NTIS HC $7.75

An Experimental and Theoretical Investigation of the Liquefaction Dynamics of a Phase Change Material in a Normal Gravity Environment

CSM-CPR-R272

(NASA-CR-129911) AN EXPERIMENTAL AND THEORETICAL INVESTIGATION OF THE LIQUEFACTION DYNAMICS OF A PHASE CHANGE
R.L. Bain, et al (Colorado School of Mines) 21 Jan. 1972 113 p CSCL 07D

N73-13131

Unclas
G3/06 16587

Chemical and Petroleum-Refining Engineering Department
Colorado School of Mines
Golden, Colorado 80401

AN EXPERIMENTAL AND THEORETICAL INVESTIGATION OF THE LIQUEFACTION DYNAMICS OF A PHASE CHANGE MATERIAL IN A NORMAL GRAVITY ENVIRONMENT

by

R. L. Bain

F. J. Stermole

J. O. Golden

Annual Summary Report No. 2

21 Nov. 1970 - 31 December 1971

Contract NAS 8-30511, Mod 2

for

National Aeronautics and Space Administration

George C. Marshall Space Flight Center

Huntsville, Alabama 35812

CSM-CPR-R272

January 21, 1972

Preface

This work was prepared by Colorado School of Mines, Golden, Colorado, under Contract NAS 8-30511, Mod. 2, "Research in Phase Change Thermal Control Technology" and under Colorado School of Mines Foundation Contracts F-6911 and F-6915. The work was administered under the direction of the Space Sciences Laboratory, George C. Marshall Space Flight Center, with Miss Barbara Richard acting as the contracting officers' technical representative.

This report covers work from 21 Nov. 1970 to 31 Dec. 1971.

The work at Colorado School of Mines was carried out by R. L. Bain under the direction of F. J. Stermole and J. O. Golden, principal investigators.

Abstract

The goal of this study was to experimentally and theoretically investigate the role of gravity-induced free convection upon the liquefaction dynamics of a cylindrical paraffin slab under normal gravity conditions.

The experimental equipment consisted of a test cell, a fluid-loop heating system, and a multipoint recorder. The test chamber was annular in shape with an effective radius of 1.585 cm and a length of 5.08 cm. The heating chamber was a 1.906 cm diameter tube going through the center of the test chamber, and connected to the fluid loop heating system.

By means of the heating chamber step changes in the inside wall temperatures were imposed on the test chamber. Temperature responses were measured by means of sixteen iron-constantan thermocouples mounted in the test chamber; hot wall temperature was also measured. N-octadecane, a high chain normal paraffin with an even number of carbon atoms, was used as the test material. All experimental runs were made with the longitudinal axis of the test cell in the vertical direction to insure that convection was not a function of the angular axis of the cell. Ten melting runs were made (five sets of reproduced data) at various hot-wall temperatures. Also, two pure-conduction solidification runs were made to determine an experimental latent heat of fusion.

The physical system was modeled using the energy equation and the ideal-viscous flow velocity approximation. An Implicit Alternating-Direction (IAD) technique was used to approximate the partial differential equations in the computer solution. The IAD technique was used to eliminate the time step stability requirement inherent in an explicit finite difference solution. However, because of numerical dispersion effects introduced by ignoring the second order partial in the Taylor's series expansion with respect to time, a time restriction was placed on the implicit solution in order to minimize the dispersion error. A latent heat of fusion of approximately 0.75 literature value was used in the theoretical solution. This value was determined by using a one-dimensional pure conduction model to predict the temperature results of the pure conduction solidification runs; the latent heat was varied until a match was obtained between data and theory. This new value was then used in the IAD program to model liquefaction.

Experimental runs were made with the total temperature gradient of the liquid phase varying from a low of 16.5°K to a high of 27.8°K. There was very good agreement between data and theoretical prediction at the low temperature gradient levels. As the gradient became larger the deviation between theory and data became larger; all phase change times were predicted correctly, but final temperatures were not.

The study has shown that with further refinements of the ideal-viscous flow model we should be able to predict temperature responses and phase-change times accurately; but the present model can only be used for theoretical prediction when liquid phase temperature gradients are small.

Table of Contents

List of Figures

Introduction

Phase change thermal control techniques have received increasing attention (references 5, 6, and 7) in the last several years for spacecraft thermal design. Because of inherent advantages of simplicity and reliability a passive solid-liquid phase change material can be used in the walls of spacecraft as packaging around sensitive electronic equipment to absorb or release energy to maintain constant temperature of the electronic equipment. However, this system is limited by the heat rejection or absorption capacity of the material used.

A previous study (1) has determined the property requirements of phase change materials in order that they be good thermal control devices. The material should be non-toxic, chemically-inert and stable, noncorrosive, have small density variations, and have a high latent heat of fusion. The material should also melt in 50- to 150°F range; n-paraffins with an even number of carbon atoms are the most widely used materials for this purpose. In this study, n-octadecane was used as the test material.

An earlier study (2) at the Colorado School of Mines dealt with the problem of gravity-induced free convection in the melting of a finite paraffin slab in a rectangular cell. Problems were encountered in reproducibility of experimental data, due to the presence of air bubbles in the test material. Because of these problems, it was difficult to be certain that the theoretical model was actually modeling the phase-change phenomena. Therefore, the present study has been undertaken to determine whether or not the model, coupling of an ideal-viscous flow model with the energy equations, will actually predict the experimental phase change phenomena. Also, the investigation is studying the phase change problem in another coordinate geometry, a cylindrical geometry. The experiments have been designed as to minimize the effects of air bubbles in the test cell.

All phase-change experiments, such as ground tests made in high gravity fields, must take into account the effect of gravity-induced free convection. Either the experiments must be designed to eliminate convection or the convection must be mathematically modeled. It is important to determine at what gravity level gravity-induced free convection may be neglected. This will enable designers of phase-change thermal control devices for spacecraft to determine whether or not gravity-induced free convection is an important design factor under low gravity conditions such as periods of thrust.

Other effects, such as electrically-induced convection or magnetically-induced convection, may also be important design factors. Since experiments to study these other effects will be made in a high gravity field, the effect of gravity must be determined before effects of these other forces can be studied completely and accurately.

Literature Survey

Many articles have appeared in the literature related to solid-liquid phase change problems and to gravity-induced free convection. This literature survey deals with only a small portion of the published material. The first treatment of liquefaction and solidification phenomena is that presented by Carslaw and Jaeger (3) in which they discuss the moving interface surface involved in the phase change problem. However, they developed only approximate mathematical models for semi-infinite bodies; no exact solutions were given for finite bodies.

Two studies have previously been completed at this institution which concern the unidimensional phase-change phenomena of high-chain normal paraffins. Both studies use the one-dimensional interface equation given by Arpaci (4). The first study was completed by P. R. Pujado (5). In his study Pujado presented a theoretical model for the unidimensional melting of a finite paraffin slab. The theoretical model was developed using finite difference methods to approximate the solution of the partial differential equations governing the physical system. The finite difference approximations were solved on an IBM-Model 360 digital computer. The model solved two-phase, unidimensional heat conduction equations with a moving interface and variable thermal properties. Mr. Pujado stated that the theoretical model neglected free convection in the liquid phase portion of the system and concluded that the errors in his results were probably due to the existence of free convection in the test cell. Mr. Pujado compared the results of his study to an investigation conducted earlier by Northrop Corporation (1) and found the results agreed very closely with the earlier work. The second study was performed by Ukanwa, Stermole, and Golden (6). The investigation concerned the solidification of a finite amount of liquid paraffin. A unidimensional model was established for the solidification of the liquid paraffin, based on the numerical solution by computer of the two-phase heat-conduction equations with moving interface and movable boundary conditions. Constant properties were assumed for each phase. The model neglected gravity-induced convection, supercooling, and nucleation effects. A comparison was made between theoretical and experimental temperature profiles. Good agreement was obtained between theory and data, although the numerical results indicate a faster rate of solidification than that observed experimentally.

A study by Shah (7) investigated solid-liquid phase change using microphotographic equipment and temperature response data as analysis tools. A two-dimensional mathematical model was developed for temperature response of the test cell and the average interfacial velocity during the

solidification process. Because no interface equations have been developed an approximate solution was used to calculate the phase change energy change. A presentation of various phase change calculations is given by Dusinberre (8). Comparison of the results obtained from the theoretical model and experimental results for the temperature response yielded reasonably good agreement. The temperature of the interface predicted by the theoretical model was always slightly higher than the experimental data.

Grodzka and Fan (9) listed several areas of study when attempting to solve the problem of free convection in phase change thermal control equipment. They stated that free convection might be induced through the following forces: gravity, surface tension, electricity, or magnetism.

Some of the texts which are good theoretical references for convection are Carslaw and Jaeger (3), Schlichting (10), and Longwell (11). Bird, Stewart, and Lightfoot (12) was used as the reference for free convection between infinite parallel plates. Vallentine (13) was used as the basic ideal-flow reference for the development of the ideal-viscous flow model. The majority of work on free convection effects in liquids and gases has been done for infinite plate systems. Models for this type of system have been developed by Bodoia and Osterle (14), Dropkin and Globe (15), Dropkin and Somerscales (16), Gebhart (17), Koh and Price (18), and Samuels and Churchill (19).

Various papers have also been published which deal with the melting of finite slabs. Chi-Tien and Yin-Chao Yen (20) developed approximate theoretical solutions for temperature distributions and melting rate when the mode of heat transfer was natural convection caused by buoyancy forces. They gave numerical solutions for various ice-water systems. Goodman and Shea (21) used a series solution to solve the problem of unidimensional melting of a finite slab.

Wilkes and Churchill (22) made a study of temperatures in a closed rectangular system to determine the theoretical effects of gravity induced convection. The theoretical model was developed from the basic equations of motion, energy, and continuity; the assumption of a two-dimensional flow pattern precluded the study of turbulent flow. The system of equations was solved by an implicit alternating-direction technique developed by Peaceman and Rachford (23). Instabilities in the numerical solution were noticed above certain Grashoff numbers. Fromm (24) developed another finite difference formulation for flow induced by a moving wall.

Papers have also been published which discussed other causes of free convection besides gravity. Emery (25) has studied magnetically induced convection. Pearson (26) and Nield (27) have studied the effects of interfacial tension on

convection. They concluded that for a gas-liquid interface surface tension was the controlling factor for thin liquid layers. At some critical liquid layer thickness gravity induced convection becomes the controlling factor. This may also be true for a solid-liquid interface, but no study of this phenomena has been reported in the literature.

An earlier study (2) performed at Colorado School of Mines dealt with the problem of gravity-induced free convection in the melting of a finite paraffin slab with cartesian geometry. An ideal-viscous flow model was assumed to model the flow pattern; this flow model was coupled with the energy equations, in finite difference form, to give a theoretical solution. Problems were encountered in reproducibility of experimental data, due to the presence of air bubbles in the test material. Because of these problems, it was difficult to be certain that the theoretical solution was modeling the phase-change phenomena accurately.

A. O. Ukanwa (28) performed a study to determine the effect of gravity-induced free convection upon the solidification of a finite paraffin slab. The mathematical solution coupled an assumed flow pattern, modified by gravity level, and the equations of motion into a finite-difference approximation. Close agreement was obtained between theory and experimental data. A pseudo-heat capacity was used to calculate the change of phase. In personal communication with Dr. Ukanwa, he has indicated that the magnitude of the energy change involved in the phase change was modified in the computer solution to correct for impurities in the test material and to correct for a solid-solid phase transition.

Lanz (29,30) and Von Rosenburg (31) have presented the results of studies which show that a numerical solution of a partial differential equation which includes bulk flow terms will include inherent numerical dispersion effects. These effects are caused by neglecting the second order partial differential in the finite difference approximation for the partial differential of time.

Theory

In this study a cylindrical-coordinate finite-difference model is developed to predict the transient temperature response of a phase change material to a step change in one boundary temperature. The model presents one method of calculating the effect of gravity-induced free convection upon the phase change process.

The test material used in the phase change investigation was n-octadecane. The literature values for the physical properties are taken from an earlier study (2).

Density

Solid phase = $(-0.0008336)T + 1.0918$, gm/cc

Liquid phase = $(-0.0012505)T + 1.1316$, gm/cc

Heat Capacity

Solid phase = 2.164, Watt-sec/gm °K

Liquid phase = $(0.008213)T - 0.14237$, Watt-sec/gm °K

Thermal Conductivity

Solid phase = $(-0.50054 \times 10^{-5})T + .002914$ watt/cm °K

Liquid phase = $(-0.50054 \times 10^{-5})T + .002914$ watt/cm °K

Melting Point = 300.60 °K

Liquefaction enthalpy = 243.893 watt-sec/gm

A diagram of the nodal system and boundary conditions is given in figure 1.

Ideal-Viscous Flow Model

An earlier study (2) has shown that it is impractical to solve the analytical equations of motion governing the liquid phase when the driving force is gravity. Therefore, an ideal-viscous flow model is developed to approximate the flow pattern which exists in the liquid phase. The velocity profile used in the model is an approximate profile obtained by combining an ideal flow system for flow in a cul-de-sac region (13) with a viscous flow solution for flow between infinite parallel plates. A maximum velocity is imposed on the ideal-viscous flow pattern, using either a driving velocity calculated from the buoyancy force term or the maximum velocity calculated from the liquid phase energy equation stability criteria.

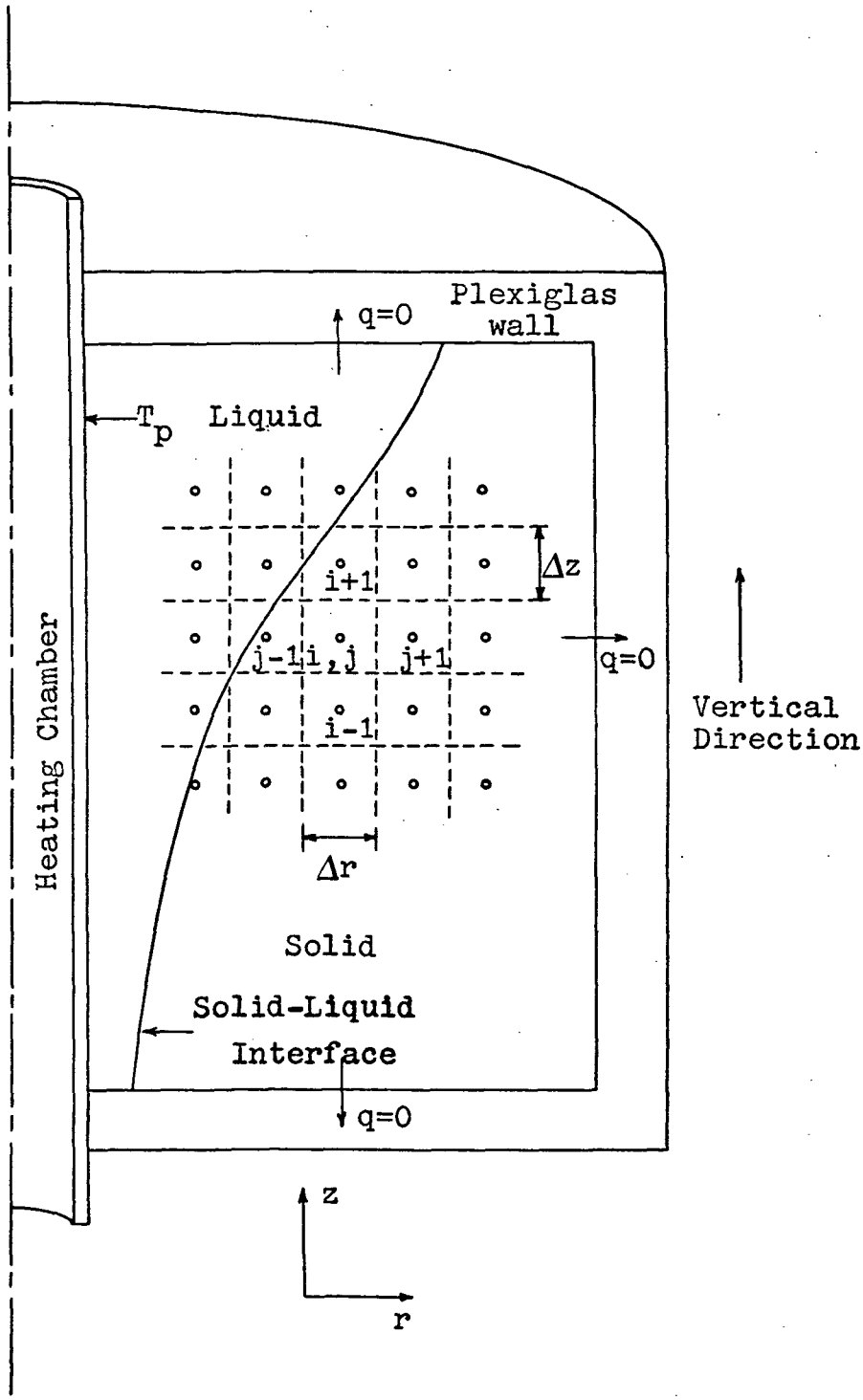

Figure 1. Model Network Diagram

The velocity profile for unidimensional flow between infinite vertical plates is developed by Bird, Stewart, and Lightfoot (12). The velocity profile is

$$v_p = \frac{\overline{\rho}\beta g b^2 \Delta T}{12\mu} (\eta^3 - \eta) \qquad (1)$$

where $\eta = y/b$.

Since a maximum velocity has been determined the velocity profile should be given as a function of the maximum velocity. The equation for velocity now becomes

$$v_p = v_{max} \left(\frac{\eta^3 - \eta}{\eta_o^3 - \eta_o}\right) \qquad (2)$$

where $\eta_o = \pm \frac{1}{\sqrt{3}}$ (from centerline)

The ideal flow velocity profiles are developed by the use of complex variable transformations; the flow pattern under consideration is shown in the following diagram.

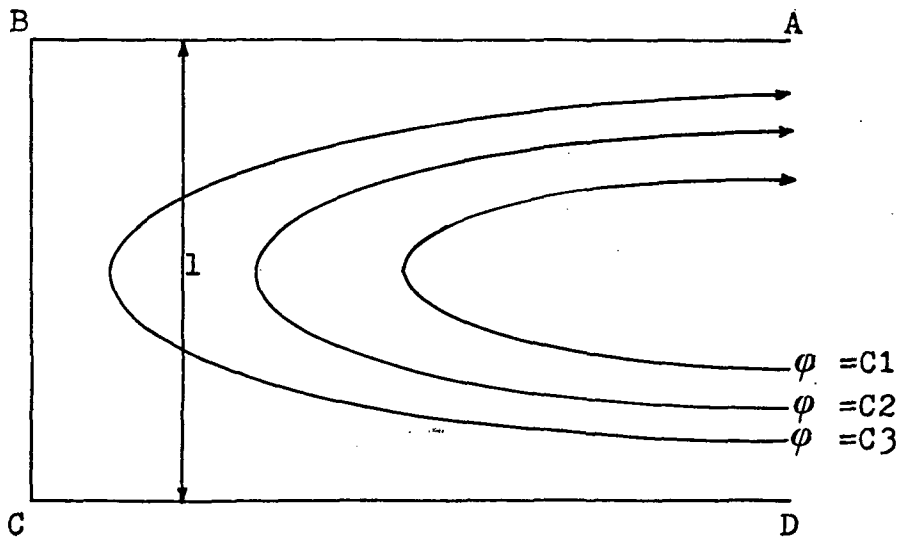

The basic assumptions made in the conformal transformation process are that (1) the flow pattern being studied is irrotational flow of a perfect fluid and that (2) the complicated flow pattern can be transformed by use of complex variables into parallel uniform flow.

The flow pattern shown above is assumed to be a complex z-plane flow within straight-wall boundaries. Since we are investigating ideal flow within a simple polygon, a Schwarz-Christoffen transformation (13) may be used to obtain a parallel uniform flow pattern.

If the polygon is in the z-plane and the new plane is the t-plane, then

$$\frac{dz}{dt} = A'(a-t)^{-\gamma/\pi}(b-t)^{-\varepsilon/\pi}(c-t)^{-\zeta/\pi} \tag{3}$$

where A' = a complex constant
a,b,c = real constants in ascending order of magnitude
γ,ε,ζ = external defection angles of the polygon

for the flow pattern under study

$$\frac{\gamma}{\pi} - = - \frac{\varepsilon}{\pi} = - \frac{\zeta}{\pi} = - \frac{1}{2}$$

The boundary conditions for the transformation are

@ A, $t = -\infty$
@ B, $t = -1$
@ C, $t = +1$
@ D, $t = +\infty$

Therefore,

$$z = A' \int \frac{dt}{\sqrt{(1-t)(-1-t)}} + B' \tag{4}$$

or $z = A' \cosh^{-1}(t) + B'$ (5)

Applying the boundary conditions

@ C, $t = 1$, $z = 0$

$0 = \cosh^{-1}(1) + B'$

$\therefore B' = 0$

@ B, $t = -1$, $z = i1$

$i1 = A' \cosh^{-1}(-1)$

$i1 = A'i\pi$

$A' = 1/\pi$

Therefore,

$$z = \frac{1}{\pi} \cosh^{-1}(t) \tag{6}$$

According to definition, as given by Vallentine (13), uniform ideal flow should have a source at $-\infty$ and a sink at $+\infty$. However, the above t-plane flow pattern gives a source at $+\infty$ and a sink at $-\infty$. Therefore, $w = -t$, where w is a new complex plane, and

$$w = -\cosh\left(\frac{\pi z}{l}\right) \tag{7}$$

where $z = x + iy$

then

$$w = -\cosh\left(\frac{\pi x}{l} + \frac{i\pi y}{l}\right) \tag{8}$$

or $$w = -\cosh\left(\frac{\pi x}{l}\right)\cos\left(\frac{\pi y}{l}\right) - i \sinh\left(\frac{\pi x}{l}\right)\sin\left(\frac{\pi y}{l}\right) \tag{9}$$

By definition of complex flow

$$\phi = -\cosh\left(\frac{\pi x}{l}\right)\cos\left(\frac{\pi y}{l}\right) \tag{10}$$

$$\psi = -\sinh\frac{\pi x}{l}\sin\frac{\pi y}{l} \tag{11}$$

The stream function is defined by the following equations

$$u = \psi_y \tag{12}$$

$$v = -\psi_x \tag{13}$$

Substituting into equation (11) and differentiating, we obtain

$$u = -\frac{\pi}{l}\sinh\left(\frac{\pi x}{l}\right)\cos\left(\frac{\pi y}{l}\right) \tag{14}$$

and $$v = \frac{\pi}{l}\cosh\left(\frac{\pi x}{l}\right)\sin\left(\frac{\pi y}{l}\right) \tag{15}$$

The liquid phase is split into three regions, as shown below.

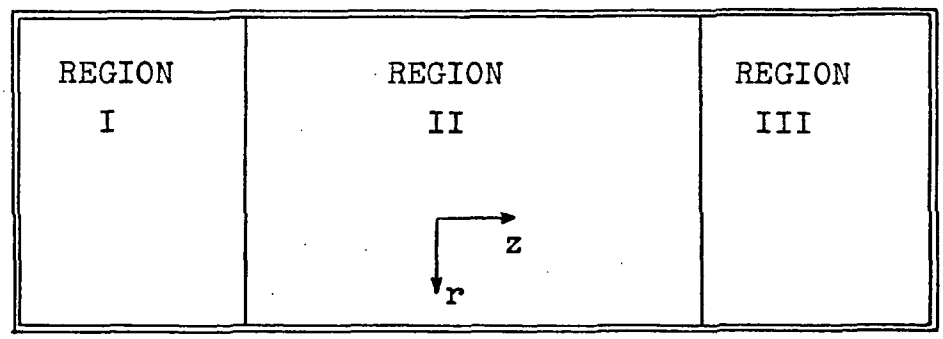

Region I flow is governed by equations (11), (14), and (15) with appropriate boundary equations. Region II is governed by equation (2) with a given maximum velocity. Region III is governed by another set of ideal flow equations; but assuming symmetrical flow it is not necessary to develop the equations for this region.

The ideal flow regions are coupled to the viscous flow region by assuming the velocities in the viscous flow region are the boundary values for the ideal flow region. All y velocities are zero at this boundary. By use of equation (11) values of the stream function may be calculated at the ideal-viscous flow boundary. Since there can be no flow across a line of constant stream function, velocities in the ideal flow region can be related to boundary velocities at calculated values of the stream function at the boundary. By this method a pseudo-viscous flow pattern can be imposed upon the ideal flow regions.

The actual liquid phase in the test cell does not have a constant depth. The velocities calculated by the ideal-viscous flow model are imposed on the liquid phase at any point by assuming the depth of the liquid at that point to be the depth of the cell in the ideal-viscous flow model.

The flow pattern calculated is only an approximation, but with the small magnitude of allowable velocities calculated by stability criteria the velocities calculated should give fairly accurate flow patterns in the liquid phase.

Finite Difference Formulation of the Energy Equations

The basic energy equations (12) governing the solid and liquid phases are given below.

Solid phase

$$T_t = \alpha_s\left(T_{zz} + \frac{1}{r}T_r + T_{rr}\right) \tag{16}$$

Liquid phase

$$T_t + uT_z + vT_r = \alpha_l\left(T_{zz} + \frac{1}{r}T_r + T_{rr}\right) \tag{17}$$

Boundary conditions

$$@\ z = 0,\ q|_z = 0$$

$$@\ z = L,\ q|_z = 0$$

$$@\ r = R,\ T = T_p$$

$$@\ r = d,\ T = T_f$$

$$@\ r = R_2,\ q|_r = 0$$

Because of the small node size needed in the finite difference solution, an implicit method of solution is

developed. The implicit formulation eliminates the stability criteria with respect to time step. An implicit alternating-direction technique has been developed by Peaceman and Rachford (23) which is inherently stable with respect to time and spatial increments.

The method involves the use of two successive time steps, each of duration Δt. Over the first time step, the derivatives in the R direction are solved implicitly, and the derivatives in the z-direction are solved explicitly. The procedure is reversed for the second time step. Let T^* denote temperatures computed at the end of the first time step, and T^o denote values at the end of the second time step. The r direction has an j subscript; the z direction has an i subscript. The following definitions are needed:

$i = 1,N$; where 1 and N are boundaries, N_i = 1^{st} liquid node in z direction for any given j.

$j = 1,M$; where M_j = 1^{st} solid node in r direction for any given i, and 1 and M are boundaries.

The solid phase finite difference approximations of equation (16) are given below.

First Time Step (Implicit in r - explicit in z)

@ an interior node

$$A_1T^*(i,j-1) + B_1T^*(i,j) + C_1T^*(i,j+1) = D_1 \tag{18}$$

where

$$A_1 = \frac{\alpha_s \Delta t}{\Delta r}\left(\frac{1}{\Delta r} + \frac{1}{2r}\right) \tag{19}$$

$$B_1 = 1.0 + \frac{2\alpha_s \Delta t}{(\Delta r)^2} \tag{20}$$

$$C_1 = -\frac{\alpha_s \Delta t}{\Delta r}\left(\frac{1}{\Delta r} + \frac{1}{2r}\right) \tag{21}$$

$$D_1 = T(i,j) + \frac{\alpha_s \Delta t}{(\Delta z)^2}\left(T(i+1,j) + T(i-1,j) - 2T(i,j)\right) \tag{22}$$

@ $j = M_j$

$$B_1T^*(i,j) + C_1T^*(i,j+1) = D_2 \tag{23}$$

where

$$D_2 = D_1 - A_1T(i,j-1) \tag{24}$$

@ $j = M-1$

$$A_1T^*(i,j-1) + B_1T^*(i,j) = D_3 \tag{25}$$

where

$$D_3 = D_1 - C_1 T(i,M) \tag{26}$$

If only one solid node is present for any given i, then

$$T^*(i,M-1) = D_4, \quad j = M-1 \tag{27}$$

where

$$D_4 = (D_3 - A_1 T(i,M-2))/B_1 \tag{28}$$

If only two solid nodes are present for any given i, then

$$T^*(i,j) = F_1/G_1, \quad \text{for} \quad j = M-1 \tag{29}$$

$$T^*(i,j) = D_5/B_1 - C_1 T^*(i,M-1)/B_1, \quad \text{for } j = M-2 \tag{30}$$

where

$$D_5 = D_1 - A_1 T(i,j-1), \quad \text{for} \quad j = M-2 \tag{31}$$

$$D_6 = D_1 - C_1 T(i,j+1), \quad \text{for} \quad j = M-1 \tag{32}$$

$$F_1 = D_5/B_1 - D_6/A_1 \tag{33}$$

$$G_1 = C_1/B_1 - B_1/A_1 \tag{34}$$

Second Time Step (implicit in z - explicit in r)

@ an interior node

$$A_7 T^o(i-1,j) + B_7 T^o(i,j) + C_7 T^o(i+1,j) = D_7 \tag{35}$$

where

$$A_7 = -\frac{\alpha_s \Delta t}{(\Delta z)^2} \tag{36}$$

$$B_7 = 1.0 + \frac{2\alpha_s \Delta t}{(\Delta z)^2} \tag{37}$$

$$C_7 = -\frac{\alpha_s \Delta t}{(\Delta z)^2} \tag{38}$$

$$D_7 = \frac{\alpha_s \Delta t}{(\Delta r)^2}\left(T^*(i,j+1)+T^*(i,j-1)-2T^*(i,j)\right) + \frac{\alpha_s \Delta t}{2r\Delta r}\left(T^*(i,j+1)-T^*(i,j-1)\right)+T^*(i,j) \tag{39}$$

@ i = 2

$$B_7 T^o(i,j) + C_7 T^o(i+1,j) = D_8 \tag{40}$$

where

$$D_8 = D_7 - A_7 T^*(i-1,j) \tag{41}$$

@ $i = N_i - 1$

$$A_7 T^o(i-1,j) + B_7 T^o(i,j) = D_9 \tag{42}$$

where

$$D_9 = D_7 - C_7 T^*(i+1,j) \tag{43}$$

If only one solid node is present for any given i, then

$$T^o(2,j) = D_{10}\ ,\ i = 2 \tag{44}$$

where

$$D_{10} = (D_7 - A_7 T^*(1,j))/B_7 \tag{45}$$

If only two solid nodes are present for any given j, then

$$T^o(i,j) = F_7/G_7\ ,\ \text{for}\ \ i = 3 \tag{46}$$

$$T^o(i,j) = D_{11}/B_7 - C_7 T^o(3,j)/B_7,\ i = 2 \tag{47}$$

where

$$D_{11} = D_7 - A_7 T^*(i-1,j),\ \ \text{for}\ \ i = 2 \tag{48}$$

$$D_{12} = D_7 - C_7 T^*(i+1,j),\ \ \text{for}\ \ i = 3 \tag{49}$$

$$F_7 = D_{11}/B_7 - D_{12}/A_7 \tag{50}$$

$$G_7 = C_7/B_7 - B_7/A_7 \tag{51}$$

In the computer program, all coefficients that have r in the denominator must be calculated as a function of radial position.

The liquid phase finite difference approximations of equation (17) are given below.

First Time Step (implicit in r - explicit in z)

@ an interior node

$$A_{13} T^*(i,j-1) + B_{13} T^*(i,j) + C_{13} T^*(i,j+1) = D_{13} \tag{52}$$

where

$$A_{13} = \frac{\Delta t}{\Delta r}\left(-\frac{v(i,j)}{2} - \frac{\alpha_1}{\Delta r} + \frac{\alpha_1}{2r}\right) \tag{53}$$

$$B_{13} = 1.0 + \frac{2\alpha_1 \Delta t}{(\Delta r)^2} \tag{54}$$

$$C_{13} = \frac{\Delta t}{\Delta r}\left(\frac{v(i,j)}{2} - \frac{\alpha_1}{\Delta r} - \frac{\alpha_1}{2r}\right) \tag{55}$$

$$D_{13} = \frac{\Delta t u(i,j)}{2\Delta z}\left(T(i-1,j) - T(i+1,j)\right) + T(i,j) + \frac{\Delta t \alpha_1}{(\Delta z)^2}\left(T(i+1,j) + T(i-1,j) - 2T(i,j)\right) \tag{56}$$

@ j = 2

$$B_{13}T^*(i,j) + C_{13}T^*(i,j+1) = D_{14} \tag{57}$$

where

$$D_{14} = D_{13} - A_{13}\,T(i,1) \tag{58}$$

@ j = M_j - 1

$$A_{13}T^*(i,j-1) + B_{13}T^*(i,j) = D_{15} \tag{59}$$

where

$$D_{15} = D_{13} - A_{13}T(i,M_j) \tag{60}$$

If only one liquid node is present for any given i, then

$$T^*(i,2) = D_{16}\ ,\quad j = 2 \tag{61}$$

where

$$D_{16} = (D_{15} - C_{13}T(i,3))/B_{13} \tag{62}$$

If only two liquid nodes are present for any given i, then

$$T^*(i,j) = F_{13}/G_{13}\ ,\ \text{for } j = 3 \tag{63}$$

$$T^*(i,j) = D_{17}/B_{13} - C_{13}T^*(i,3)/B_{13},\ j = 2 \tag{64}$$

where

$$D_{17} = D_{13} - A_{13}T(i,j-1),\ \text{for } j = 2 \tag{65}$$

$$D_{18} = D_{13} - C_{13}T(i,j+1),\ \text{for } j = 3 \tag{66}$$

$$F_{13} = D_{17}/B_{13} - D_{18}/A_{13} \tag{67}$$

$$G_{13} = C_{13}/B_{13} - B_{13}/A_{13} \tag{68}$$

Second Time Step (implicit in z - explicit in r)

@ an interior node

$$A_{19}T^\circ(i-1,j) + B_{19}T^\circ(i,j) + C_{19}T^\circ(i+1,j) = D_{19} \tag{69}$$

where

$$A_{19} = \frac{\Delta t}{\Delta z}\left(-\frac{u(i,j)}{2} - \frac{\alpha_1}{\Delta z}\right) \tag{70}$$

$$B_{19} = 1.0 - \frac{2\alpha_1 \Delta t}{(\Delta z)^2} \tag{71}$$

$$C_{19} = \frac{\Delta t}{\Delta z}\left(\frac{u(i,j)}{2} - \frac{\alpha_1}{\Delta z}\right) \tag{72}$$

$$D_{19} = \frac{v(i,j)\Delta t}{2\Delta r}\,(T^*(i,j-1) - T^*(i,j+1)) + T^*(i,j) + \frac{\alpha_1 \Delta t}{(\Delta r)^2}\,(T^*(i,j+1) + T^*(i,j-1) - 2T^*(i,j)) + \frac{\alpha_1 \Delta t}{2r\Delta r}\,(T^*(i,j+1) - T^*(i,j-1)) \quad (73)$$

@ $i = N_i$

$$B_{19}T^\circ(i,j) + C_{19}T^\circ(i+1,j) = D_{20} \quad (74)$$

where

$$D_{20} = D_{19} - A_{19}T^*(i-1,j) \quad (75)$$

@ $i = N-1$

$$A_{19}T^\circ(i-1,j) + B_{19}T^\circ(i,j) = D_{21} \quad (76)$$

where

$$D_{21} = D_{19} - C_{19}T^*(i+1,j) \quad (77)$$

If only one liquid node is present for any given j, then

$$T^\circ(i,j) = D_{22},\ i = N-1 \quad (78)$$

where

$$D_{22} = (D_{21} - C_{19}T^*(N,j))/B_{19} \quad (79)$$

If only two liquid nodes are present for any given j, then

$$T^\circ(i,j) = F_{19}/G_{19},\ \text{for } i = N-2 \quad (80)$$

$$T^\circ(i,j) = D_{23}/B_{19} - C_{19}T^\circ(N-2,j)/B_{19},\ i = N-1 \quad (81)$$

where

$$D_{23} = D_{19} - A_{19}T^*(i-1,j),\ i = N-2 \quad (82)$$

$$D_{24} = D_{19} - C_{19}T^*(i+1,j),\ i = N-1 \quad (83)$$

$$F_{19} = D_{23}/B_{19} - D_{24}/A_{19} \quad (84)$$

$$G_{19} = C_{19}/B_{19} - B_{19}/A_{19} \quad (85)$$

Consider the solid phase energy equation. In particular, let equation 18 be applied to each point j = 3, 4, ..., M-2 in the i^{th} column. Equations (23) and (25) hold for j = 2 and j = M-1, respectively. A system of simultaneous equations results, but there are a maximum of three unknowns in each equation. A non-iterative method for the solution of this system of equations, known as the tridiagonal matrix regression technique, is available. These equations are of the form

$$
\begin{aligned}
b_2 s_2 + c_2 s_3 &= d_2 \\
a_3 s_2 + b_3 s_3 + c_3 s_4 &= d_3 \\
&\cdots \\
a_{M-2} s_{M-3} + b_{M-2} s_{M-2} + c_{M-2} s_{M-1} &= d_{M-2} \\
a_{M-1} s_{M-2} + b_{M-1} s_{M-1} &= d_{M-1}
\end{aligned}
\tag{86}
$$

where s_j = unknown temperature at node i,j. The values of a_j, b_j, and c_j are determined from equations (19), (20), and (21). The values of d_1, d_j, and d_{M-1} are determined from equations (24), (22), and (26) respectively. The matrix of the coefficients of temperature is a trigonal matrix. The solution of equation (86) takes advantage of the tridiagonal properties of the coefficient matrix. The values of s_j satisfying equation (86) are given by

$$s_{M-1} = g_{M-1} \tag{87}$$

$$s_l = g_l - f_l s_{l+1}, \text{ for } l = M-2, M-3, \ldots, 3,2 \tag{88}$$

where the g's and f's are determined by the recursion formulae

$$w_2 = b_2 \tag{89}$$

$$w_l = b_l - a_l f_{l-1}, \text{ for } l = 3,4,\ldots M-2,M-1 \tag{90}$$

$$f_l = c_l/w_l, \text{ for } l = 2,3,\ldots,M-2,M-1 \tag{91}$$

$$g_2 = d_2/w_2 \tag{92}$$

$$g_l = (d_l - a_l g_{l-1})/w_l, \text{ for } l = 2,3,\ldots,M-2,M-1 \tag{93}$$

This regression technique is used to solve both solid and liquid phase energy equations. During the first time step each row, j = 2,...,M-1, is solved by the above technique, going explicitly from i = 2,...,N-1. During the second time step the procedure is reversed, using the appropriate energy equations.

This solution of the energy equations, coupled with the phase change calculations, gives a theoretical solution of the liquefaction of the test material under the influence of gravity-induced free convection.

Phase Change Calculations

A summary of various phase change calculation techniques is given by Dusinberre (8). A variation of the method of "excess degrees" was used as a calculation procedure in this study. Since the n-octadecane used in the study was practical grade, and not the pure material, the assumption was made that

the phase-change material changed over a 1.76°K degree temperature range. The phase-change temperature range was made symmetrically around the literature value for phase change temperature. For n-octadecane the heat capacity is the same above and below the phase-change temperature; in this case when the latent heat is divided by the heat capacity we get a term with the dimensions of temperature, called "excess degrees." It is the temperature rise which would occur if the amount of heat, equal to the latent heat, were added and no phase change took place. The procedure for calculating the phase change is given below. After each iteration a test is run on solid phase temperatures.

Given:

$$T_s(i,j) \cdot R \cdot T_f \tag{94}$$

If, $T_s(i,j) < T_f$, the node is still solid (95)

If, $T_s(i,j) \geq T_f$, the node is changing phase (96)

If equation (96) is applicable for the node being investigated, then the following procedure is followed.

Given:

$$T_e(i,j) \cdot R \cdot \Delta H_f / C_p \tag{97}$$

If, $T_e(i,j) < \Delta H_f / C_p$, the node has not changed phase (98)
and the temperature is given by

$$T_s(i,j) = T_{fo} + T_e(i,j) * C_p * 1.76 / \Delta H_f \tag{99}$$

If, $T_e(i,j) \geq \Delta H_f / C_p$ (100)

the node has changed phase and the liquid phase temperature is given by

$$T_l(i,j) = T_{fo} + 1.76 + (T_e(i,j) * C_p - \Delta H_f) / C_p \tag{101}$$

Numerical Dispersion Effects

Von Rosenburg (31) and Lantz (30) state that finite difference solutions of partial differential equations which have bulk flow velocity terms include numerical dispersion effects caused by ignoring the second order partial differential with respect to time in the Taylor's series expansion used to derive the finite difference approximation for the partial of the variable with respect to time. Both explicit and implicit solutions exhibit these numerical dispersion effects.

When the second partial with respect to time is left in the Taylor's series expansion and a partial differential equation is derived from the finite difference equation, equation (17) becomes

$$T_t + \frac{\Delta t}{2} T_{tt} + uT_z + vT_r = \frac{\alpha_1}{r} T_r + \alpha_1 T_{rr} + \alpha_1 T_{zz} \quad (102)$$

The procedure for calculating the numerical dispersion terms is

(1) rearrange equation (17) and solve for T_t

(2) substitute T_t, from step 1, into equation (102) for term $\frac{\Delta t}{2} T_{tt}$

(3) rearrange the resulting equation.

When this is done, equation (102) becomes

$$T_t + uT_z + (v + \frac{v\Delta t}{2r})T_r = \frac{\alpha_1}{r} (1.0 + \frac{\Delta t \alpha_1}{2r^2})T_r$$
$$+ (\alpha_1 + \frac{\Delta t \alpha_1 v}{2r} - \frac{\Delta t v^2}{2} - \frac{\Delta t \alpha_1^2}{2r})T_{rr}$$
$$+ \alpha_1 (10 - \frac{\Delta t u^2}{2})T_{zz}$$
$$+ (\frac{\Delta t v \alpha_1}{r} - \Delta t v u)T_{rz} \quad (103)$$

To minimize the effect of numerical dispersion the magnitude of the time step in the finite difference solution must be reduced until numerical dispersion coefficients, all coefficients which include Δt in the above equation, are negligible, and a convergent solution is obtained when the time step is varied.

Stability Criteria

Although the implicit solution developed in this study has eliminated the time step stability criteria, stability criteria still exist which limit the magnitudes of allowable velocities (30) in the program. The stability criteria for velocities from the finite difference formulation of equation (17) are given below.

$$|u| \leq 2\alpha_1/\Delta z \quad (104)$$

$$-v \leq \frac{\alpha_1 (r/\Delta r - 1)}{r}, \text{ for } v < 0 \quad (105)$$

$$v \leq \frac{\alpha_1 (r/\Delta r + 1)}{r}, \text{ for } v > 0 \quad (106)$$

Equipment and Procedure

In this section a short discussion of the equipment and procedure used in the experimental investigation portion of this study is given. The test cell, figures 2 and 3, consisted of an annular test chamber, a tubular heating chamber, and an expansion chamber. The heating chamber was aluminum pipe with an outside diameter of 1.906 cm. The outside diameter of the test chamber was 5.08 cm; the height of test chamber was 5.08 cm. The test chamber was drilled in a 10.16 cm by 10.16 cm by 7.62 cm block of plexiglas. The expansion chamber, 7.62 cm by 7.62 cm by 2.54 cm, was machined from a 10.16 cm by 10.16 cm by 3.76 cm block. Sixteen iron-constantan thermocouples, made from 24-gauge wire, were placed in the test chamber at various positions. These positions are given below. The z-position is the distance from the bottom of the test chamber; the r-position is the distance from the inside wall.

Thermocouple No.	z-position (cm)	r-position (cm)
1	1.016	1.270
2	1.016	0.9525
3	1.016	0.635
4	1.016	0.3175
5	2.032	1.27
6	2.032	0.9525
7	2.032	0.635
8	2.032	0.3175
9	3.048	1.27
10	3.048	0.9525
11	3.048	0.635
12	3.048	0.3175
13	4.064	1.27
14	4.064	0.9525
15	4.064	0.635
16	4.064	0.3175

Thermocouples were also used to measure the heating tank temperature and the heating chamber wall temperature. The expansion chamber and test chamber were connected using 4-0.3175 cm diameter bolts. A cork gasket was placed in the test chamber to ensure that no leaks developed. Epoxy was used to seal all other openings, such as the thermocouple ports and the heating chamber port.

The heating system consisted of the following equipment: a constant temperature bath, a constant temperature controller, a centrifugal pump, a flow-meter, and lines and valves. A diagram of the heating system is given in figure 4. The flow lines consisted of 1.27-cm inside-diameter copper tubing; the valves were 1.27 cm Prier globe valves. The flow-

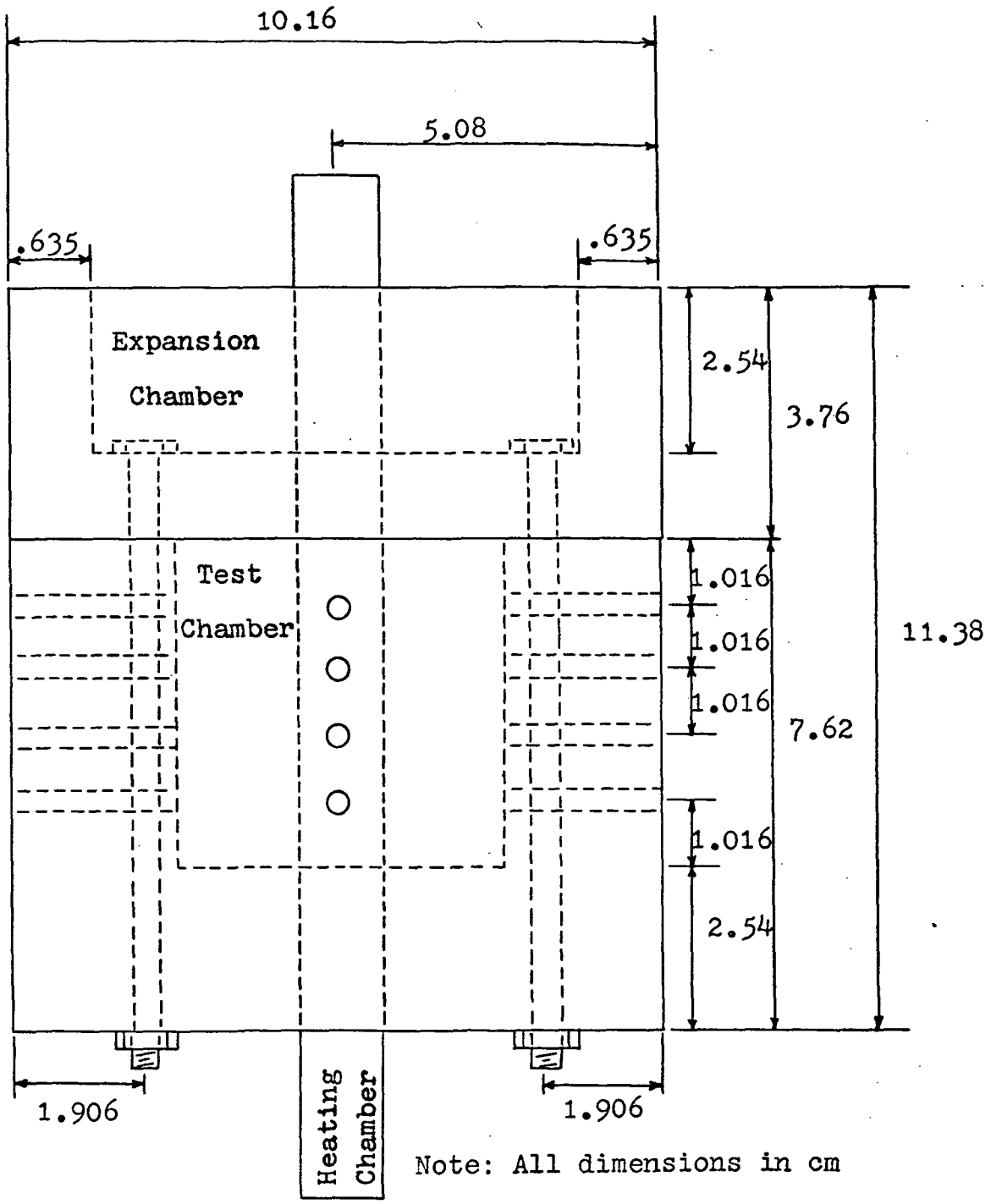

Figure 2. Test Cell - Front View

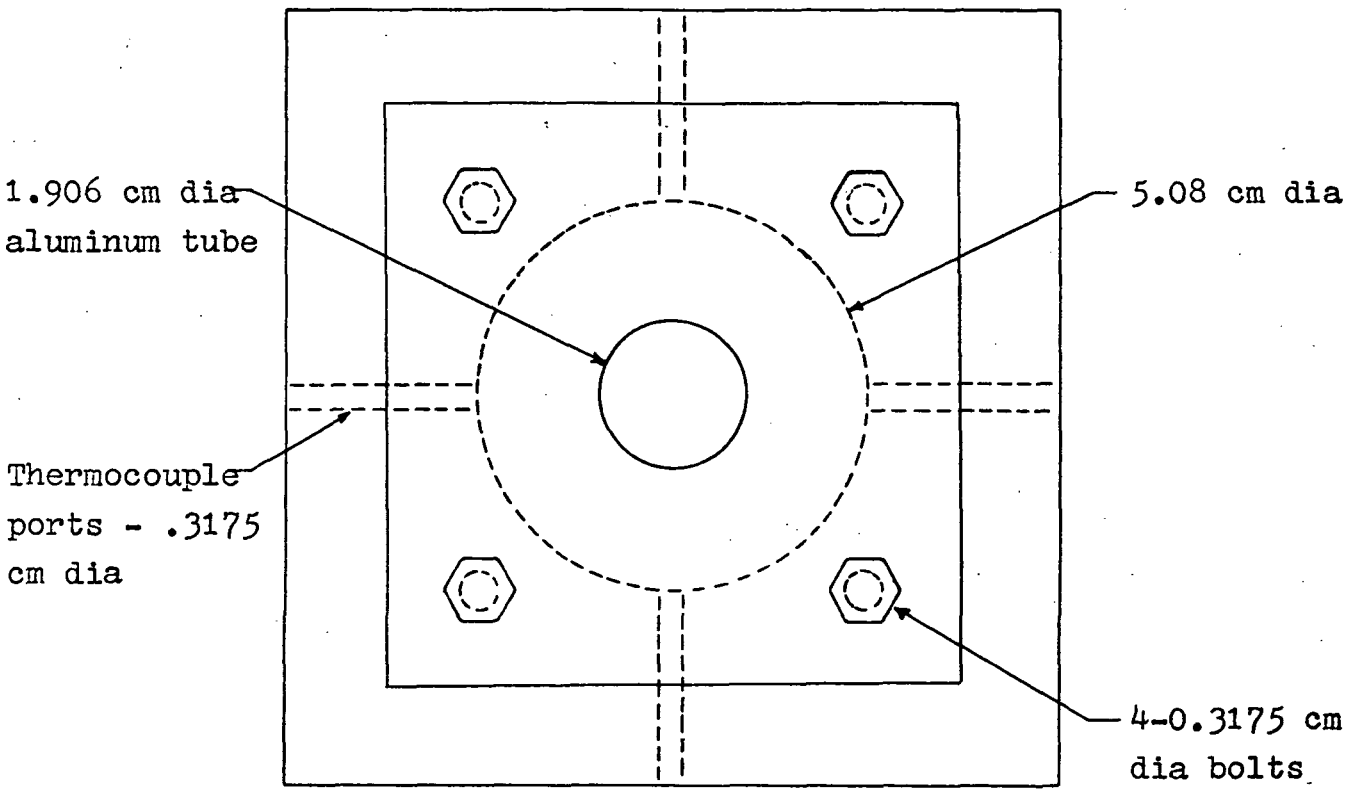

Figure 3. Test Cell - Top View

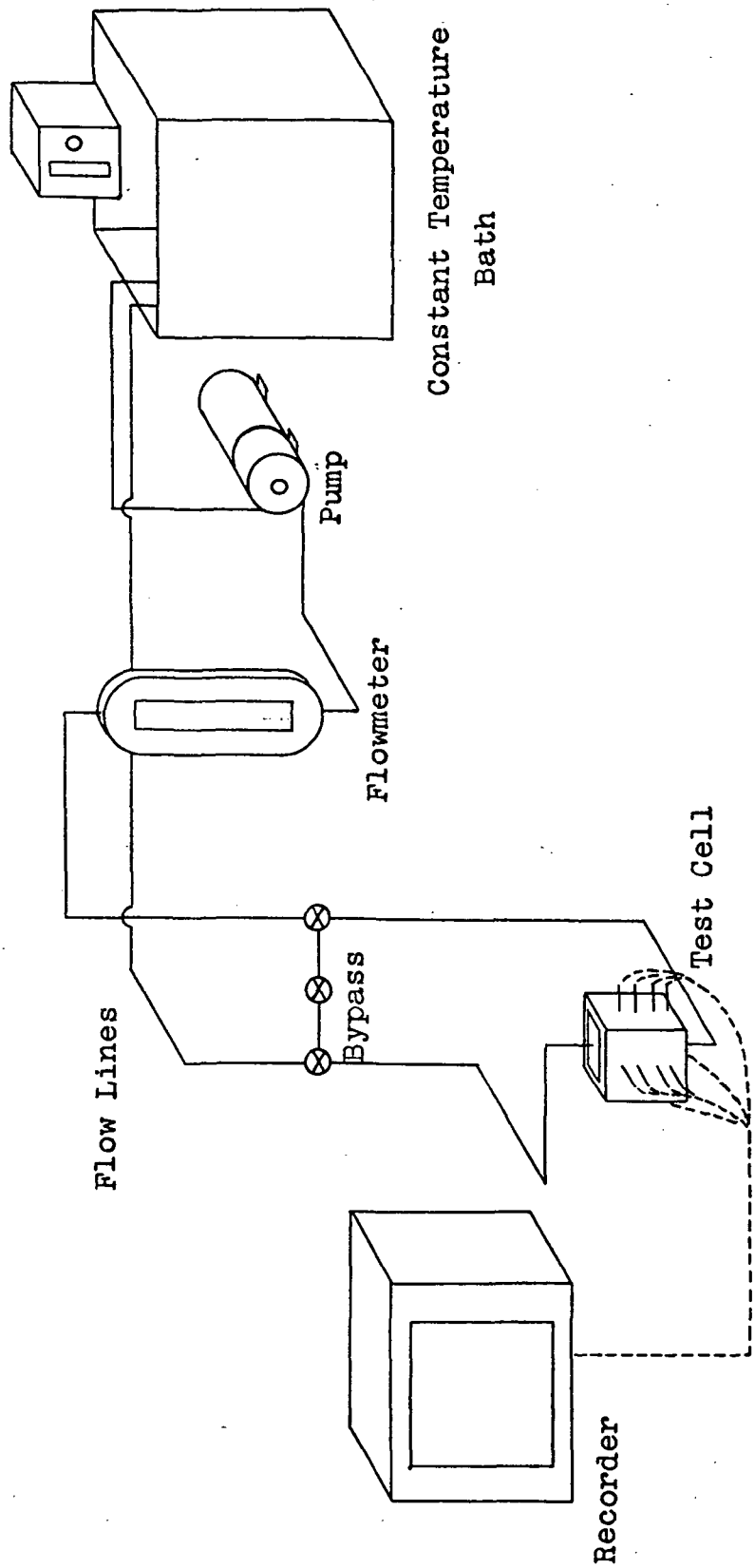

Figure 4. Flow System

meter was a Fisher and Porter Co. precision bore flowrator tube No. FP-1/2-27-G-10/83 with a 100% rated capacity of 2.3467 liters/min for a liquid with a specific gravity of 1.0.

The constant temperature bath was a 5-liter Pyrex tank. The constant temperature bath was a Hanke Company, Model E51, Constant Temperature Circulator. The circulator is designed for thermosetting open baths in the temperature range 243 to 423°K with a control accuracy of ±0.02°K. The circulator has a continuously variable heater output selections between 0 and 1000 watts. The circulating pump used to circulate the heating fluid to the test cell was a Chemical Rubber Company "No Seal" centrifugal pump, Model AB1P005N. The pump operated on 115-volt, 60 cycle/min, alternating current. The pump's rated capacity was 2.65 liters/min at a head of 30.5 cm to 1.58 liters/min at 274.5 cm under normal atmospheric conditions.

Temperatures were recorded using a Bristol Dynamaster Multipoint convertible recorder, Model 570, operating on 120 volt, 60 cycle/min, alternating current. The print speed was 2 seconds per thermocouple. The accuracy of the recorder was ±0.417 °K.

Experimental runs were made using the following procedure:

1. For a melting run the tank temperature was set approximately 1°K higher than the desired hot wall temperature. The pump was turned on and heating fluid, water, was allowed to flow through the bypass lines; this brought most of the water in the flow system to tank temperature. When the constant temperature bath reached a constant temperature, and the test cell thermocouples recorded temperatures that were within 0.278°K the experimental run was started. For a solidification run the test material was heated 5.6°K above the melt point. The constant temperature bath was filled with ice, and the flow cooled to 273.16°K. When the test material cooled to 2.78°K above the melt point the experimental run was started.

2. At the start of the experimental run the test cell was first leveled; then the run was started by switching from bypass flow to heating chamber flow. The starting point was marked on the chart paper of the temperature recorder.

3. The duration of the solidification runs was approximately forty minutes; the duration of the liquefaction runs varied from 50 minutes to 120 minutes.

Discussion of Results

In this section the results of two experimental solidification runs and ten experimental liquefaction runs are compared to theoretical temperature profiles obtained using the numerical computer solution. The experimental solidification runs were made to determine a latent heat of fusion under pure conduction conditions. All liquefaction experimental runs show the effect of gravity-induced free convection. Good agreement was obtained between theory and data for the liquefaction runs; agreement was best when the liquid-phase temperature gradient was small.

Figure 5 shows typical results from the combined experimental and theoretical determination of a latent heat of fusion to be used in the liquefaction study. During personal communication with A. O. Ukanwa and S. P. White (32) it was determined that the use of literature values of latent heat in the numerical solution of solid-liquid phase change problems being studied was not modeling the physical situation being observed experimentally. In all three investigations, two liquefaction studies and one solidification study, the test materials were all high chain normal paraffins of practical chemical grade. There are three possible justifications for varying the literature value of latent heat: (1) Since only practical chemical grade test material was used in the study, the physical properties may be different from literature values. (2) Impurities may exist in the test material, due to chemical reaction with the aluminum walls, leaching of solvents from the plexiglas walls, or other forms of contamination. (3) In an earlier study (2) and in the present study, a large number of air bubbles have been observed in the test material during the experimental runs. These air bubbles have an effect on the physical properties of a given volume of the test material.

In the computer solution the temperature response is insensitive to thermal diffusivity, making the latent heat of fusion the governing factor. The results of the comparison of theory and data shown in figure 5 indicate that a latent heat of 75 percent of literature value gives the best theoretical approximation of experimental data. Ukanwa (28) overcame the problem by using a pseudo-heat capacity to model the phase change; he stated that the method, as used in the computer solution, also changed the magnitude of the latent heat. However, this method of phase change calculation is not applicable to a liquefaction study. White, using n-octadecane as a test material, has also obtained good agreement between theory and data using a latent heat of 75 percent of literature value. The only deviations that appear between theory and data, figures 5-a, 5-b, and 5-c, occur at the phase change temperature; this indicates that a larger temperature range for phase change may be applicable. Until

the phase change takes place there is little apparent difference in the theoretical profiles for the different latent heats, see figure 5-d. Only one thermocouple is presented for each radial position; since all thermocouples for both experimental runs were within 0.7°K at any radial position the solidification was unidimensional, and only one thermocouple was needed in the presentation. The experimental data, runs C-19-2 and C-23-2, are given in Appendix A. As in the equipment and procedure section the z-position of a thermocouple is the distance from the bottom of the test cell and the r-position is the distance from the inside wall.

Figure 6 presents a comparison of experimental temperature data and theoretical temperature predictions for a liquefaction run with a hot wall temperature of 313.55°K. The agreement between experimental and theoretical results is very good for all sixteen thermocouples. Good reproducibility of experimental data is shown by the two experimental runs presented. The effect of convection is very important. For example, figures 6-a, 6-b, 6-c, and 6-d are all at R = 0.3175 cm and various z-positions. If the mode of heat transfer were pure conduction then all four thermocouples would show that the interface was flat. But thermocouple 16 shows that the node at z = 4.064 cm melts at 1980 seconds; thermocouple 12 shows that the node at z = 3.048 cm melts at 3000 seconds; thermocouple 8 shows that the node at z = 2.032 cm melts at 4800 seconds; and thermocouple 4 shows that the node at z = 1.016 cm melts at 5400 seconds. The melt pattern is definitely affected by convection. The thermocouples at other R-positions show the same effect, but with a time lag caused by their larger distances from the hot wall. At any given z-position the final liquid phase temperatures for all R-positions are approximately the same, see figures 6-d, 6-h, 6-l, and 6-p.

Figure 7 shows the effect of numerical dispersion upon the theoretical temperature profiles for a hot wall temperature of 313.55°K. For the duration of the runs, the largest effect is at z = 4.064 cm, figures 7-d, 7-h, 7-l, 7-p. The results show that the solution obtained is not yet in the convergent region. Due to computer limitations it was not possible to obtain a convergent time step. With a larger and faster computer solution it should be possible to reduce the time step far enough to eliminate the effect of numerical dispersion. At z = 2.032 cm and z = 3.048 cm, for example see figures 7-b and 7-c, there is very little effect due to numerical dispersion, due to the fact that these z-positions are in the parallel flow region and not influenced by the velocity to a large extent. At z = 1.016 cm the solution is not affected by numerical dispersion, due to the fact that temperature gradients in this region of the test cell are small. In all liquefaction computer runs the time step used was the smallest one that would allow modeling of an entire experimental run; core limitations were placed on the computer solutions that made it necessary to complete each run within a seven hour time limit.

Figure 8 presents a comparison of theoretical temperature profiles and experimental temperature profiles for a hot wall temperature of 319.11°K. There is good agreement between theory and data for all thermocouples; but larger deviations occur in the final liquid phase temperatures than occurred at a hot wall temperature of 313.55°K. The largest deviations in final liquid phase temperatures are 2.25°K, see figures 8-d, 8-h, 8-o, and 8-p; all phase change times are predicted within 180 seconds. The R = 0.3175 cm, z = 2.032 cm and z = 3.048 cm thermocouples, see figures 8-b and 8-c, show deviation between theory and data immediately after the phase change takes place; the theoretical curves show a more rapid temperature rise than the experimental data indicates should occur. This deviation is accounted for by the fact that the theoretical model assumes parallel flow in this portion of the liquid phase while experimentally the flow is not parallel in this region, because the interface is not parallel to the hot wall.

Figure 9 shows a comparison of three theoretical runs made for a hot plate temperature of 319.11°K. As in figure 7 the results show that the solution is not in the convergent region, and that numerical dispersion is still an important factor in the solution for the time steps used. The effect is of the same magnitude as that observed for figure 7.

Figures 10, 11, and 12 present theoretical temperature profiles compared to experimental temperature profiles. As in earlier runs, the experimental reproducibility of data is very good. The same trends are present as in figure 8; all phase change times are predicted very closely; deviations are present in the rate of liquid phase temperature rise for z = 2.032 cm and z = 3.048 cm for R = 0.3175 cm. Again the model does predict accurately the final liquid phase temperatures at z = 4.064 cm. For a hot wall temperature of 321.33°K, figure 10, the largest deviation in final liquid phase temperature is 2.8°K; for a hot wall temperature of 327.44°K, figure 11, the largest deviation in final liquid phase temperature is 4.4°K; for a hot wall temperature of 330.22°K, figure 12, the largest deviation in final liquid phase temperature is 5.6°K.

From the results presented in this section, it can be concluded that gravity-induced free convection is an important design factor in the use of passive solid-liquid phase-change thermal control devices. In all ground tests gravity-induced convection will affect results to some extent, even in cases where the experiments are designed to minimize the effects of gravity-induced convection. In cases where the hot wall is not horizontal one end of the test material, that at the highest elevation, will melt faster than predicted by pure conduction. With the present progress made in prediction of gravity-induced convection it is not possible to say at what gravity level convection effects may be neglected.

Figure 5. Comparison of Experimental Data for a Solidification Run to Theoretical Pure Conduction Profiles for Various Values of Latent Heat

(a) at R = 0.3175 cm
(b) at R = 0.635 cm
(c) at R = 0.9525 cm
(d) at R = 1.27 cm

Legend:

$\Delta H_{used} = K\Delta H_{literature}$

------ - K = 1.0

——— - K = 0.75

—·—·— K = 0.50

⊙ - Experimental Data

Figure 5

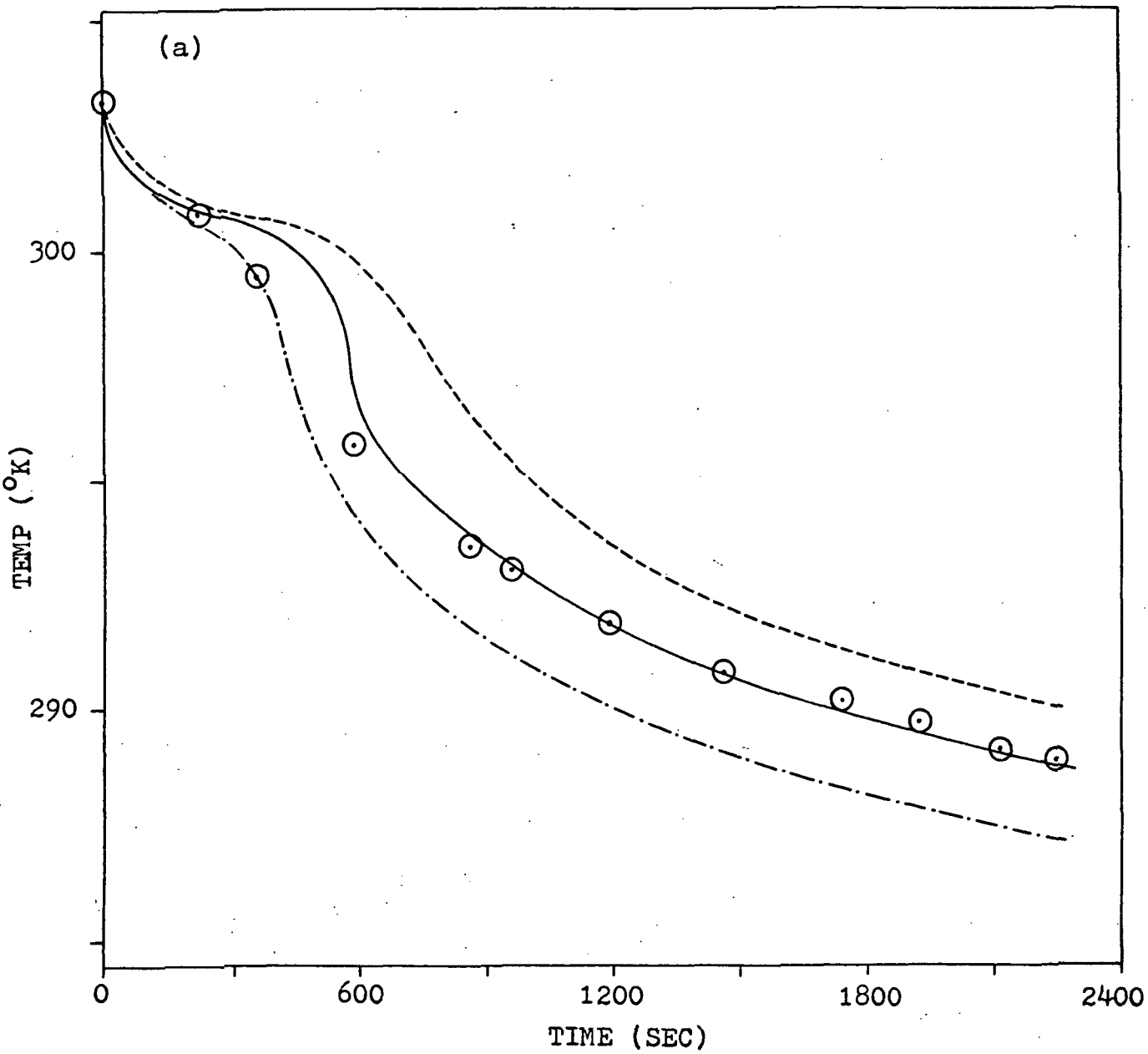

Figure 5 (cont)

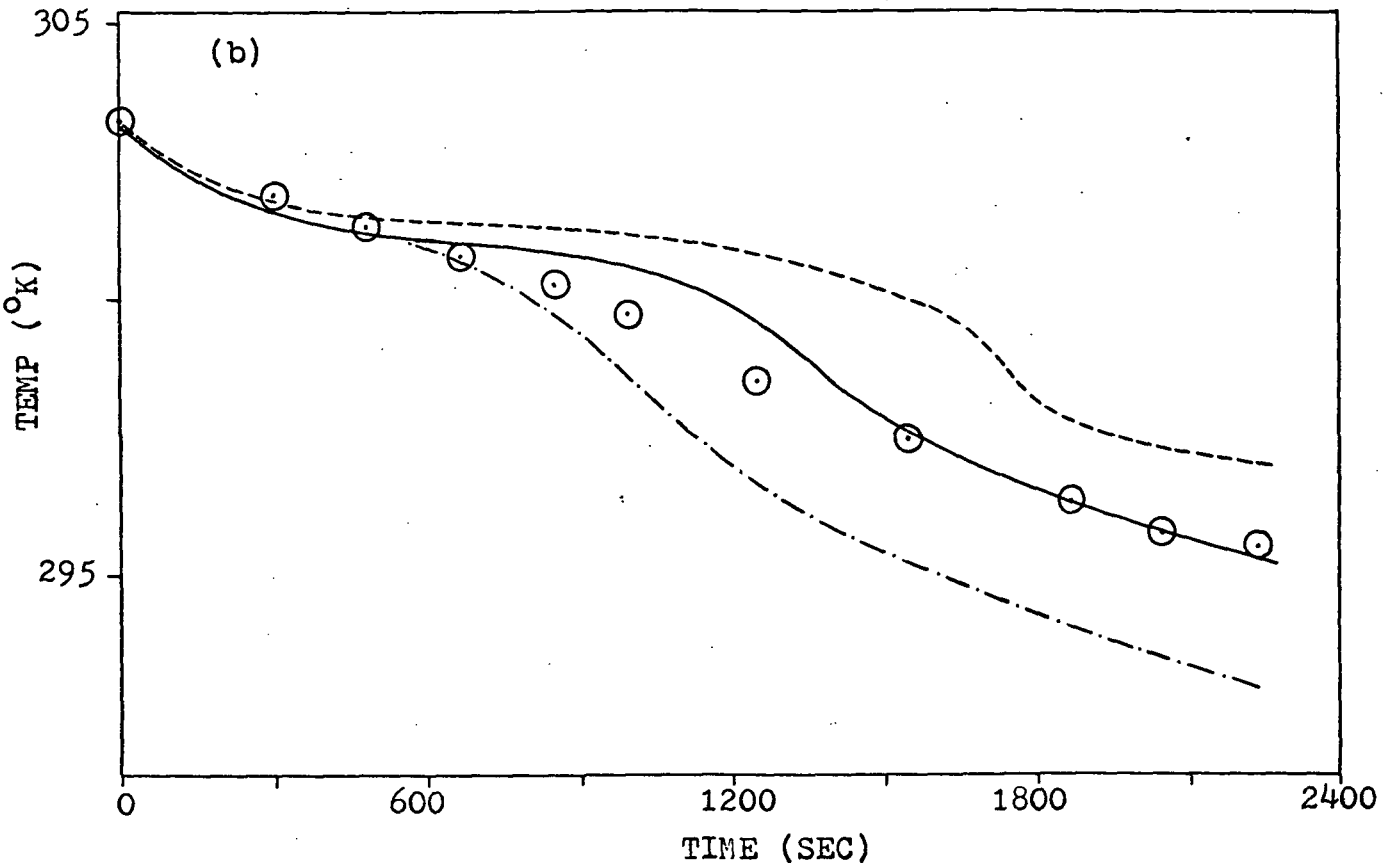

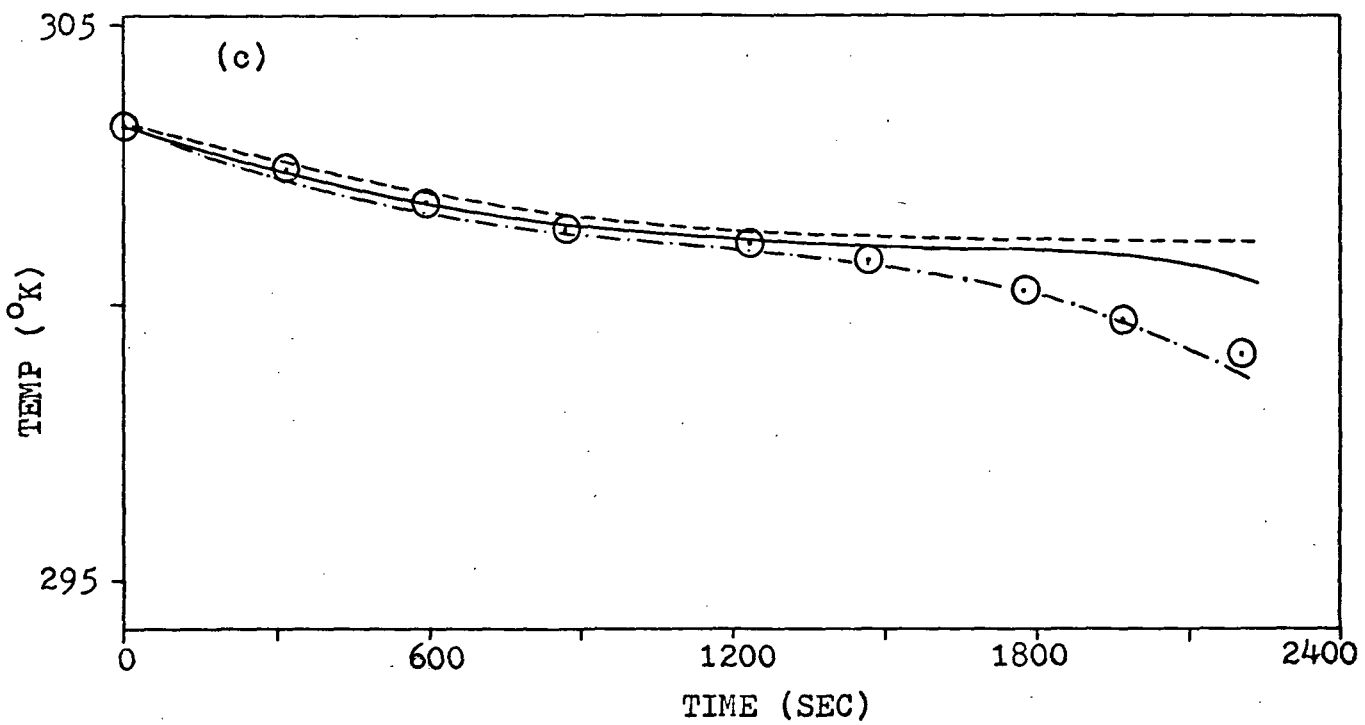

Figure 5 (cont)

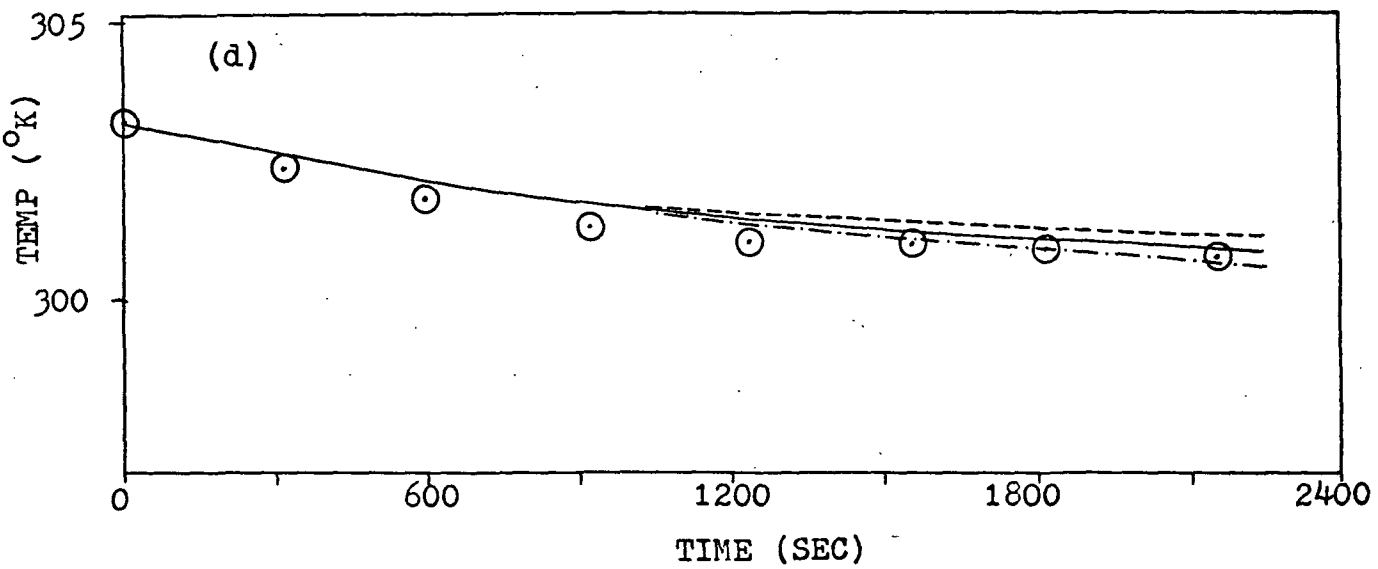

Figure 6. Comparison of Experimental Data to Theoretical Model Temperature Profiles for a Hot Wall Temperature of 313.55°K

(a) r = 0.3175 cm, z = 1.016 cm
(b) r = 0.3175 cm, z = 2.032 cm
(c) r = 0.3175 cm, z = 3.048 cm
(d) r = 0.3175 cm, z = 4.064 cm
(e) r = 0.635 cm, z = 1.016 cm
(f) r = 0.635 cm, z = 2.032 cm
(g) r = 0.635 cm, z = 3.048 cm
(h) r = 0.635 cm, z = 4.0 4 cm
(i) r = 0.9525 cm, z = 1.016 cm
(j) r = 0.9525 cm, z = 2.032 cm
(k) r = 0.9525 cm, z = 3.048 cm
(l) r = 0.9525 cm, z = 4.064 cm
(m) r = 1.270 cm, z = 1.016 cm
(n) r = 1.270 cm, z = 2.032 cm
(o) r = 1.270 cm, z = 3.048 cm
(p) r = 1.270 cm, z = 4.064 cm

Legend:

⊙ = C-13-2
⊡ = C-14-2
—— = Theoretical Model

Figure 6

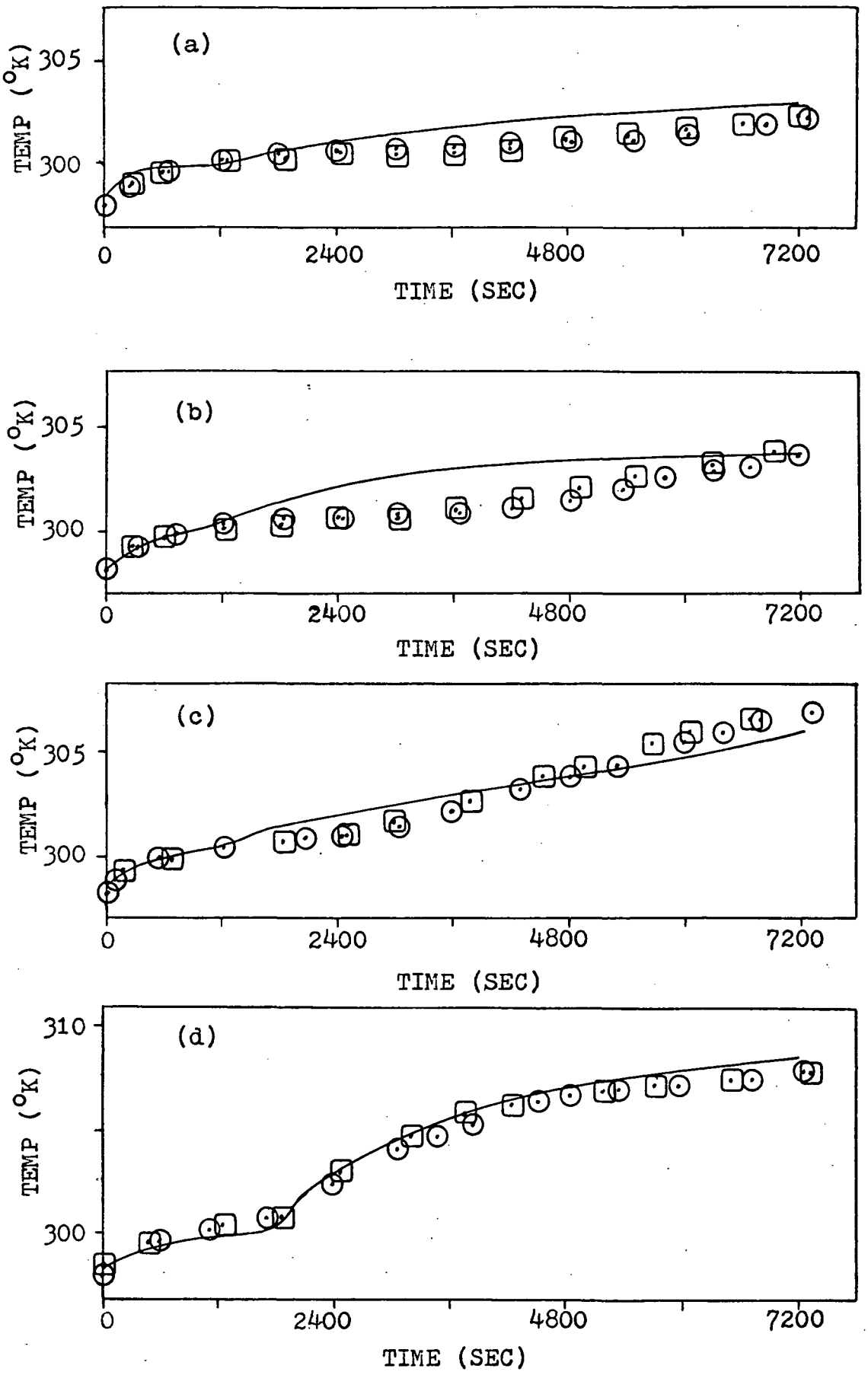
(a)
TEMP (°K)
305
300
0
2400
4800
7200
TIME (SEC)
(b)
TEMP (°K)
305
300
0
2400
4800
7200
TIME (SEC)
(c)
TEMP (°K)
305
300
0
2400
4800
7200
TIME (SEC)
(d)
TEMP (°K)
310
300
0
2400
4800
7200
TIME (SEC)

Figure 6 (cont)

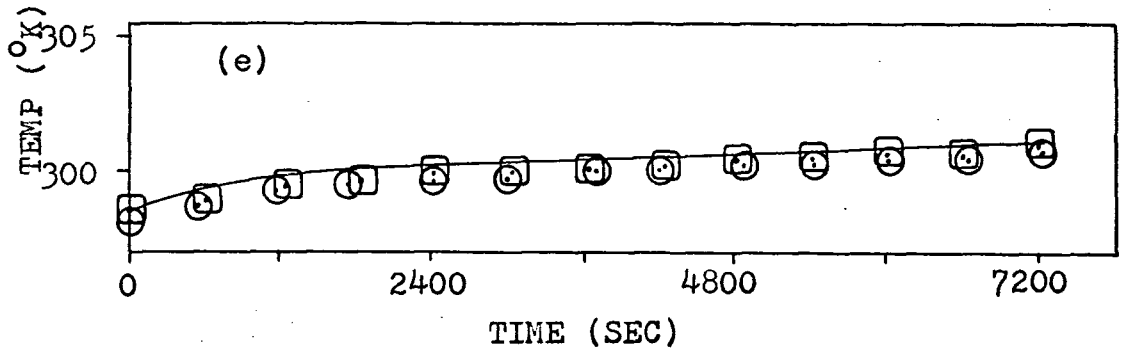

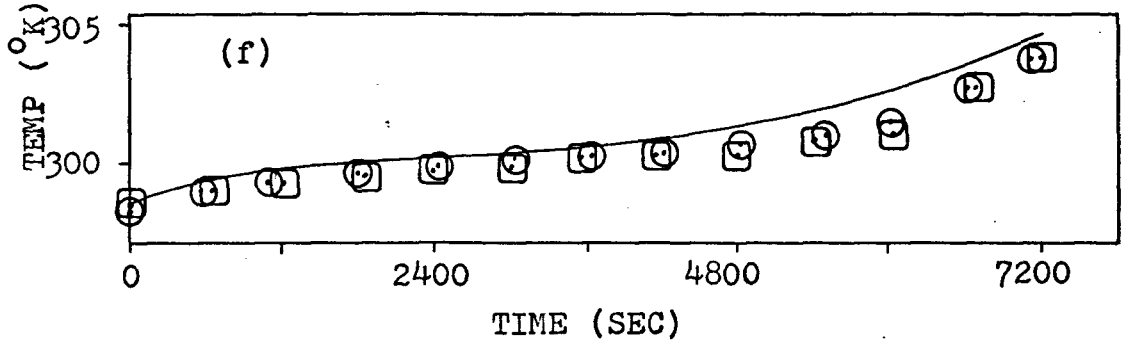

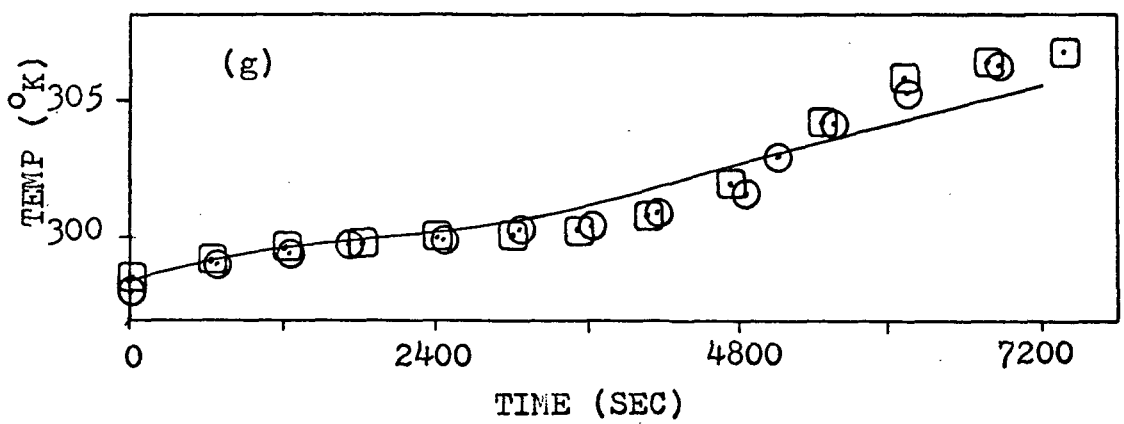

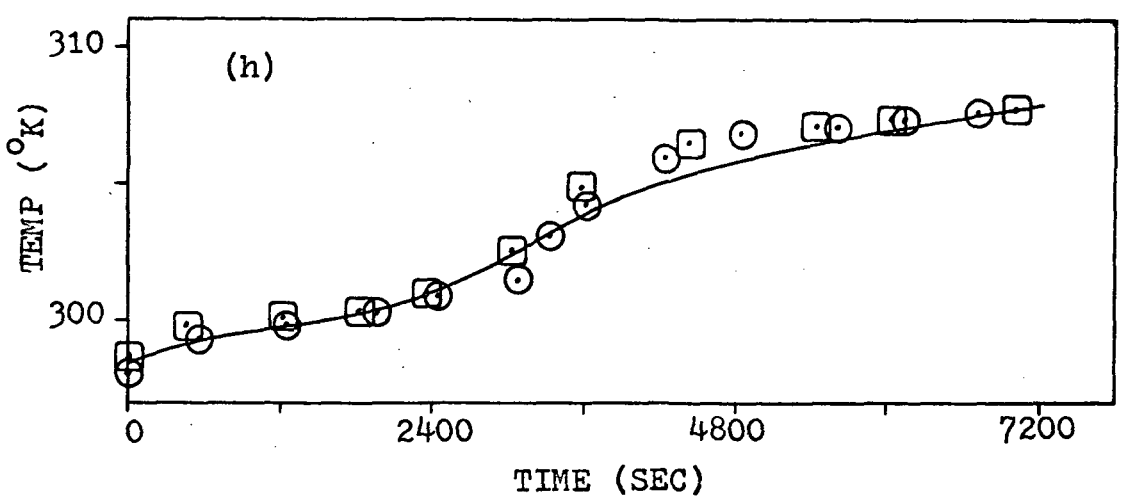

Figure 6 (cont)

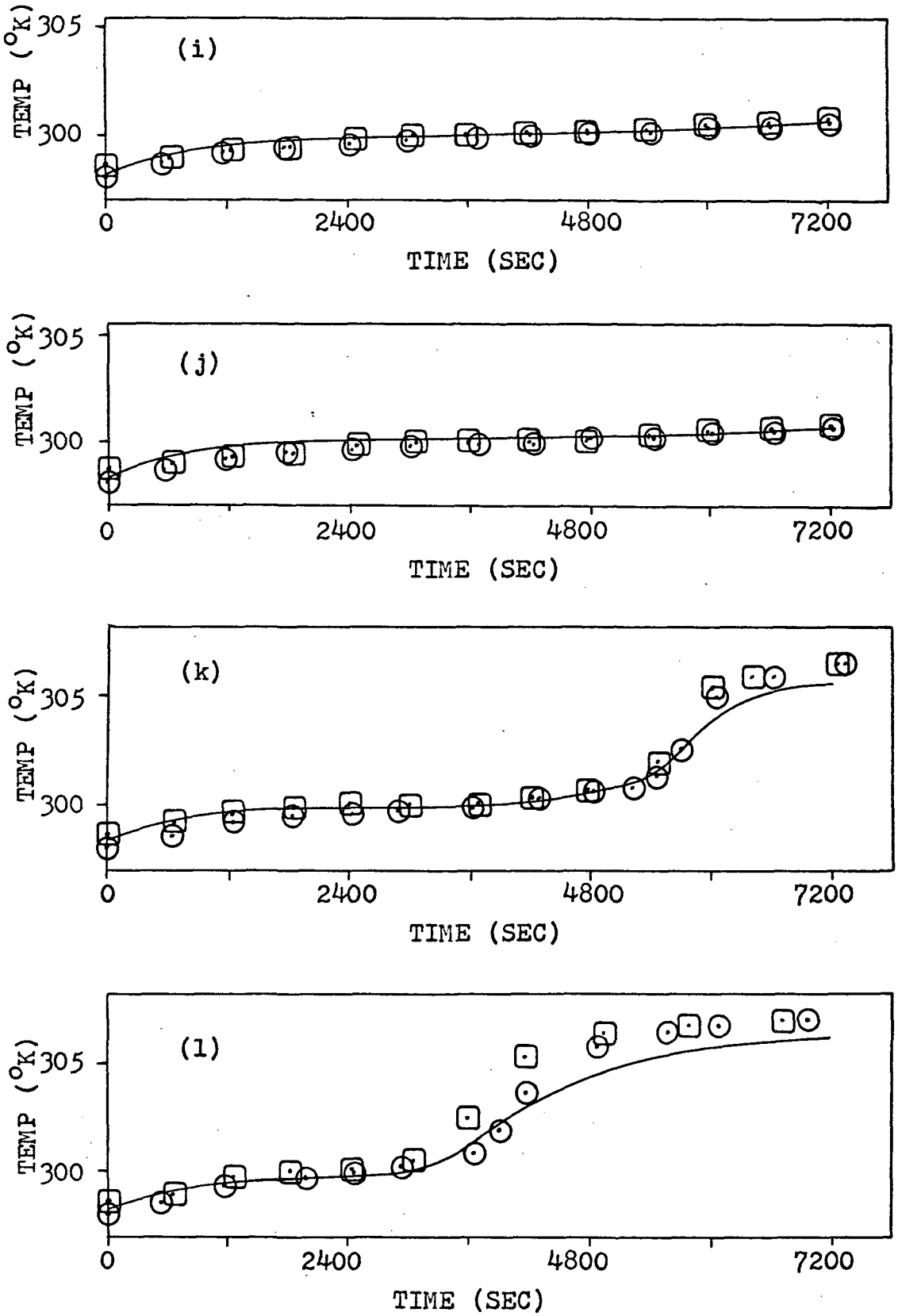

Figure 6 (cont)

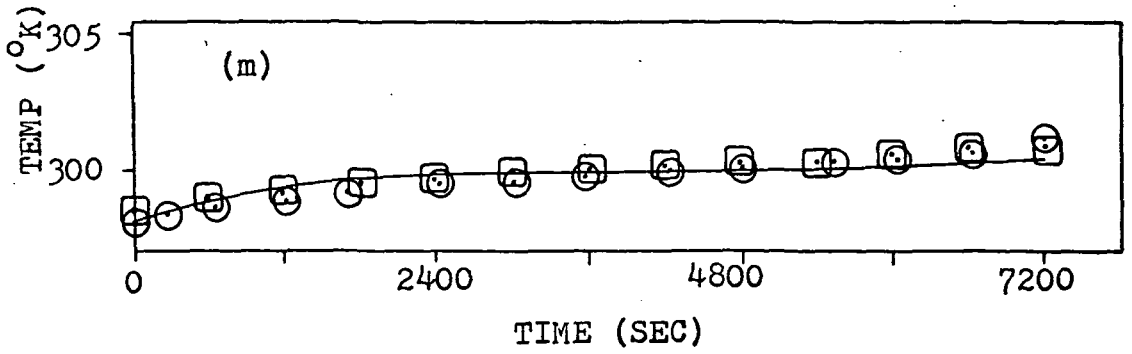

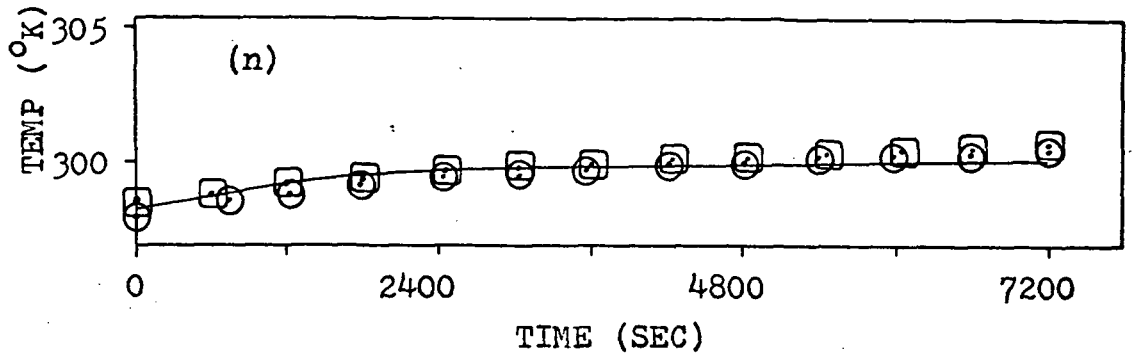

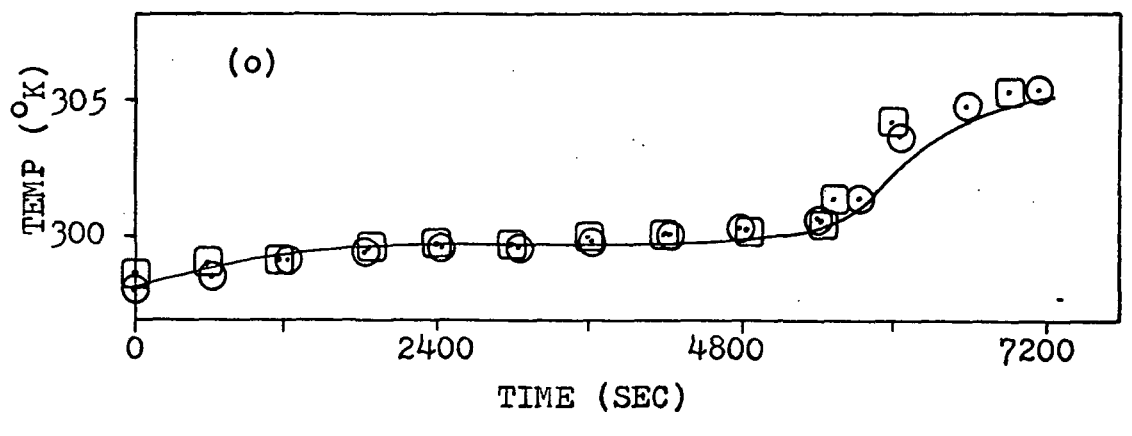

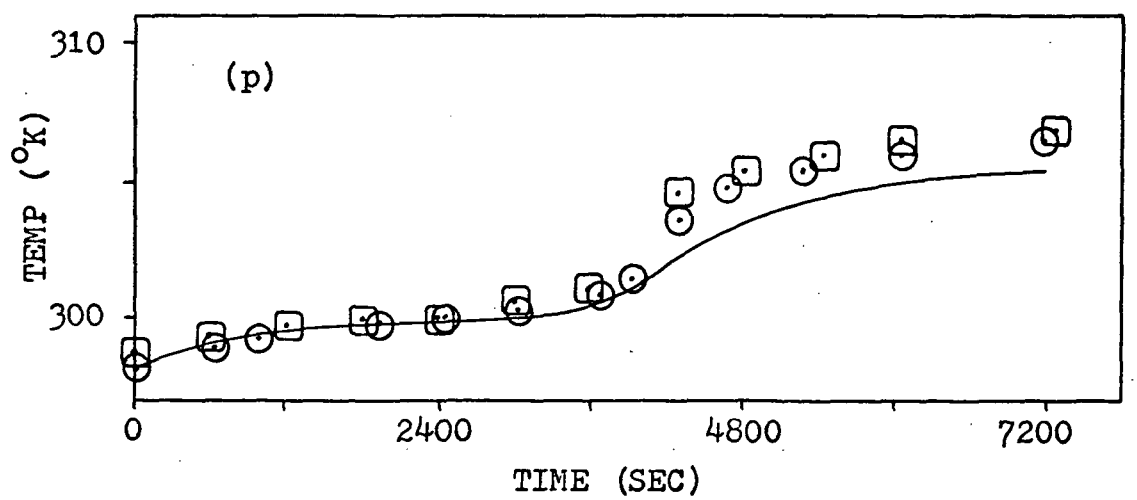

Figure 7. Effect of Numerical Dispersion Upon Theoretical Temperature Profiles for a Hot Wall Temperature of 313.55 ^{o}K

(a) r = 0.3175 cm, z = 1.016 cm
(b) r = 0.3175 cm, z = 2.032 cm
(c) r = 0.3175 cm, z = 3.048 cm
(d) r = 0.3175 cm, z = 4.064 cm
(e) r = 0.635 cm, z = 1.016 cm
(f) r = 0.635 cm, z = 2.032 cm
(g) r = 0.635 cm, z = 3.048 cm
(h) r = 0.635 cm, z = 4.064 cm
(i) r = 0.9525 cm, z = 1.016 cm
(j) r = 0.9525 cm, z = 2.032 cm
(k) r = 0.9525 cm, z = 3.048 cm
(l) r = 0.9525 cm, z = 4.064 cm
(m) r = 1.270 cm, z = 1.016 cm
(n) r = 1.270 cm, z = 2.032 cm
(o) r = 1.270 cm, z = 3.048 cm
(p) r = 1.270 cm, z = 4.064 cm

Legend:

—·—·— = 1.0 sec for time increment
——— = 1.5 sec for time increment
----- = 3.0 sec for time increment

Figure 7

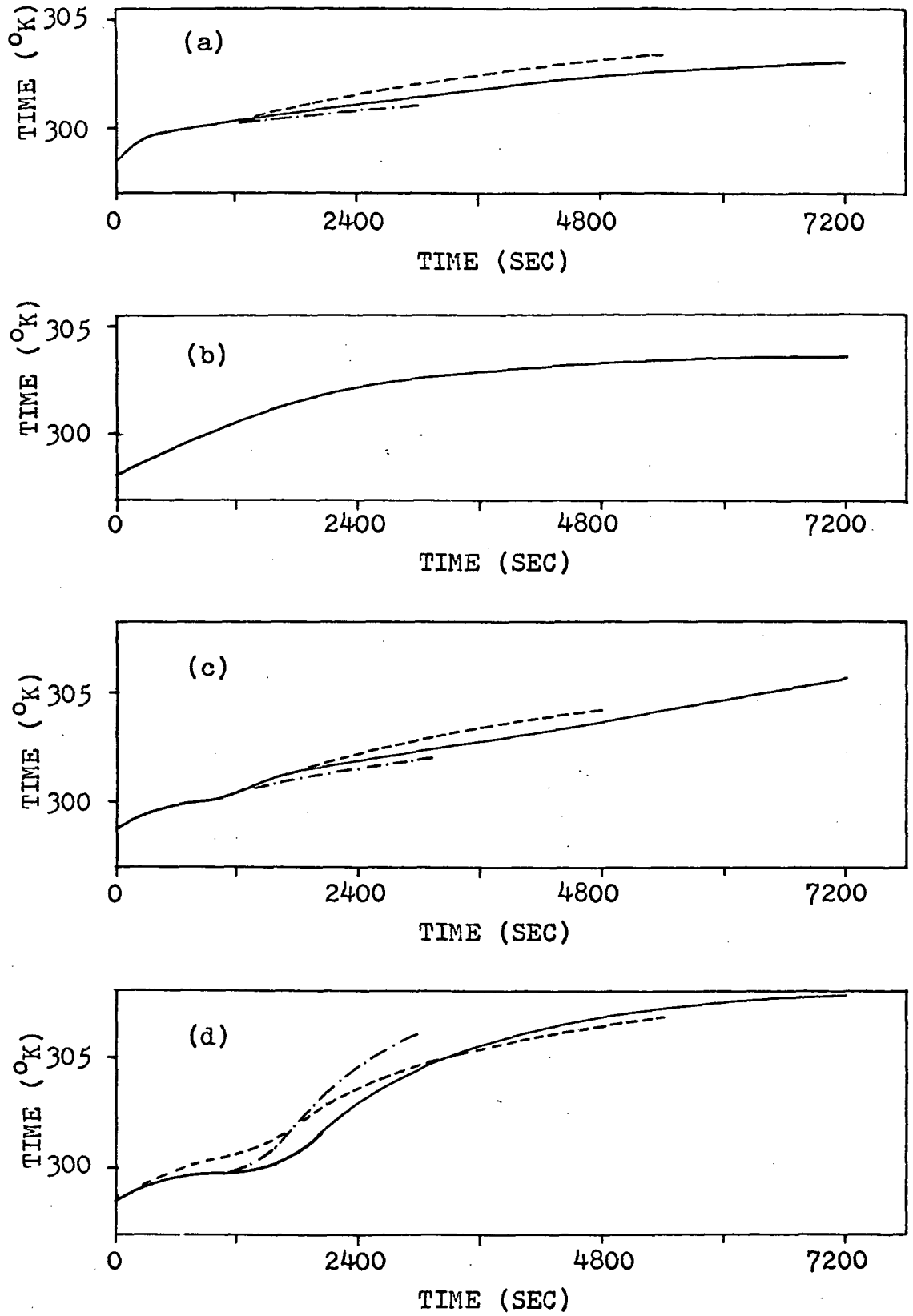
(a)
TIME (°K)
305
300
0
2400
4800
7200
TIME (SEC)
(b)
TIME (°K)
305
300
0
2400
4800
7200
TIME (SEC)
(c)
TIME (°K)
305
300
0
2400
4800
7200
TIME (SEC)
(d)
TIME (°K)
305
300
0
2400
4800
7200
TIME (SEC)

Figure 7 (cont)

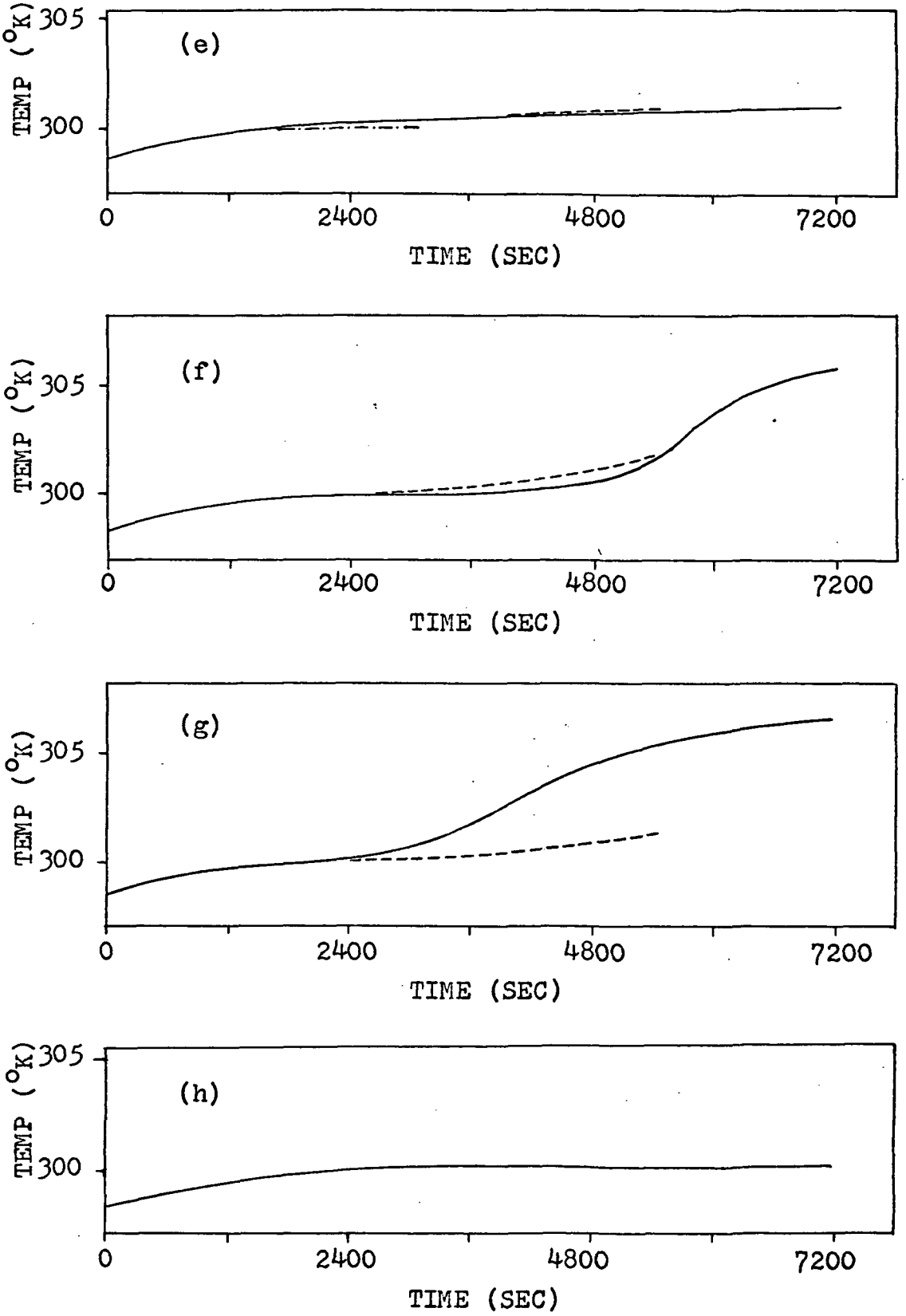

Figure 7 (cont)

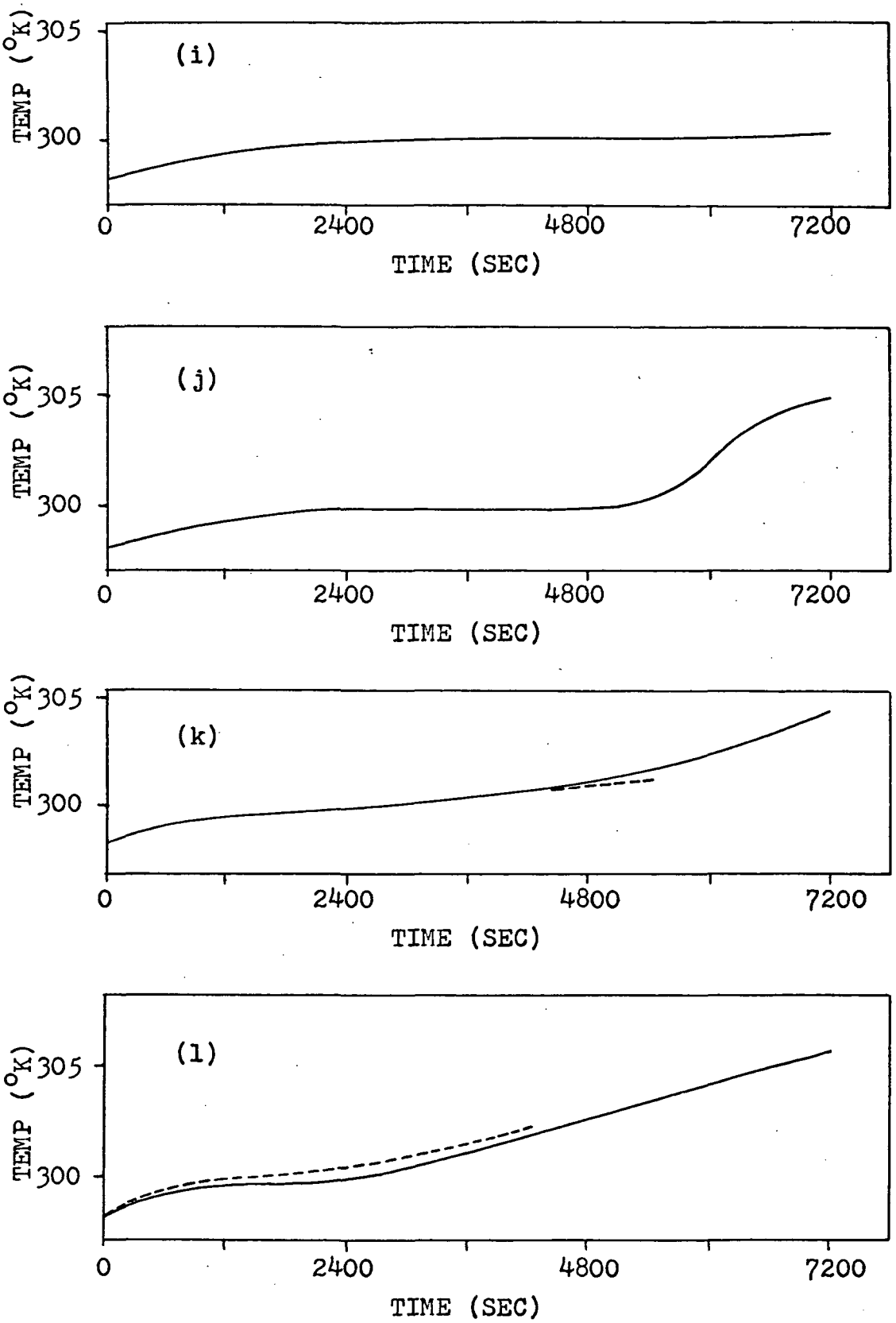

Figure 7 (cont)

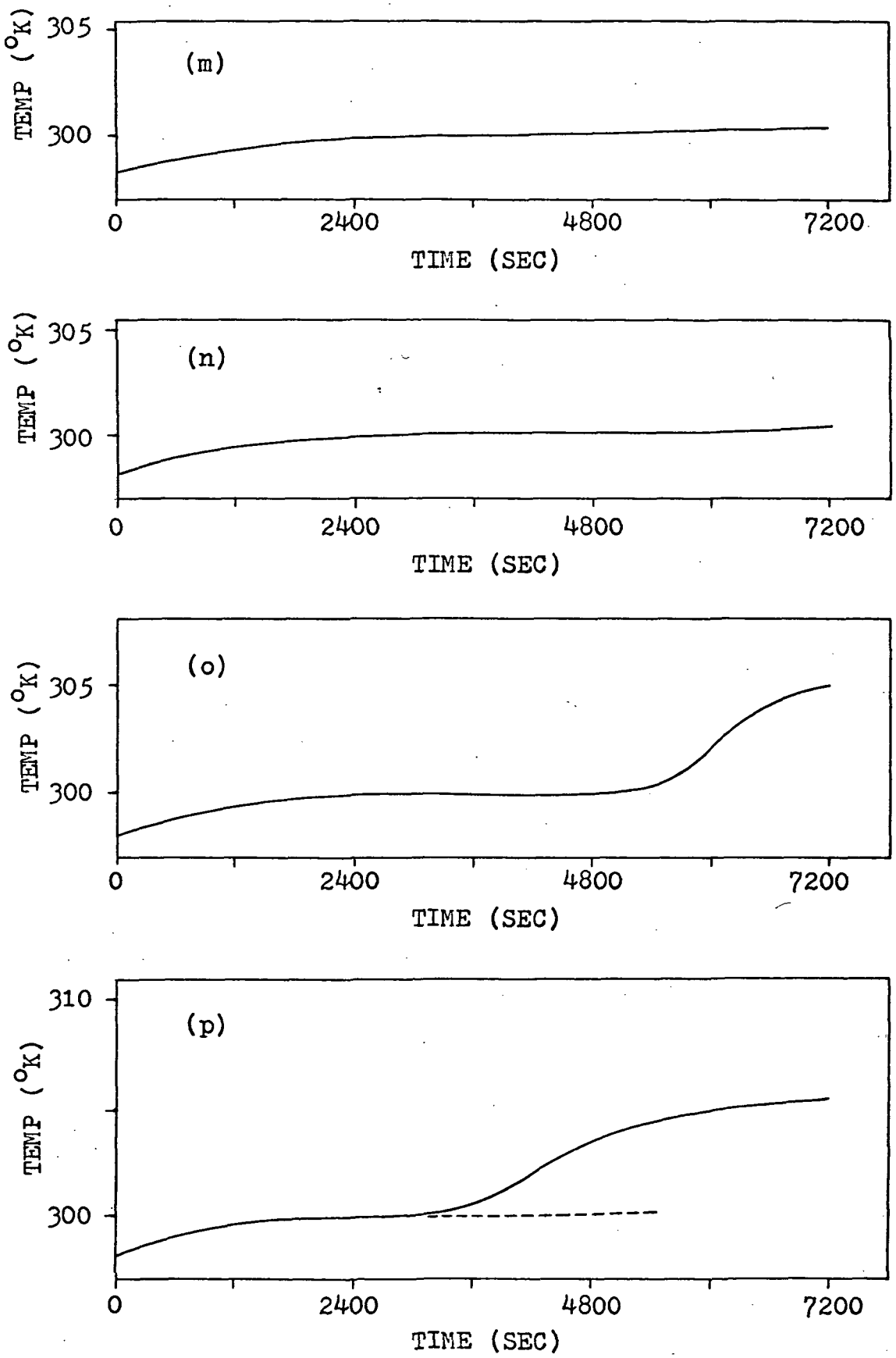

Figure 8. Comparison of Experimental Data to Theoretical Model Temperature Profiles for a Hot Wall Temperature of 319.11 ^{o}K

(a) r = 0.3175 cm, z = 1.016 cm
(b) r = 0.3175 cm, z = 2.032 cm
(c) r = 0.3175 cm, z = 3.048 cm
(d) r = 0.3175 cm, z = 4.064 cm
(e) r = 0.635 cm, z = 1.016 cm
(f) r = 0.635 cm, z = 2.032 cm
(g) r = 0.635 cm, z = 3.048 cm
(h) r = 0.635 cm, z = 4.064 cm
(i) r = 0.9525 cm, z = 1.016 cm
(j) r = 0.9525 cm, z = 2.032 cm
(k) r = 0.9525 cm, z = 3.048 cm
(l) r = 0.9525 cm, z = 4.064 cm
(m) r = 1.270 cm, z = 1.016 cm
(n) r = 1.270 cm, z = 2.032 cm
(o) r = 1.270 cm, z = 3.032 cm
(p) r = 1.270 cm, z = 4.064 cm

Legend:

⊙ = C-21-2
⊡ = C-22-2
—— = Theoretical Model

Figure 8

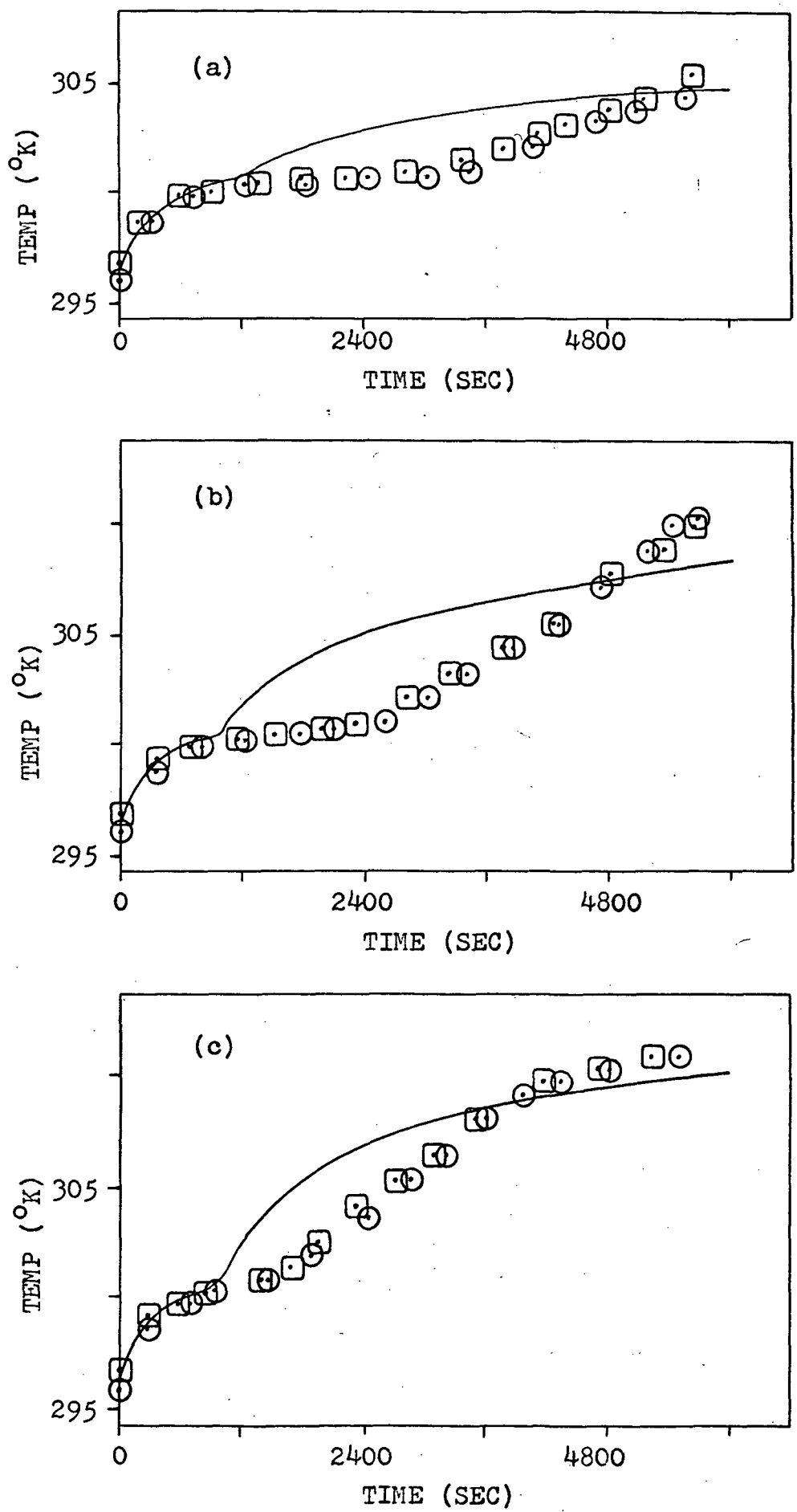
(a)
305
295
TEMP (°K)
0
2400
4800
TIME (SEC)
(b)
305
295
TEMP (°K)
0
2400
4800
TIME (SEC)
(c)
305
295
TEMP (°K)
0
2400
4800
TIME (SEC)

Figure 8 (cont)

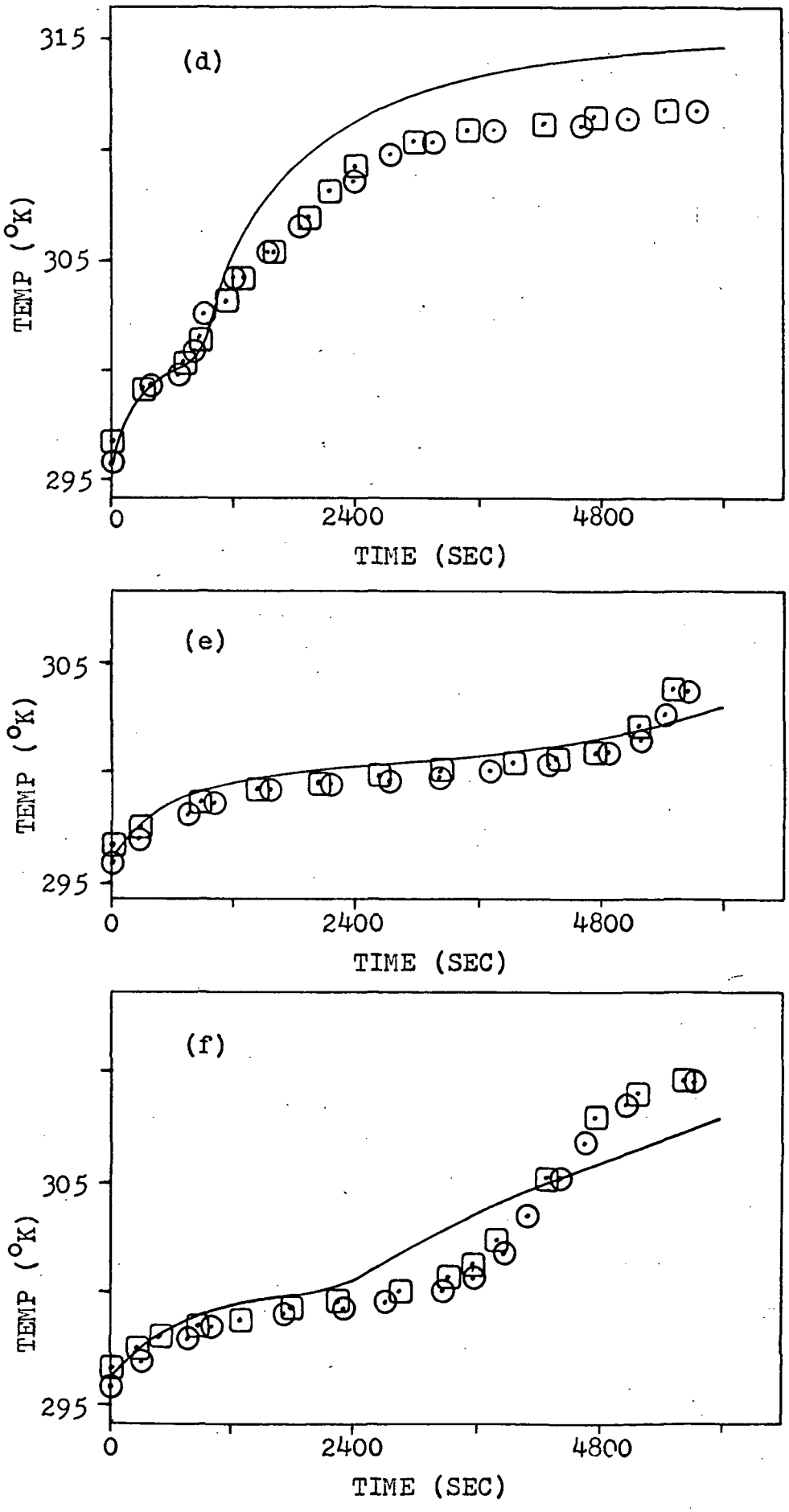

Figure 8 (cont)

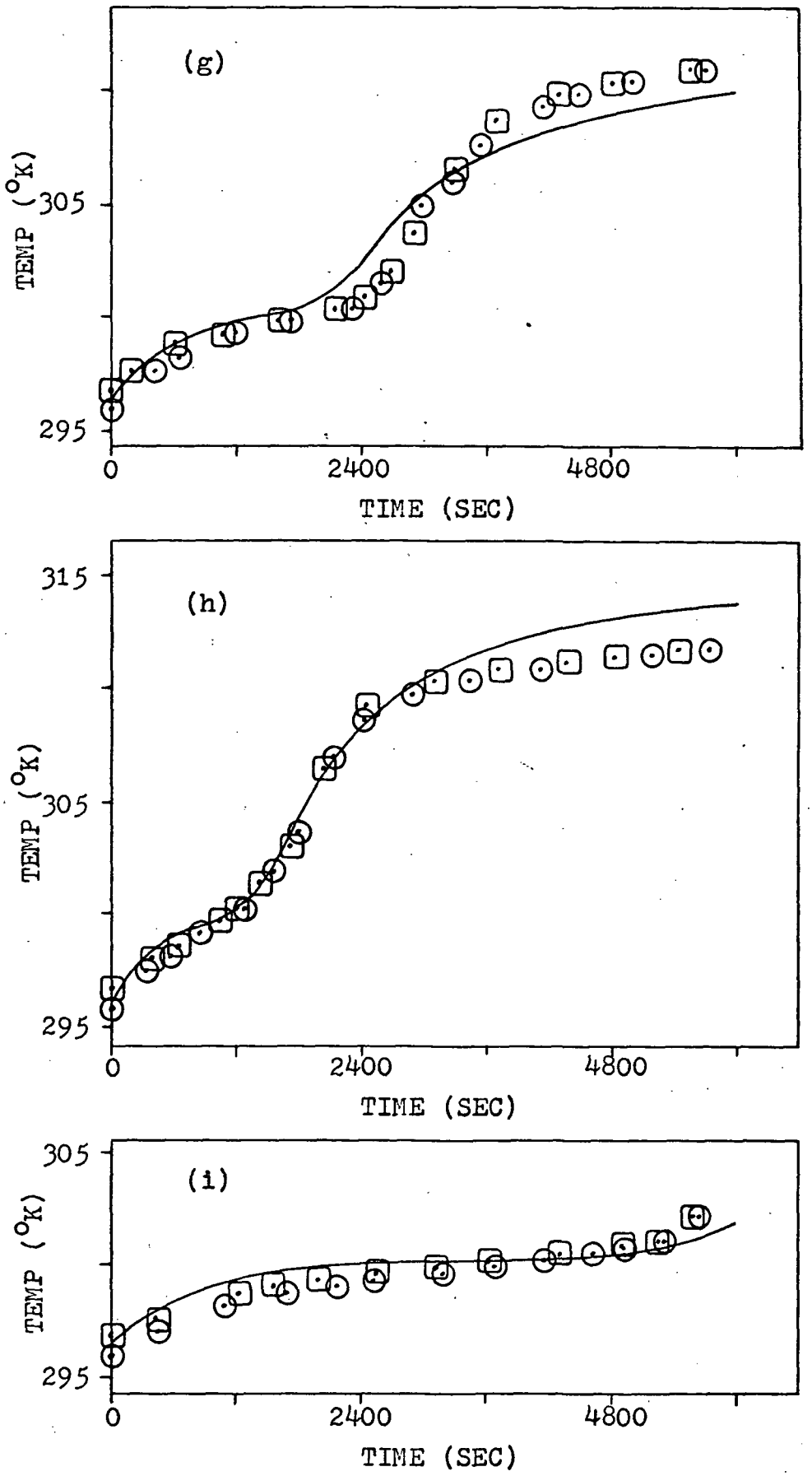

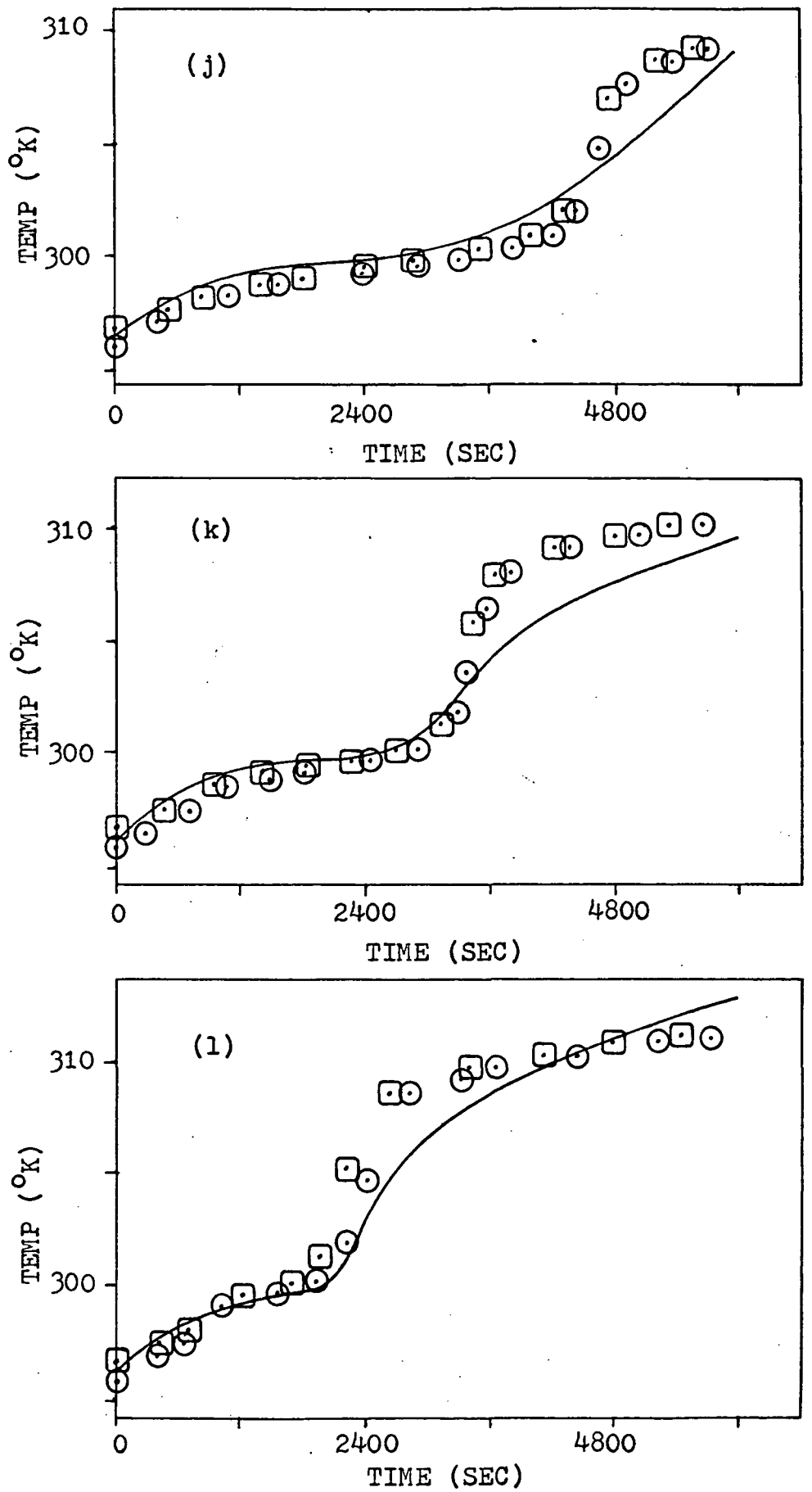
(j)
310
300
TEMP (°K)
0
2400
4800
TIME (SEC)
(k)
310
300
TEMP (°K)
0
2400
4800
TIME (SEC)
(l)
310
300
TEMP (°K)
0
2400
4800
TIME (SEC)

Figure 8 (cont)

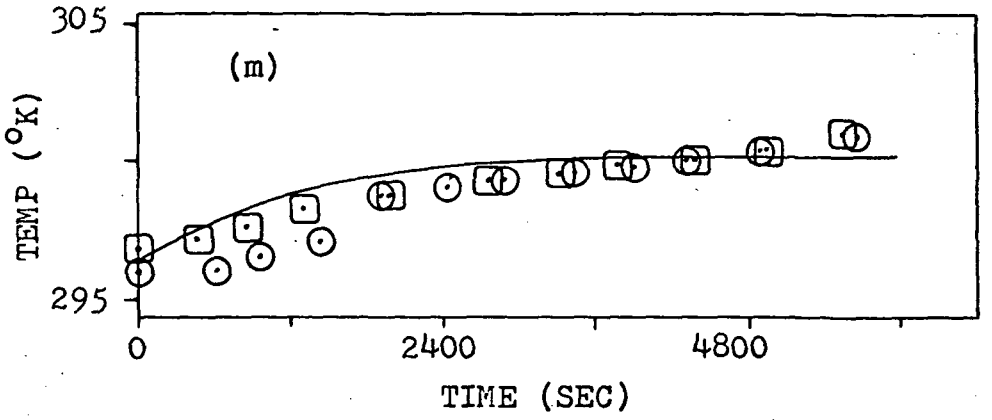

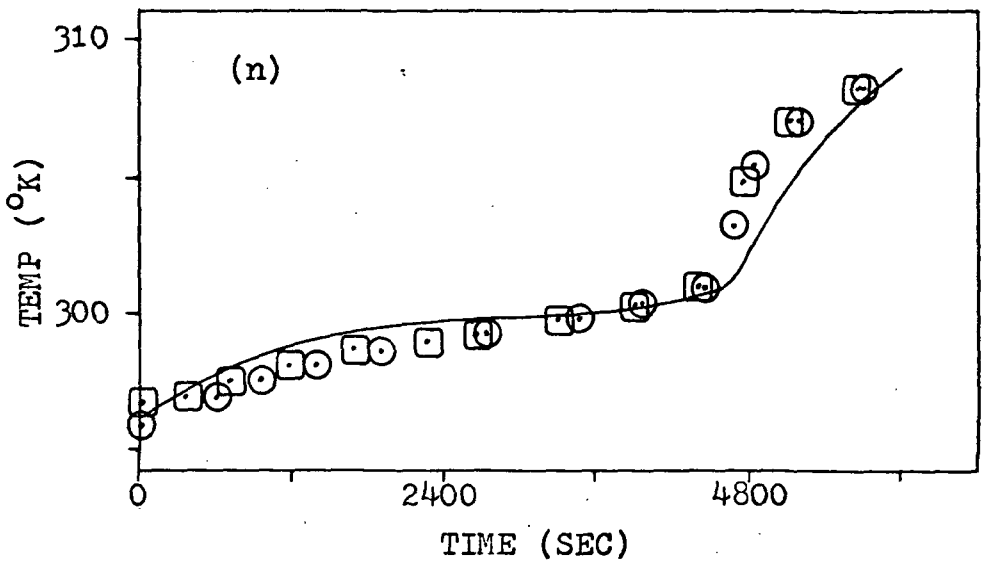

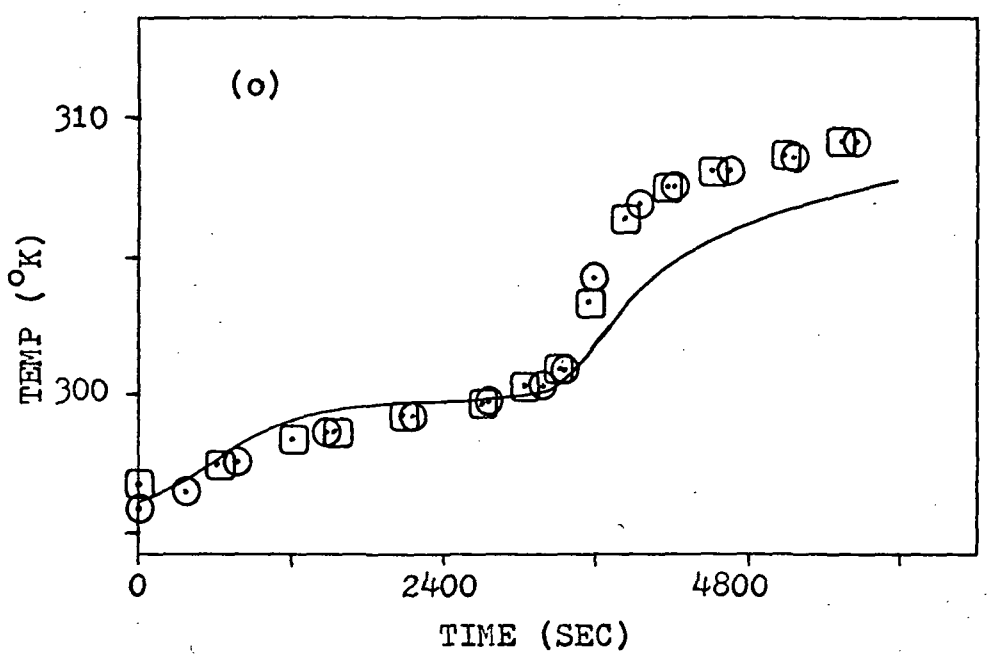

Figure 8 (cont)

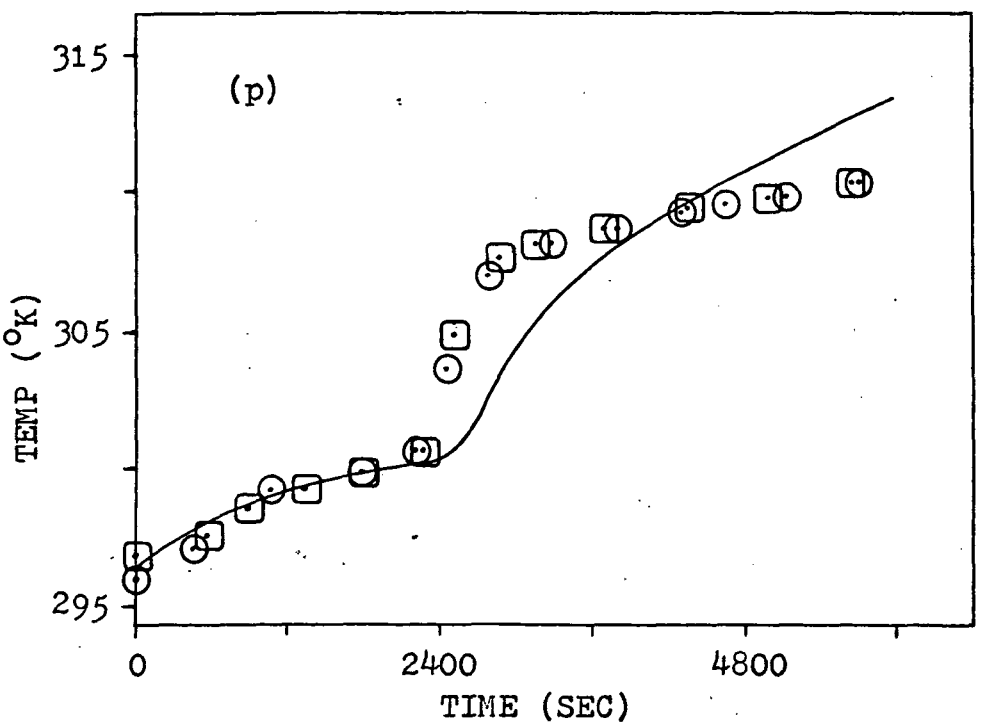

Figure 9. Effect of Numerical Dispersion Upon Theoretical Temperature Profiles for a Hot Wall Temperature of 319.11 ^{o}K

(a) r = 0.3175 cm, z = 1.016 cm
(b) r = 0.3175 cm, z = 2.032 cm
(c) r = 0.3175 cm, z = 3.048 cm
(d) r = 0.3175 cm, z = 4.064 cm
(e) r = 0.635 cm, z = 1.016 cm
(f) r = 0.635 cm, z = 2.032 cm
(g) r = 0.635 cm, z = 3.048 cm
(h) r = 0.635 cm, z = 4.064 cm
(i) r = 0.9525 cm, z = 1.016 cm
(j) r = 0.9525 cm, z = 2.032 cm
(k) r = 0.9525 cm, z = 3.048 cm
(l) r = 0.9525 cm, z = 4.064 cm
(m) r = 1.270 cm, z = 1.016 cm
(n) r = 1.270 cm, z = 2.032 cm
(o) r = 1.270 cm, z = 3.048 cm
(p) r = 1.270 cm, z = 4.064 cm

Legend:

——= 1.5 sec for time increment
----= 3.0 sec for time increment
—·— = 6.0 sec for time increment

Figure 9

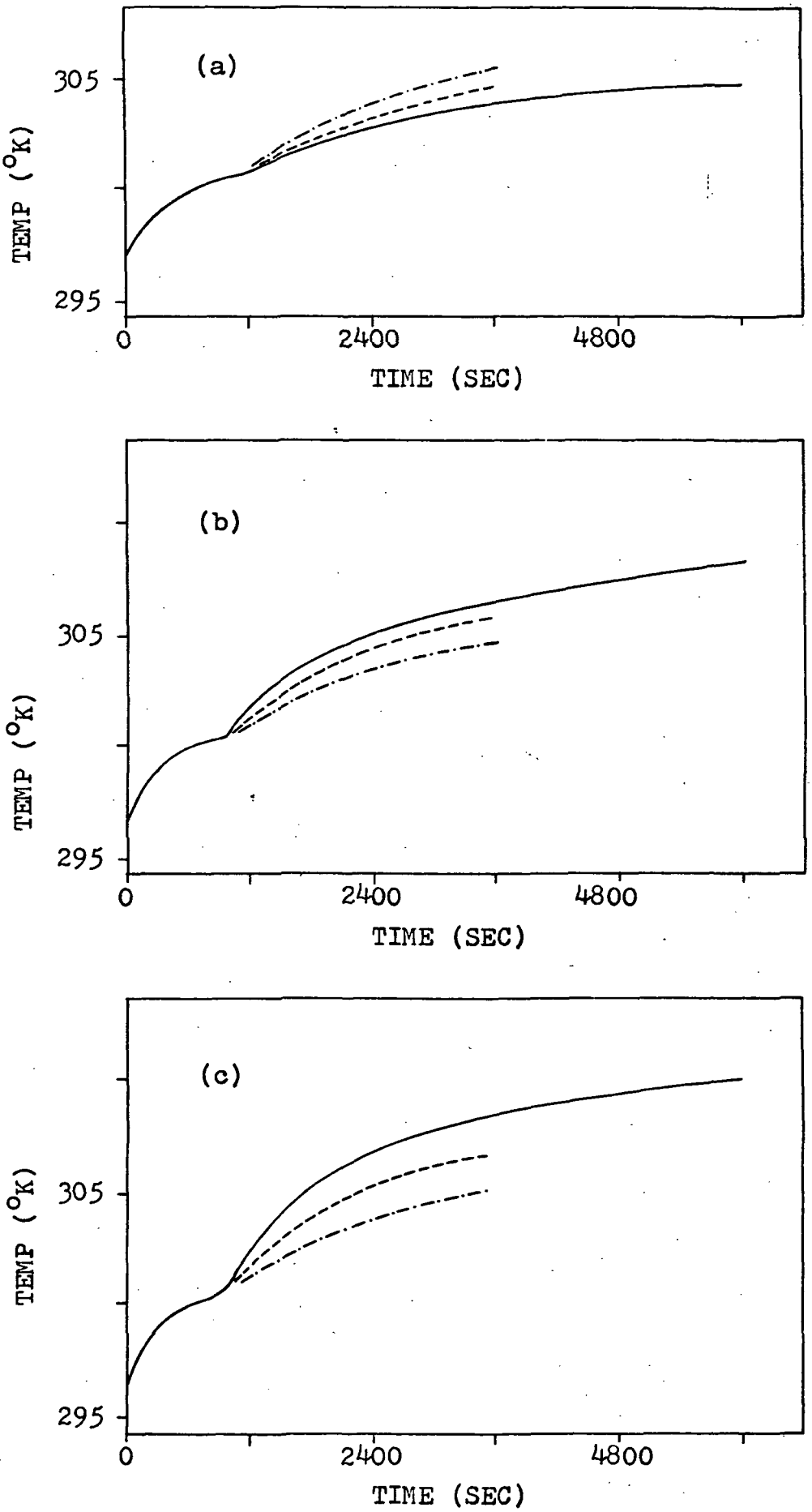
(a)
305
295
TEMP (°K)
0
2400
4800
TIME (SEC)
(b)
305
295
TEMP (°K)
0
2400
4800
TIME (SEC)
(c)
305
295
TEMP (°K)
0
2400
4800
TIME (SEC)

Figure 9 (cont)

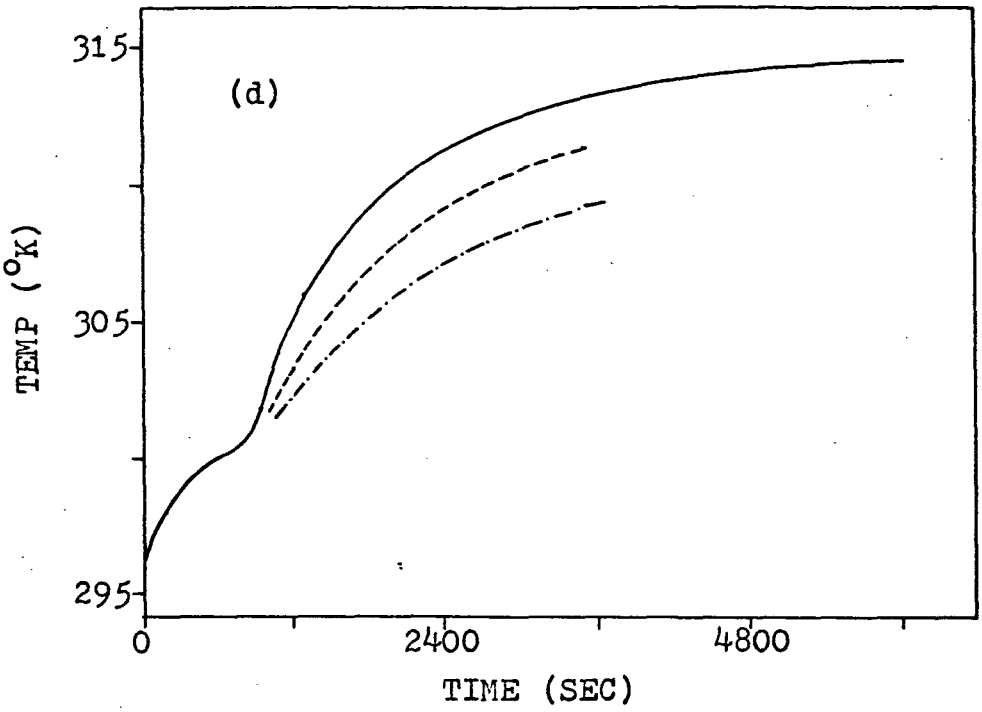

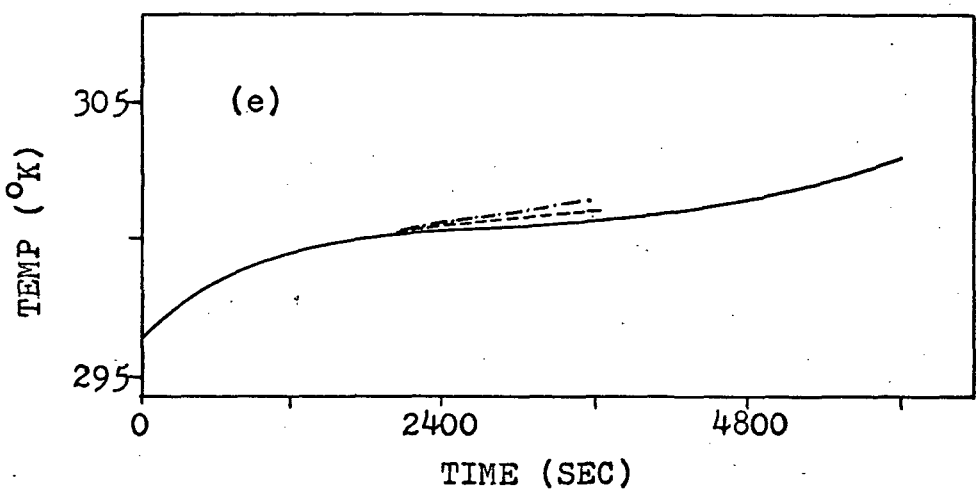

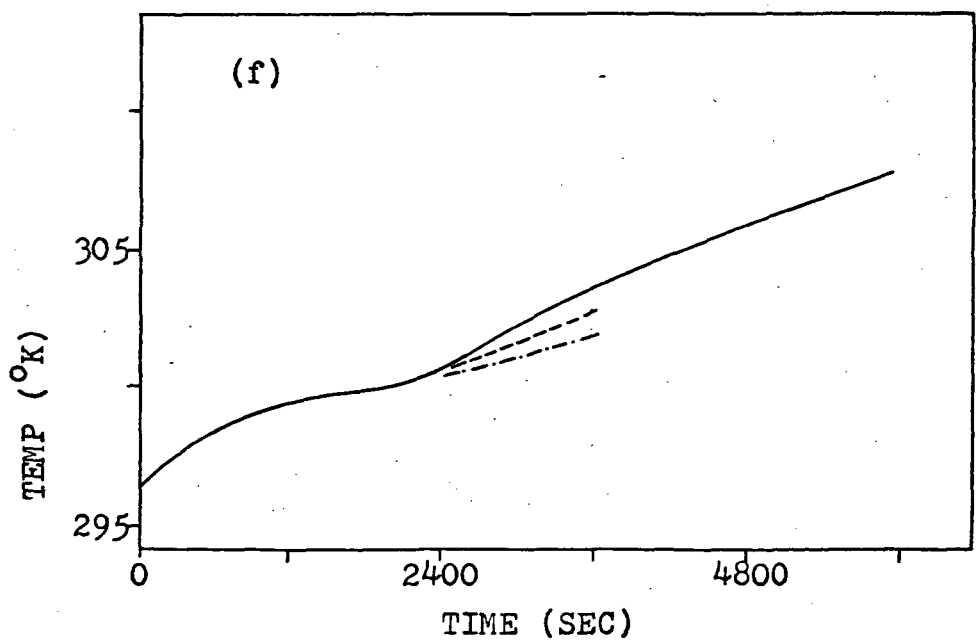

Figure 9 (cont)

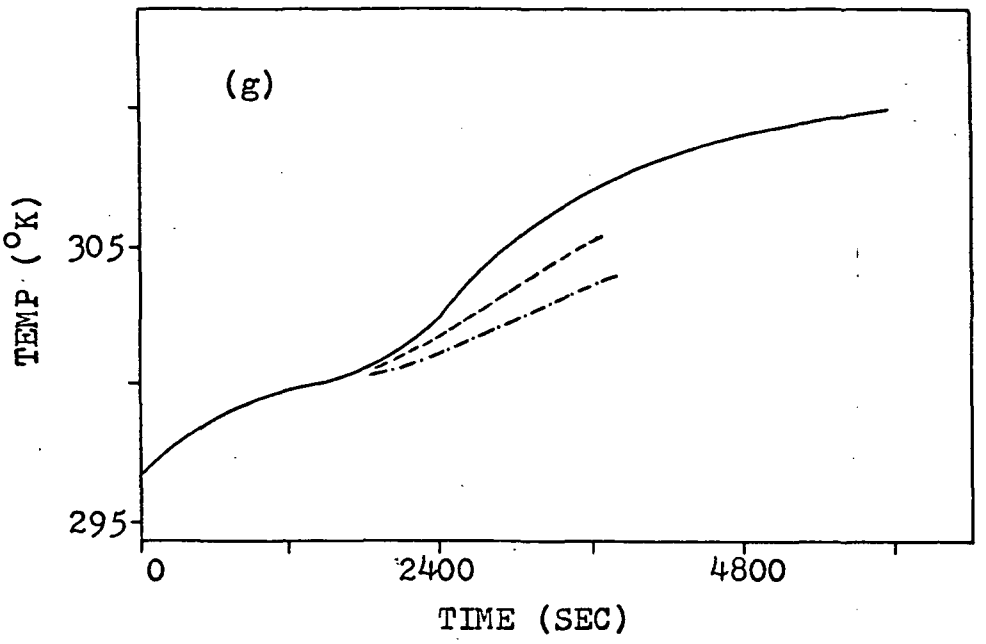

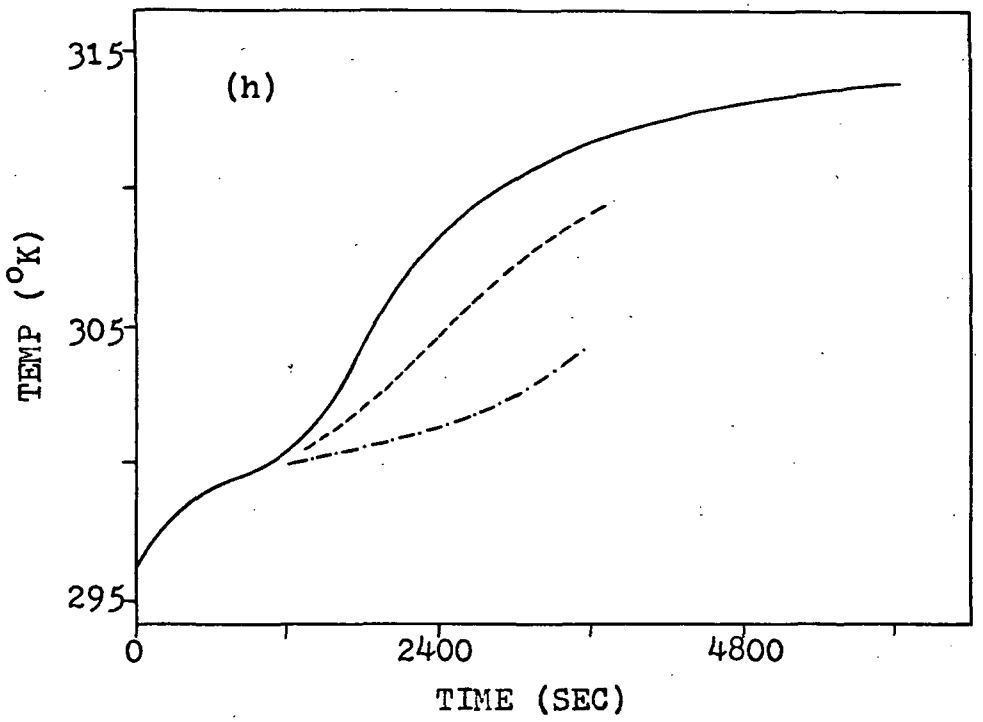

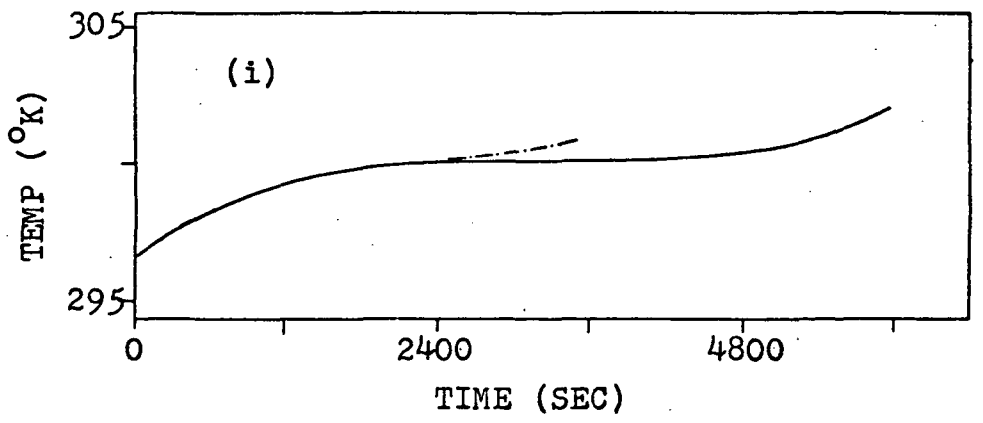

Figure 9 (cont)

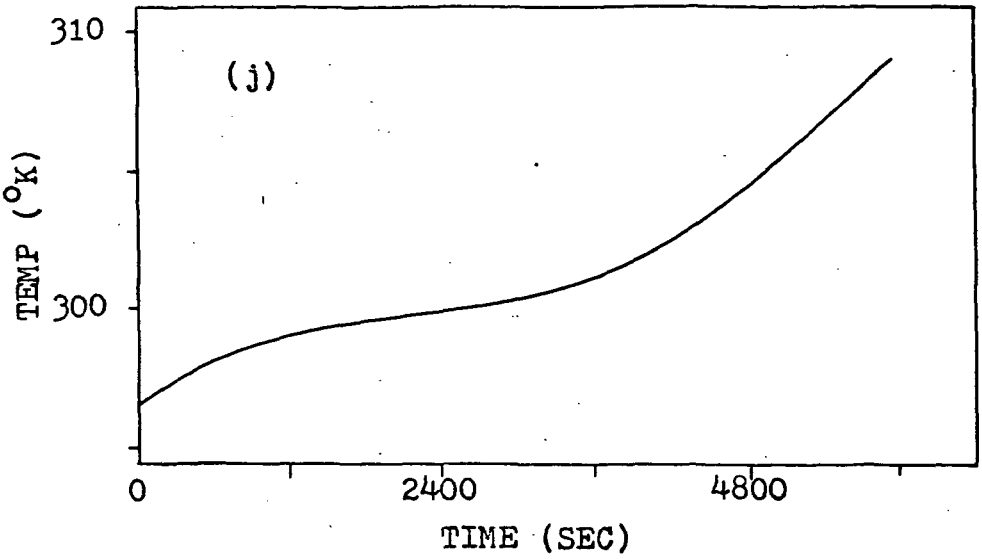

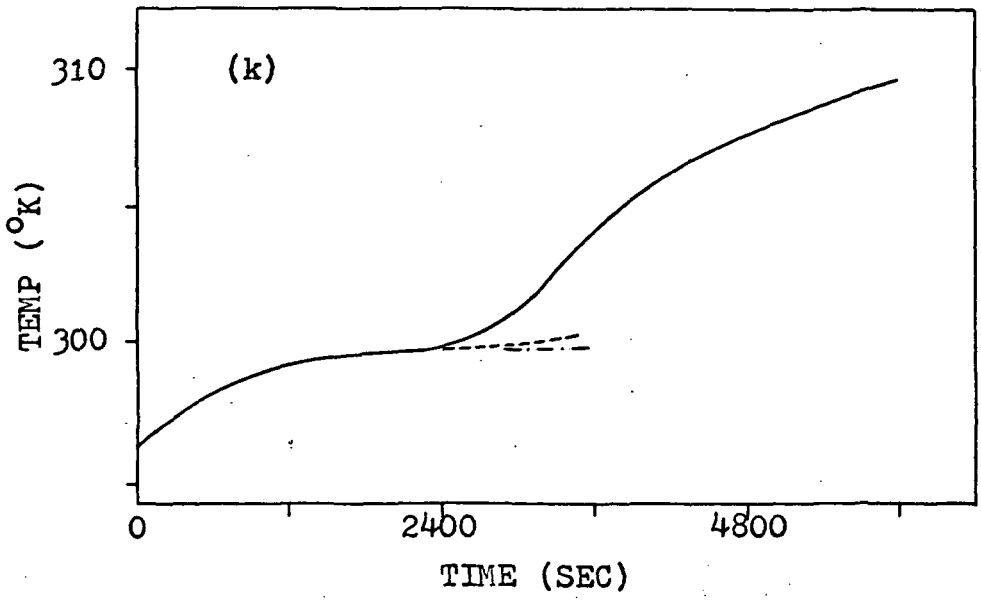

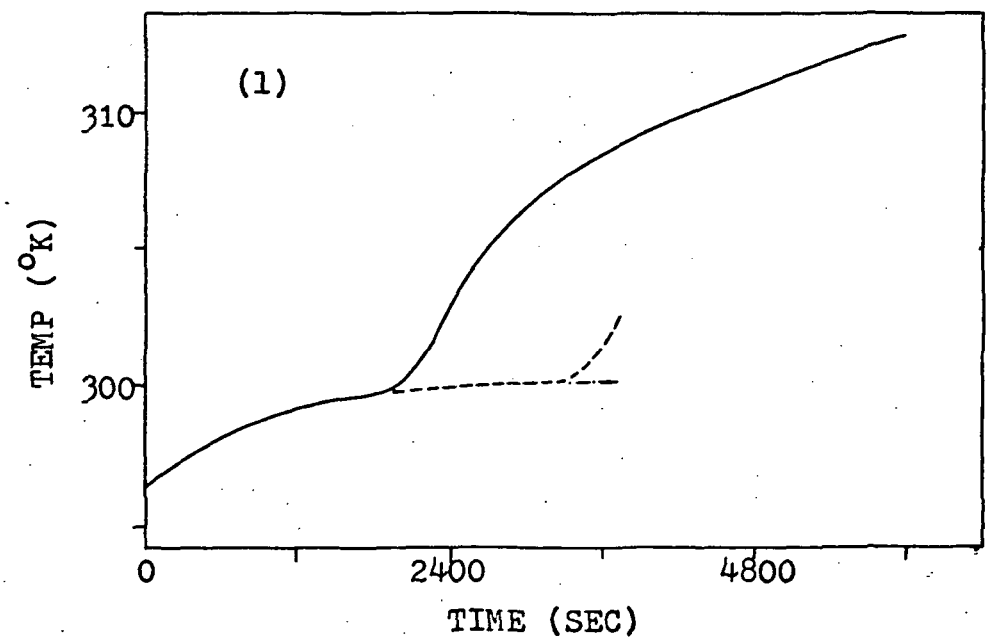

Figure 9 (cont)

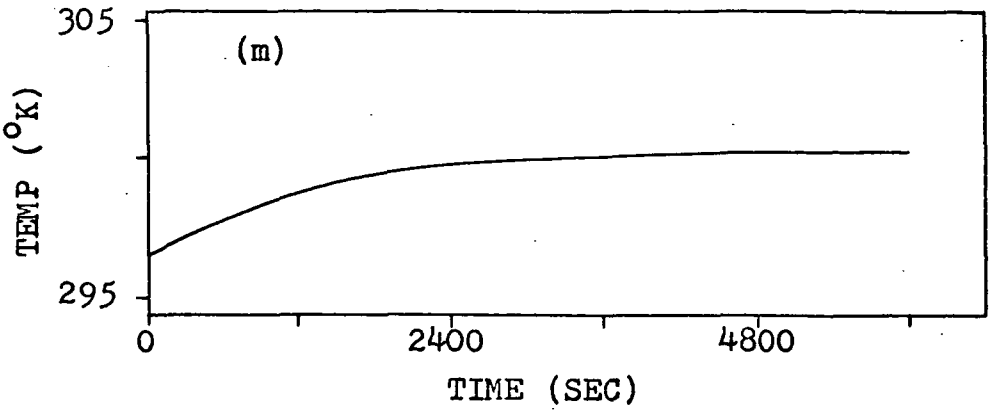

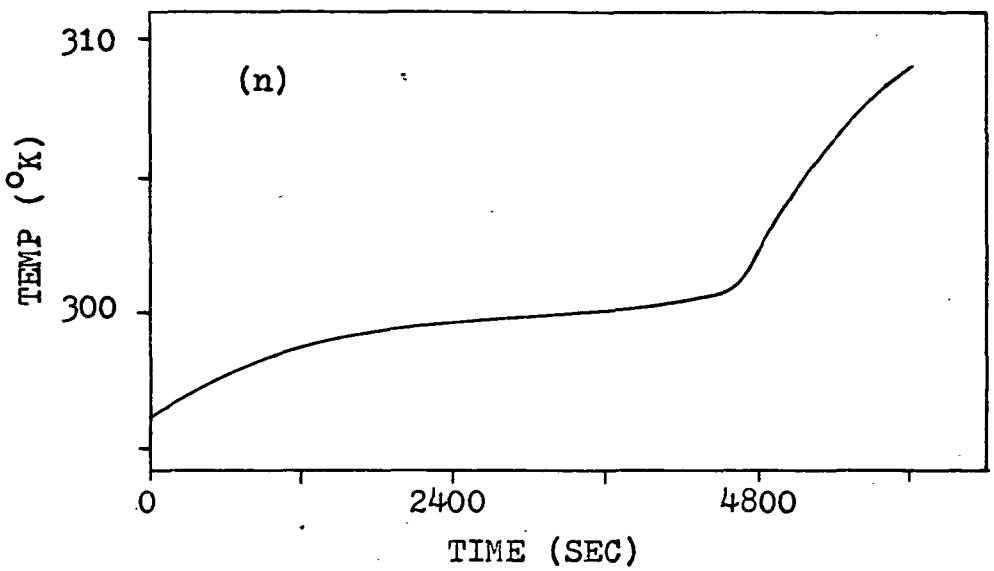

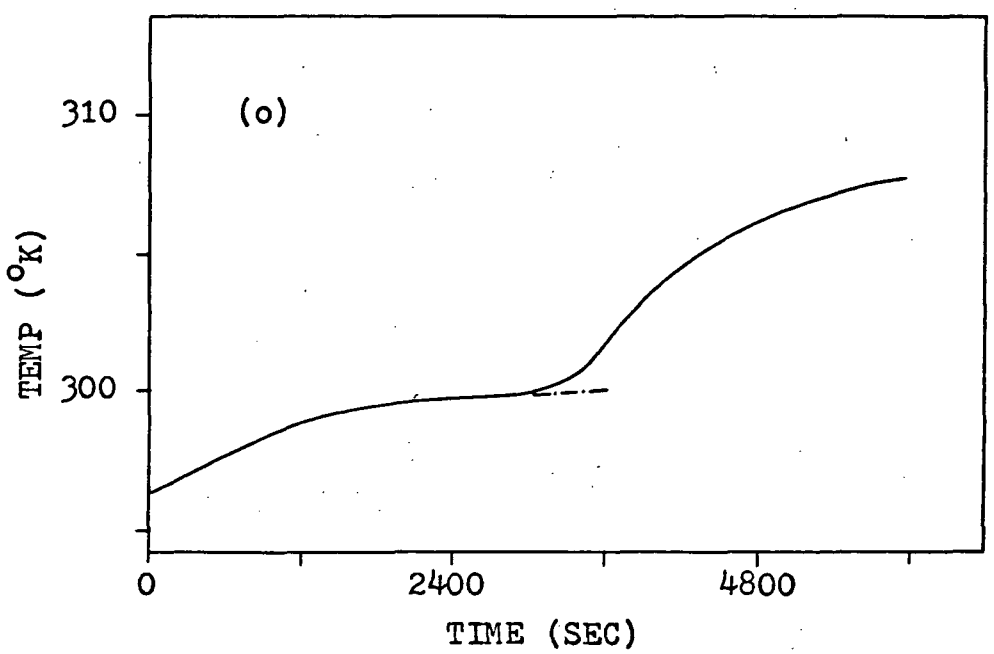

Figure 9 (cont)

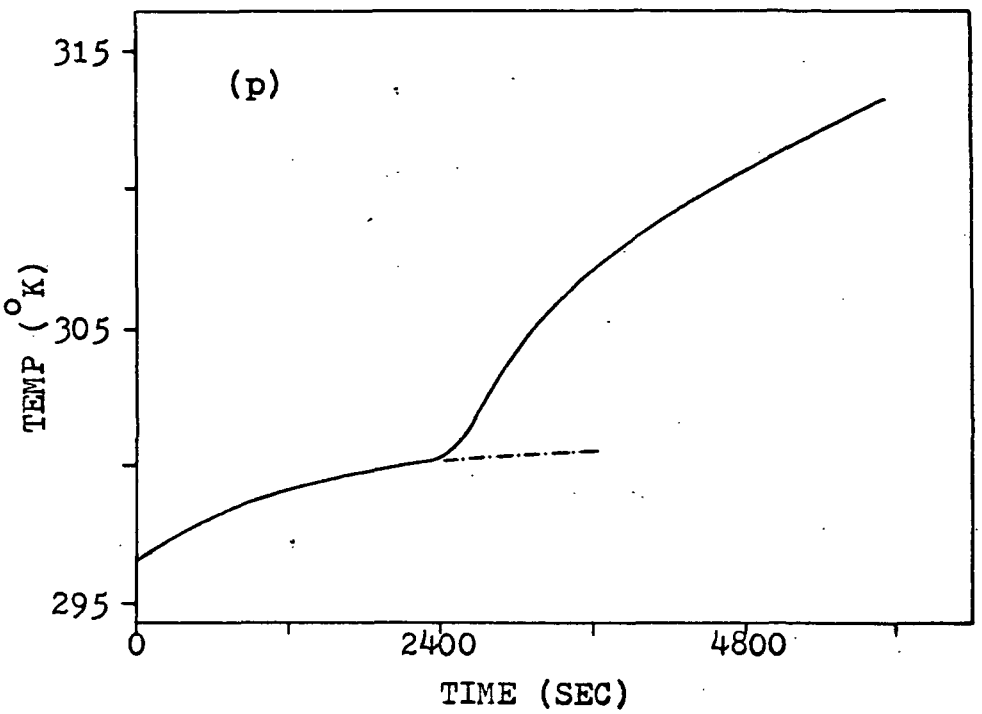

Figure 10. Comparison of Experimental Data to Theoretical Model Temperature Profiles for a Hot Wall Temperature of 321.33 ^{o}K

(a) r = 0.3175 cm, z = 1.016 cm
(b) r = 0.3175 cm, z = 2.032 cm
(c) r = 0.3175 cm, z = 3.048 cm
(d) r = 0.3175 cm, z = 4.064 cm
(e) r = 0.635 cm, z = 1.016 cm
(f) r = 0.635 cm, z = 2.032 cm
(g) r = 0.635 cm, z = 3.048 cm
(h) r = 0.635 cm, z = 4.064 cm
(i) r = 0.9525 cm, z = 1.016 cm
(j) r = 0.9525 cm, z = 2.032 cm
(k) r = 0.9525 cm, z = 3.048 cm
(l) r = 0.9525 cm, z = 4.064 cm
(m) r = 1.270 cm, z = 1.016 cm
(n) r = 1.270 cm, z = 2.032 cm
(o) r = 1.270 cm, z = 3.048 cm
(p) r = 1.270 cm, z = 4.064 cm

Legend:

⊙ = C-11-2
⊡ = C-12-2
—— = Theoretical Model

Figure 10

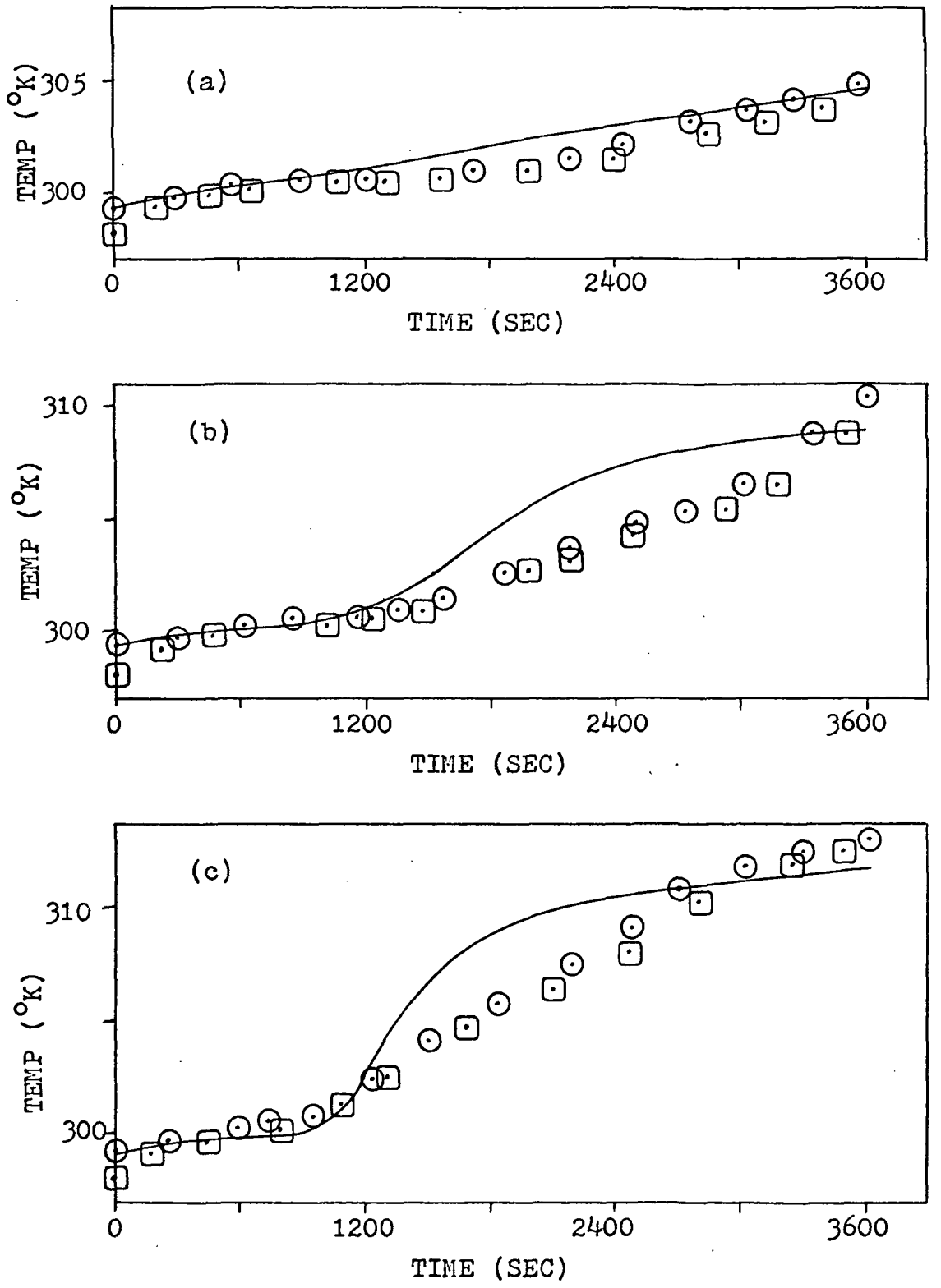
(a)
TEMP (°K)
305
300
0
1200
2400
3600
TIME (SEC)
(b)
TEMP (°K)
310
300
0
1200
2400
3600
TIME (SEC)
(c)
TEMP (°K)
310
300
0
1200
2400
3600
TIME (SEC)

Figure 10 (cont)

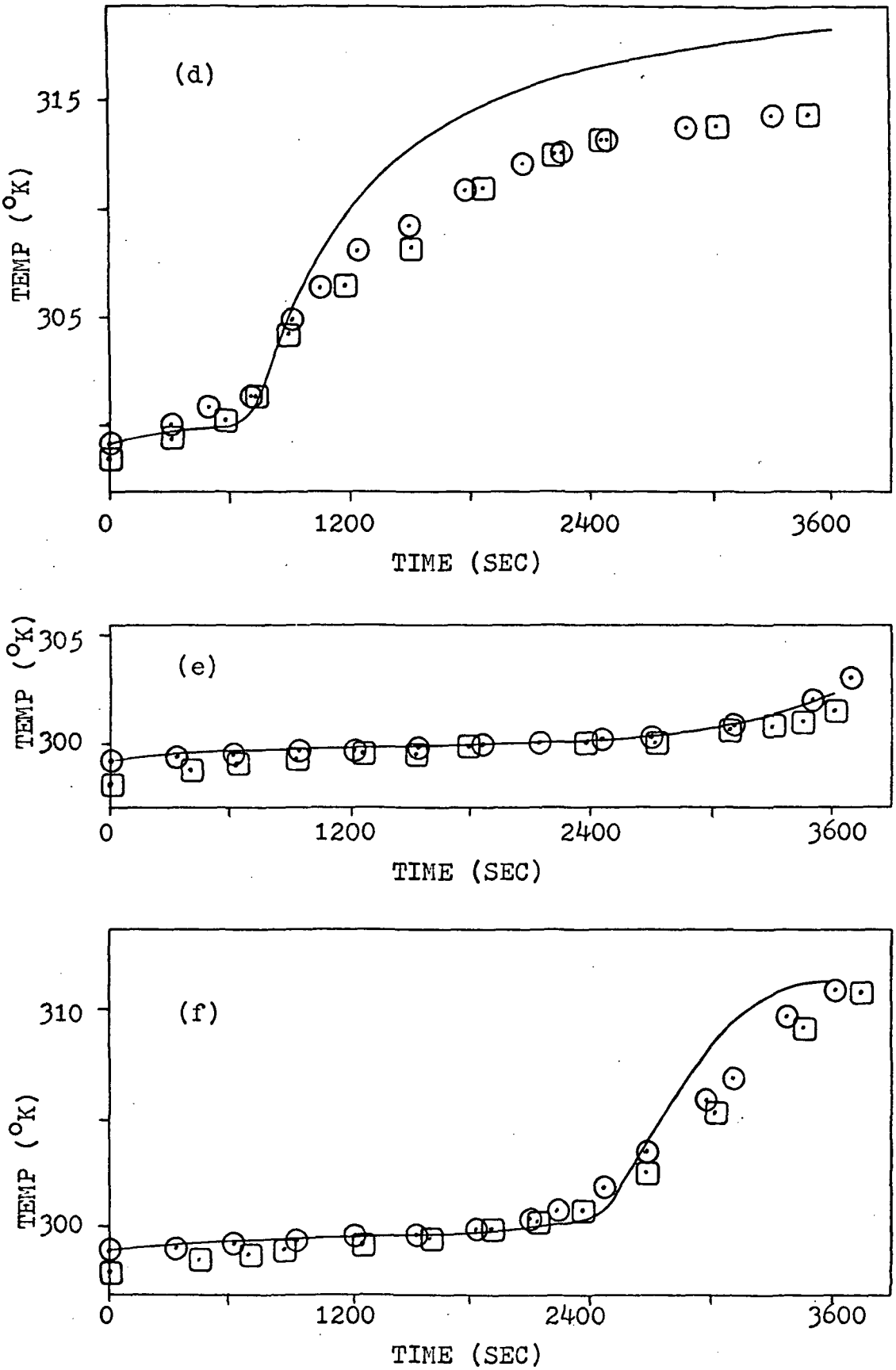

Figure 10 (cont)

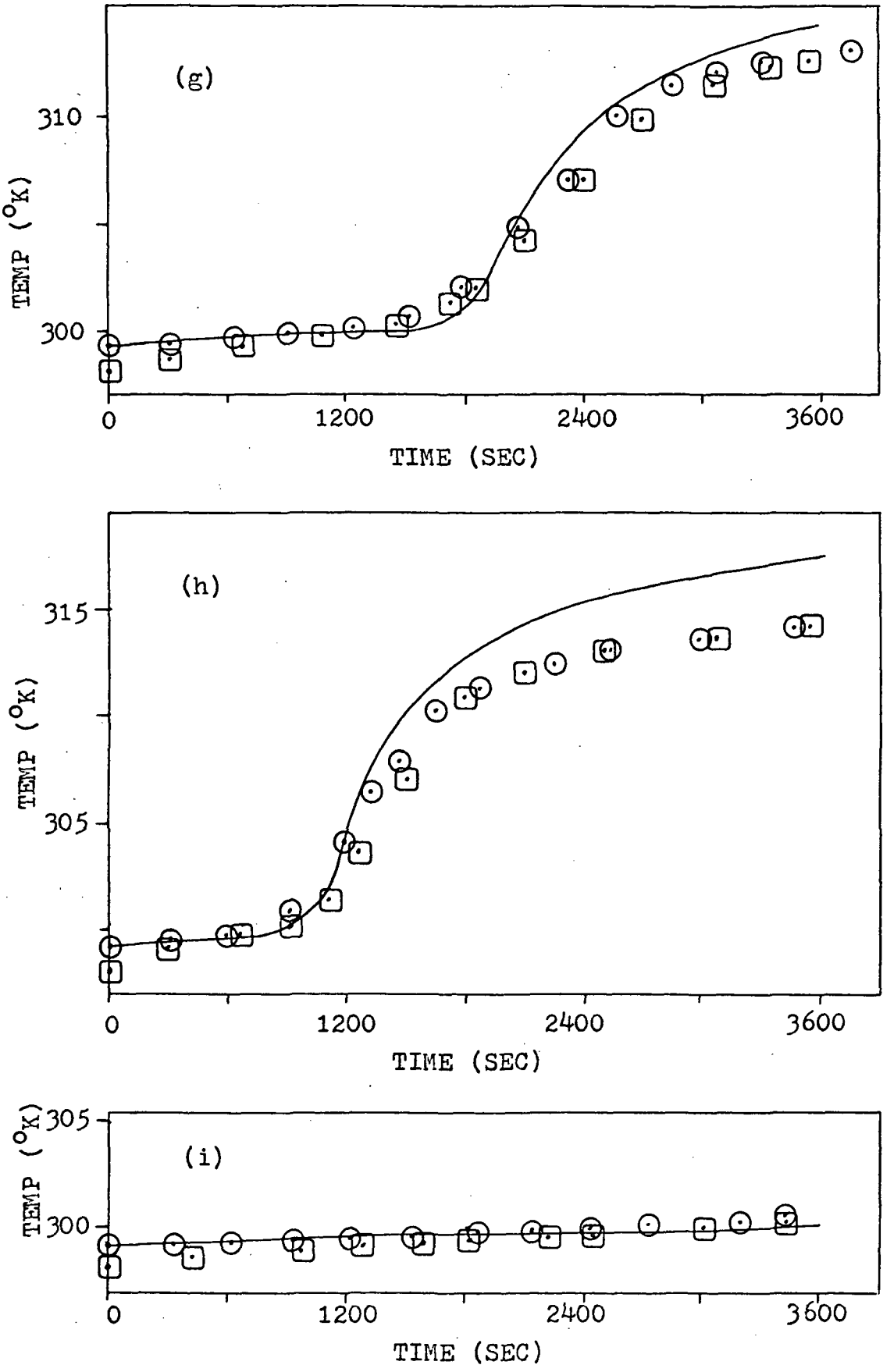

Figure 10 (cont)

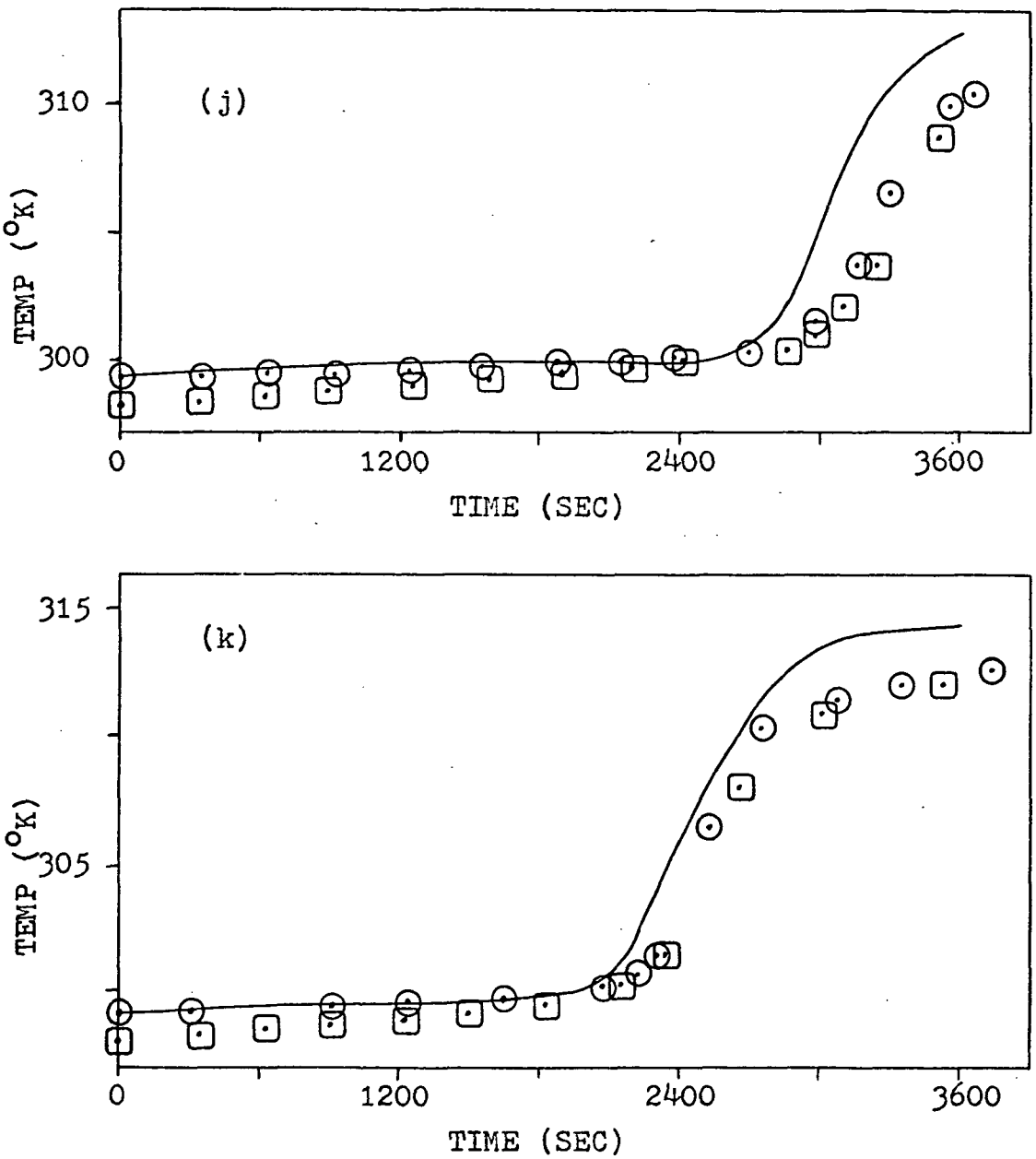

Figure 10 (cont)

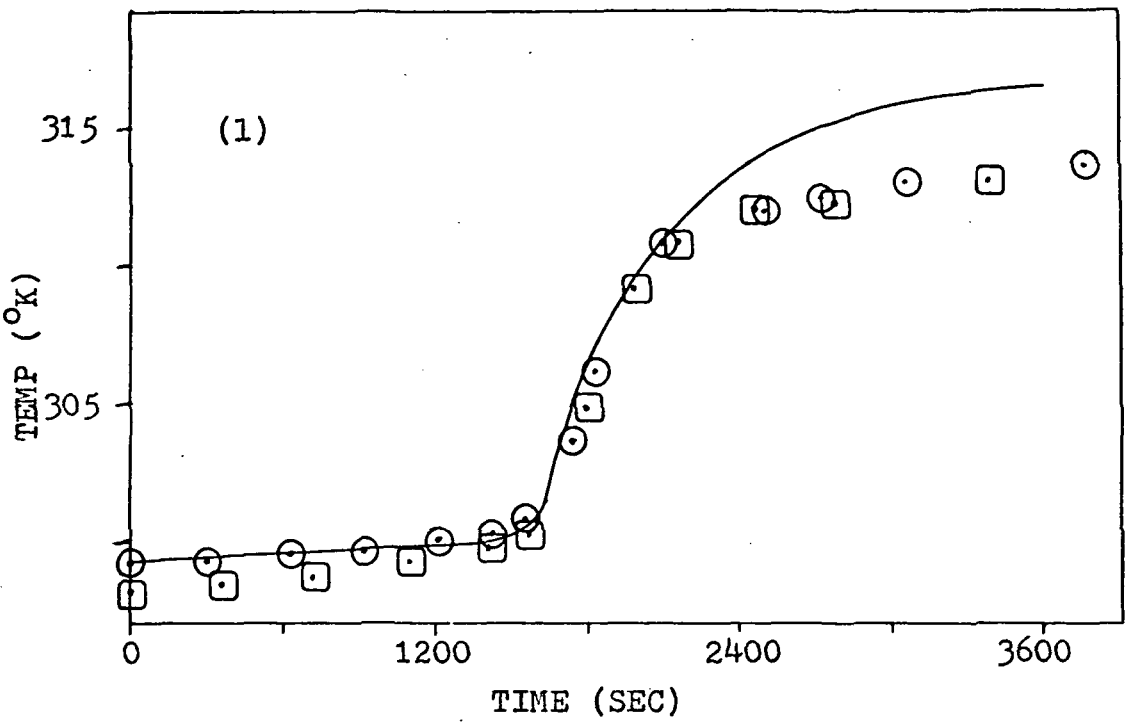

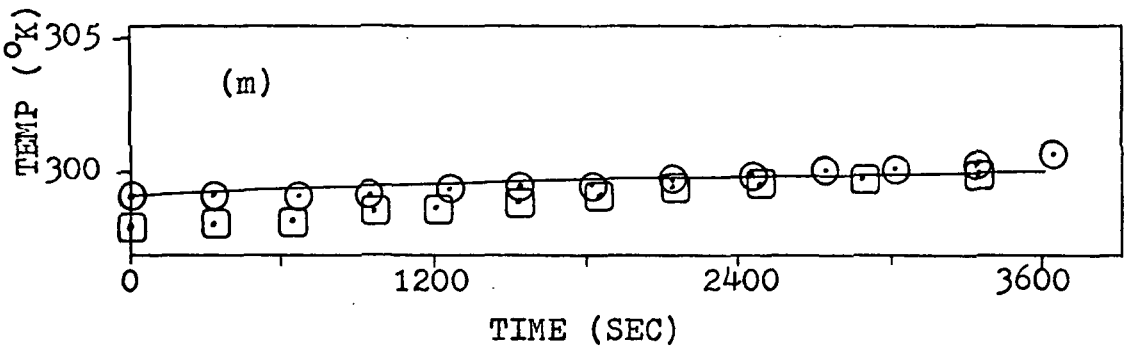

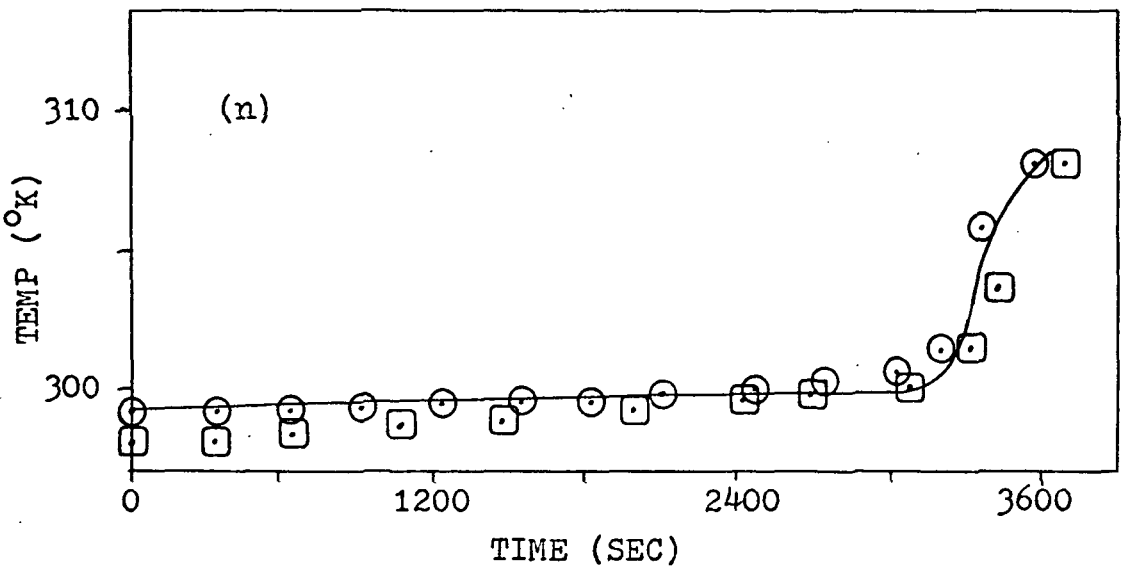

Figure 10 (cont)

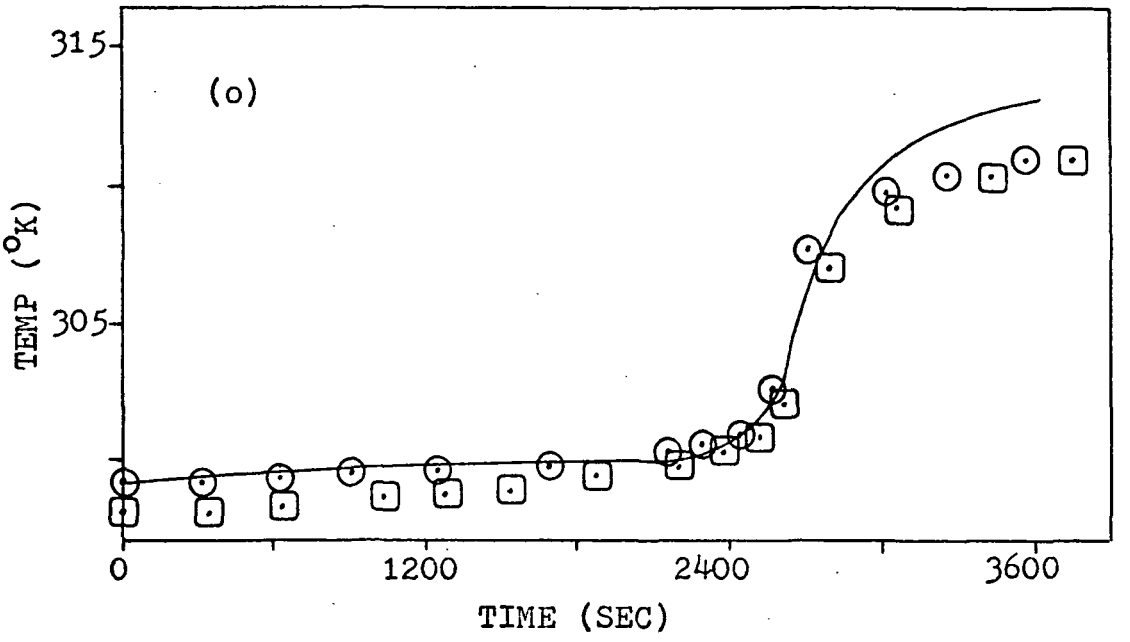

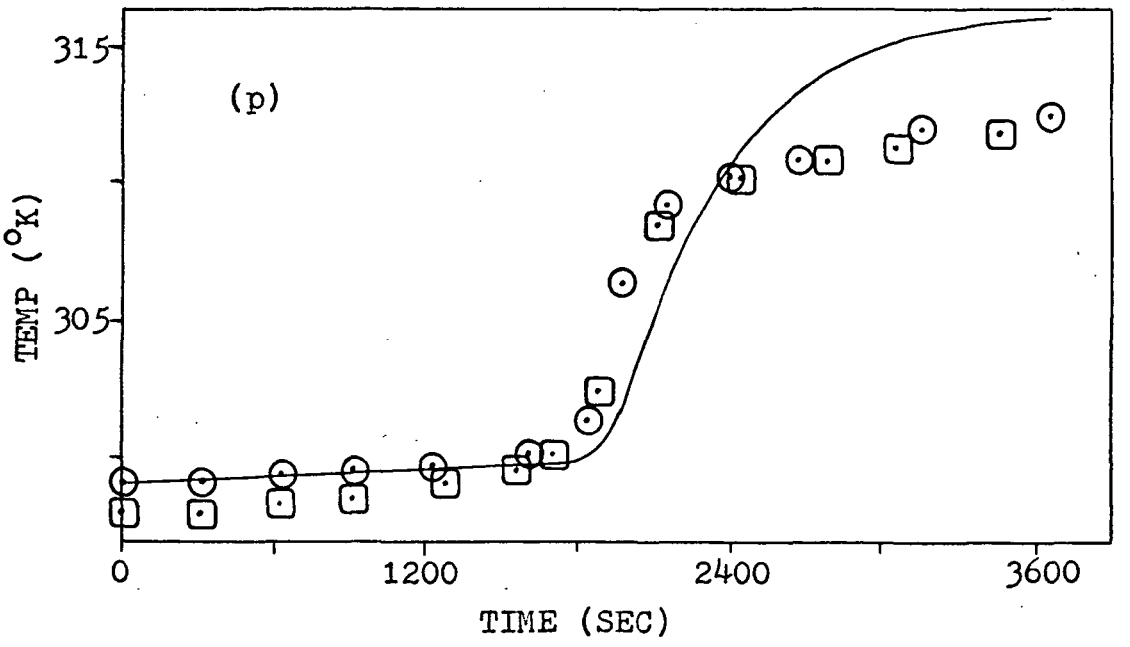

Figure 11. Comparison of Experimental Data to Theoretical Model Temperature Profiles for a Hot Wall Temperature of 327.44 ^{o}K

(a) r = 0.3175 cm, z = 1.016 cm
(b) r = 0.3175 cm, z = 2.032 cm
(c) r = 0.3175 cm, z = 3.048 cm
(d) r = 0.3175 cm, z = 4.064 cm
(e) r = 0.6350 cm, z = 1.016 cm
(f) r = 0.6350 cm, z = 2.032 cm
(g) r = 0.6350 cm, z = 3.048 cm
(h) r = 0.6350 cm, z = 4.064 cm
(i) r = 0.9525 cm, z = 1.016 cm
(j) r = 0.9525 cm, z = 3.048 cm
(k) r = 0.9525 cm, z = 3.048 cm
(l) r = 0.9525 cm, z = 4.064 cm
(m) r = 1.270 cm, z = 1.016 cm
(n) r = 1.270 cm, z = 2.032 cm
(o) r = 1.270 cm, z = 3.048 cm
(p) r = 1.270 cm, z = 4.064 cm

Legend:

⊙ = C-11-2
⊡ = C-12-2
— = Theoretical Model

Figure 11

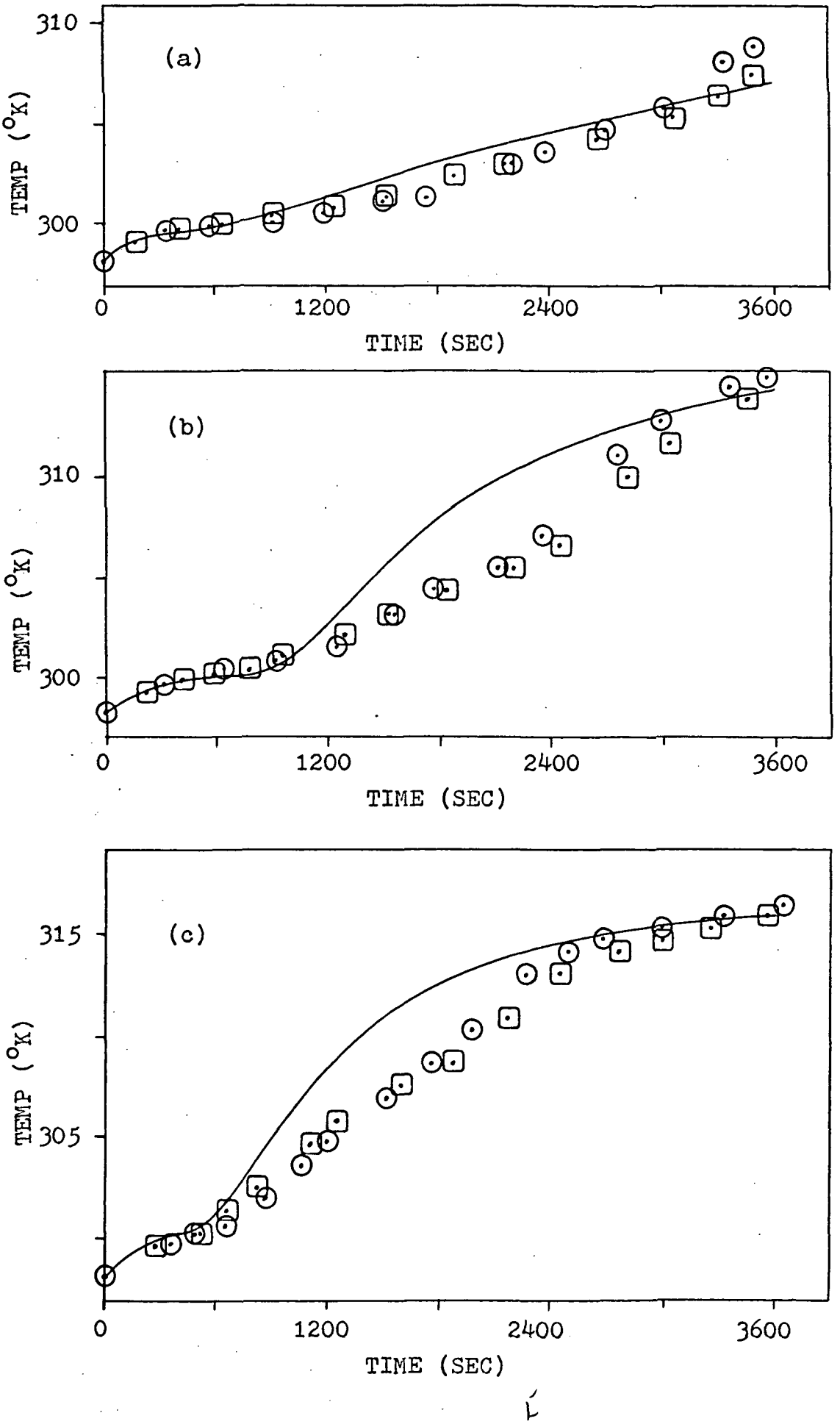
(a)
310
300
TEMP (°K)
0
1200
2400
3600
TIME (SEC)
(b)
310
300
TEMP (°K)
0
1200
2400
3600
TIME (SEC)
(c)
315
305
TEMP (°K)
0
1200
2400
3600
TIME (SEC)

Figure 11 (cont)

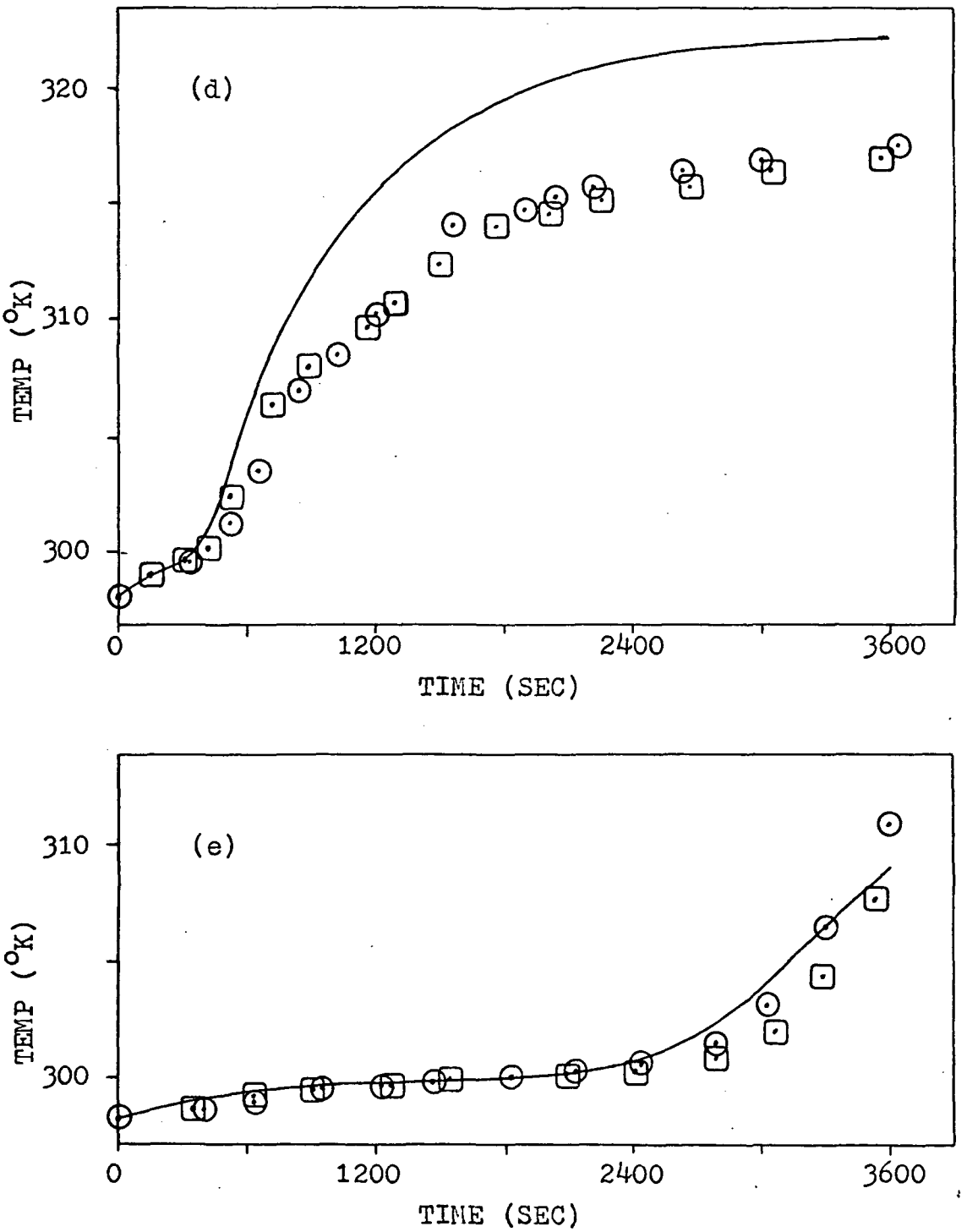

Figure 11 (cont)

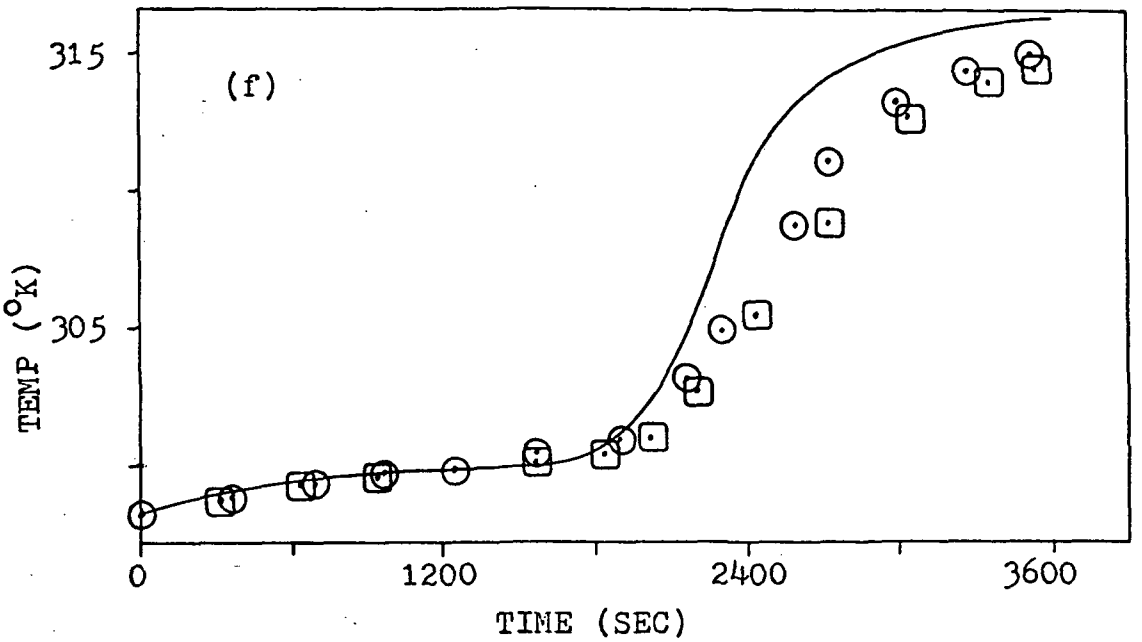

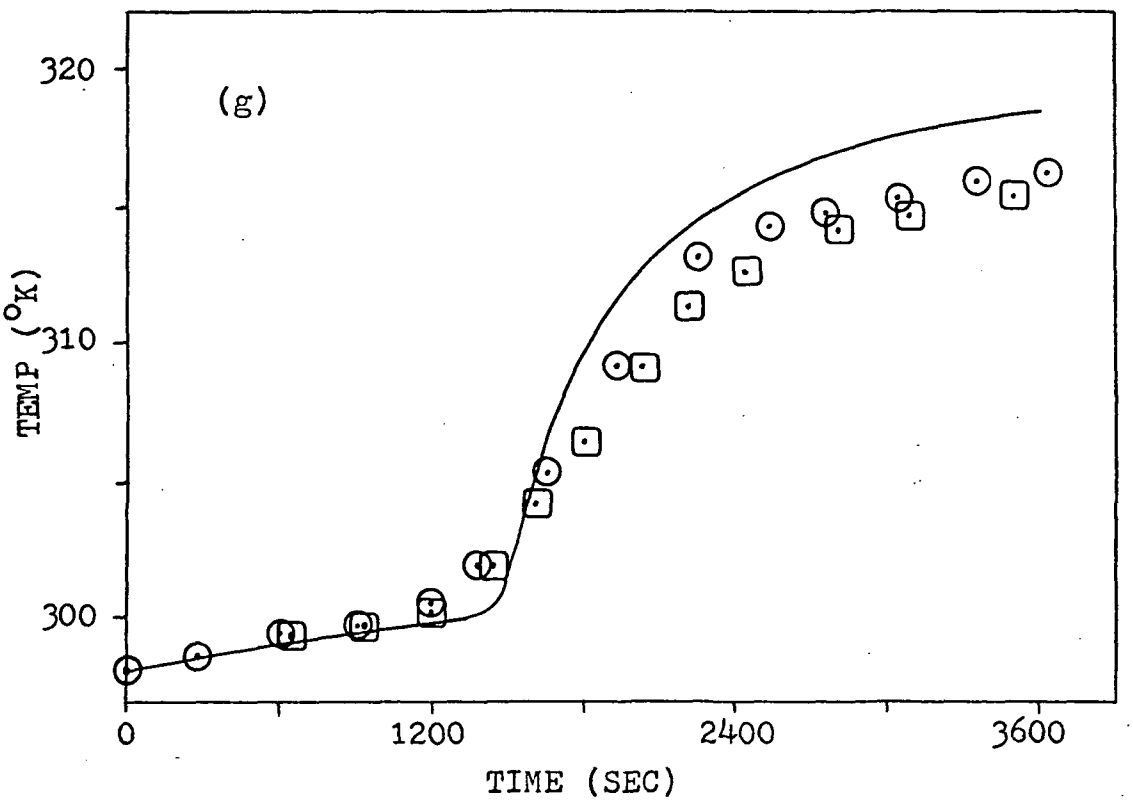

Figure 11 (cont)

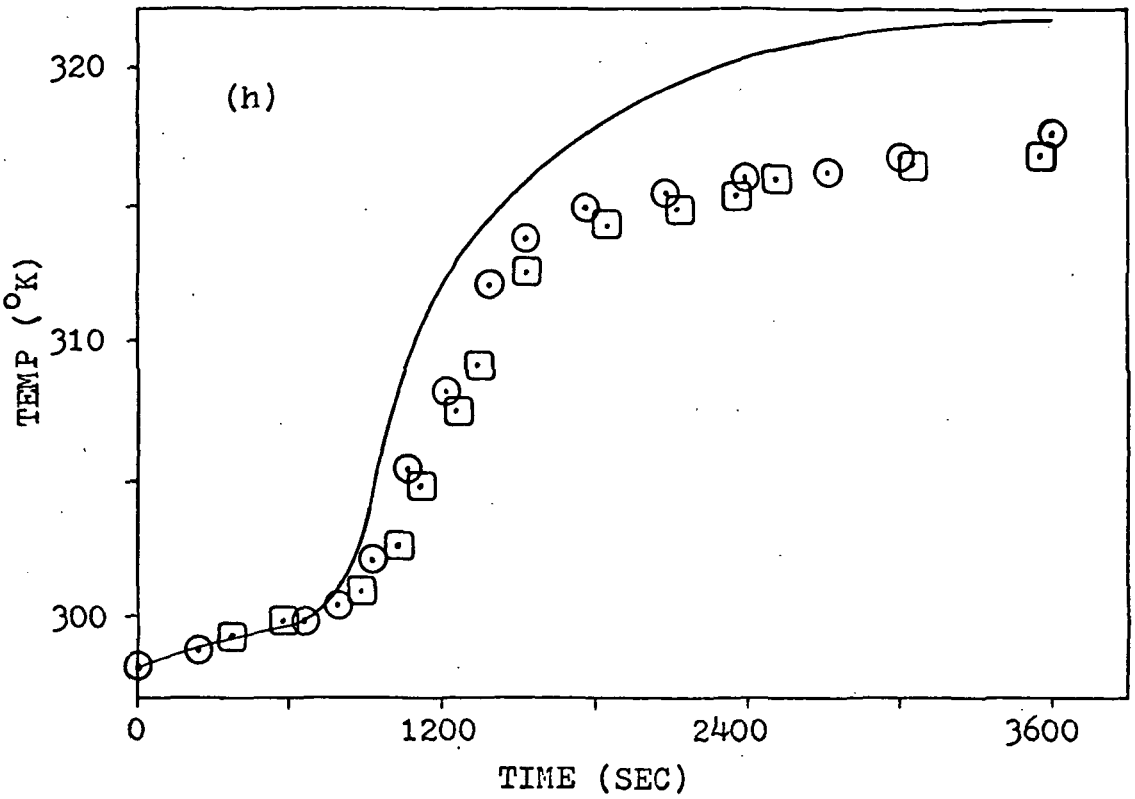

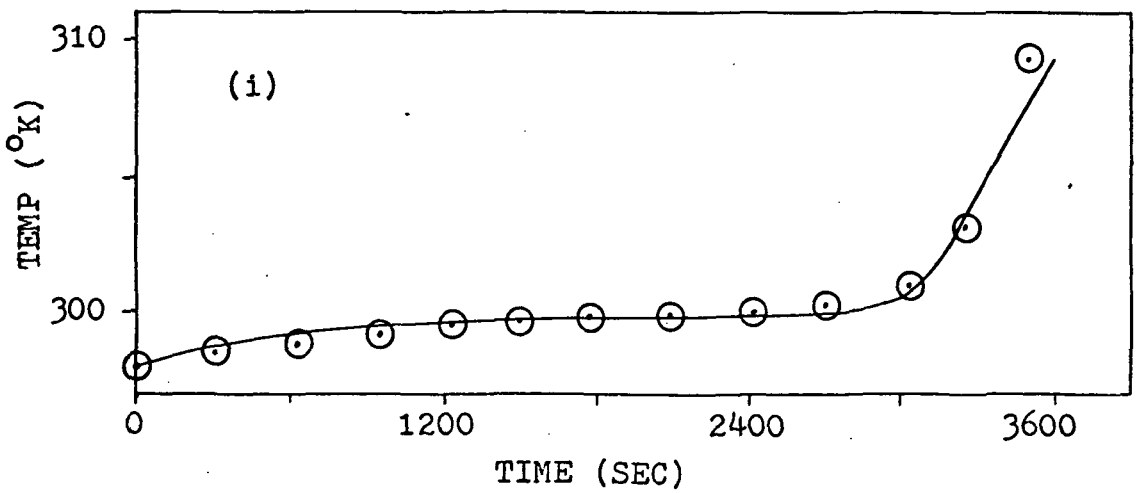

Figure 11 (cont)

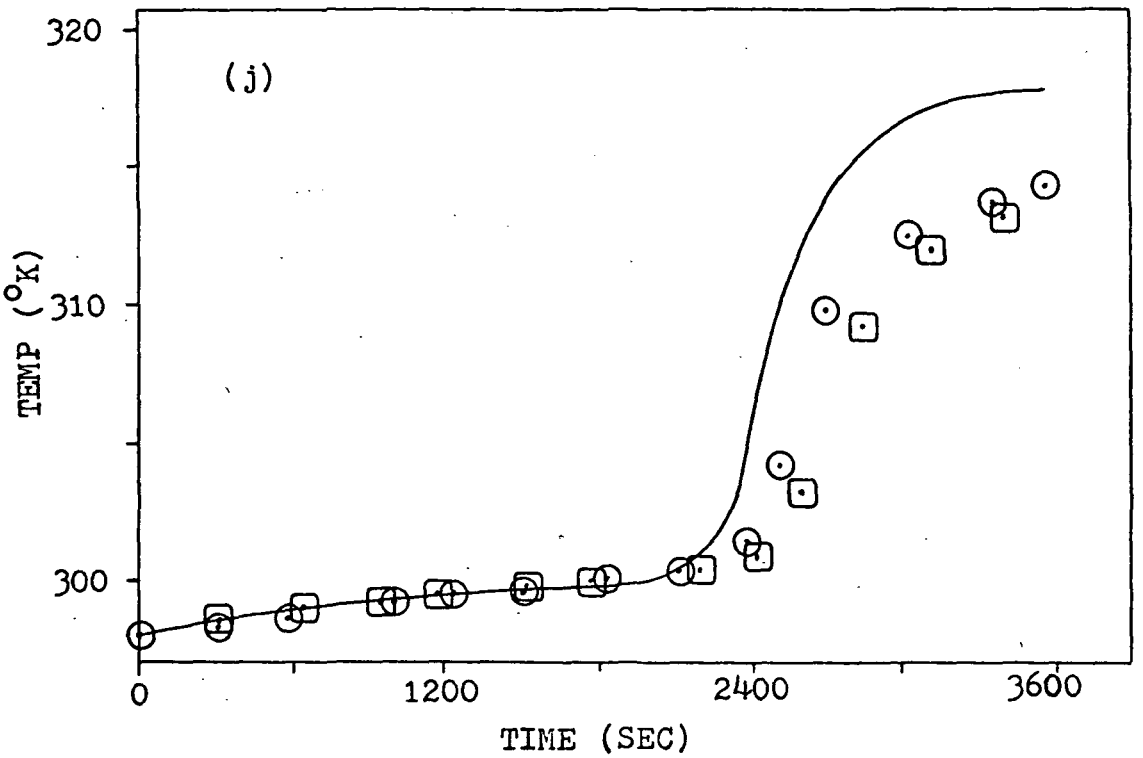

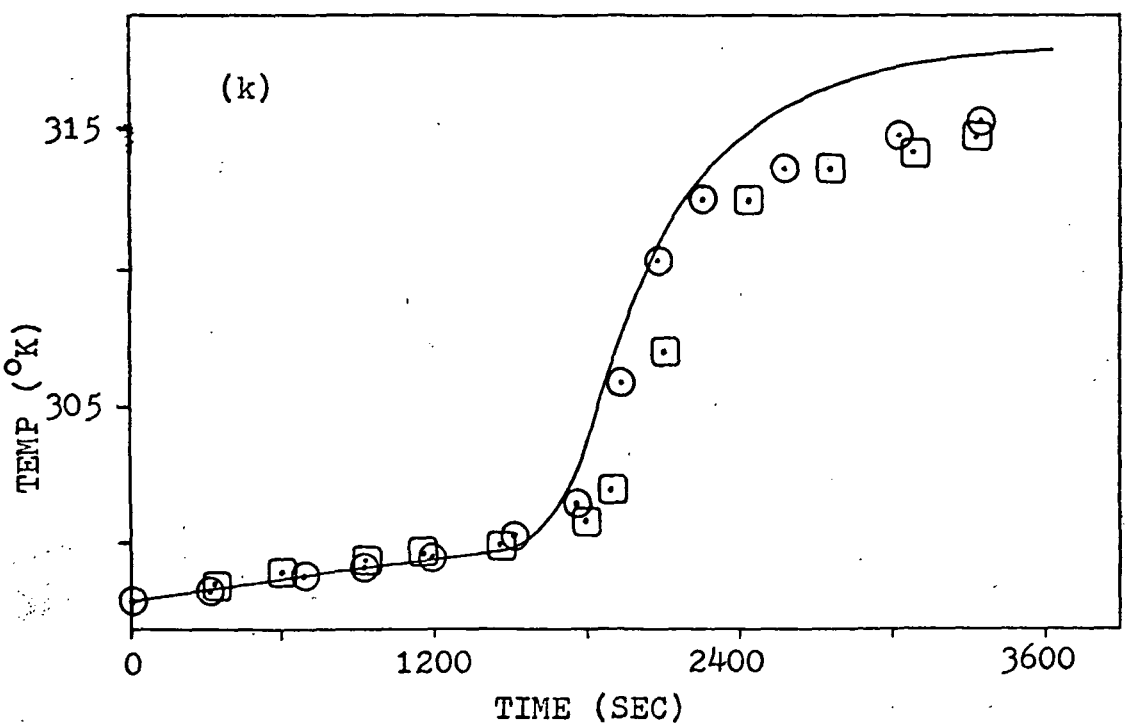

Figure 11 (cont)

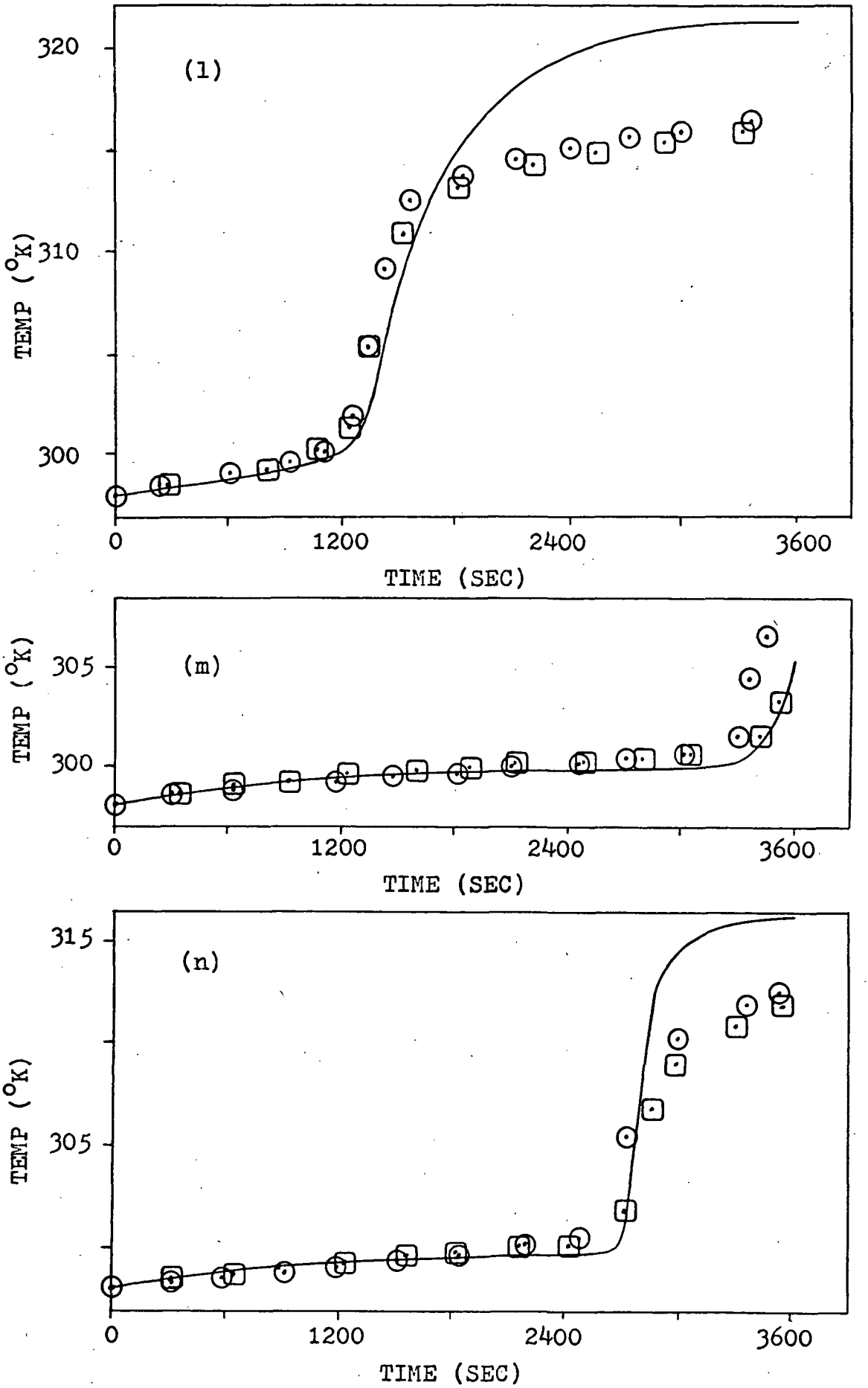

Figure 11 (cont)

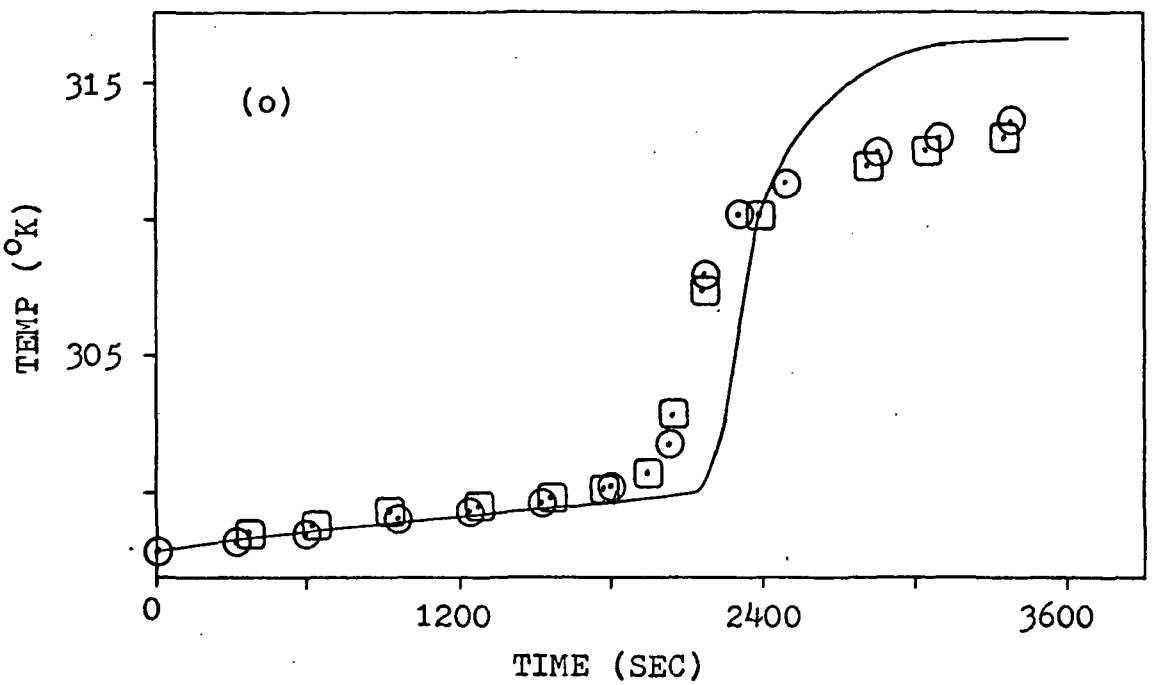

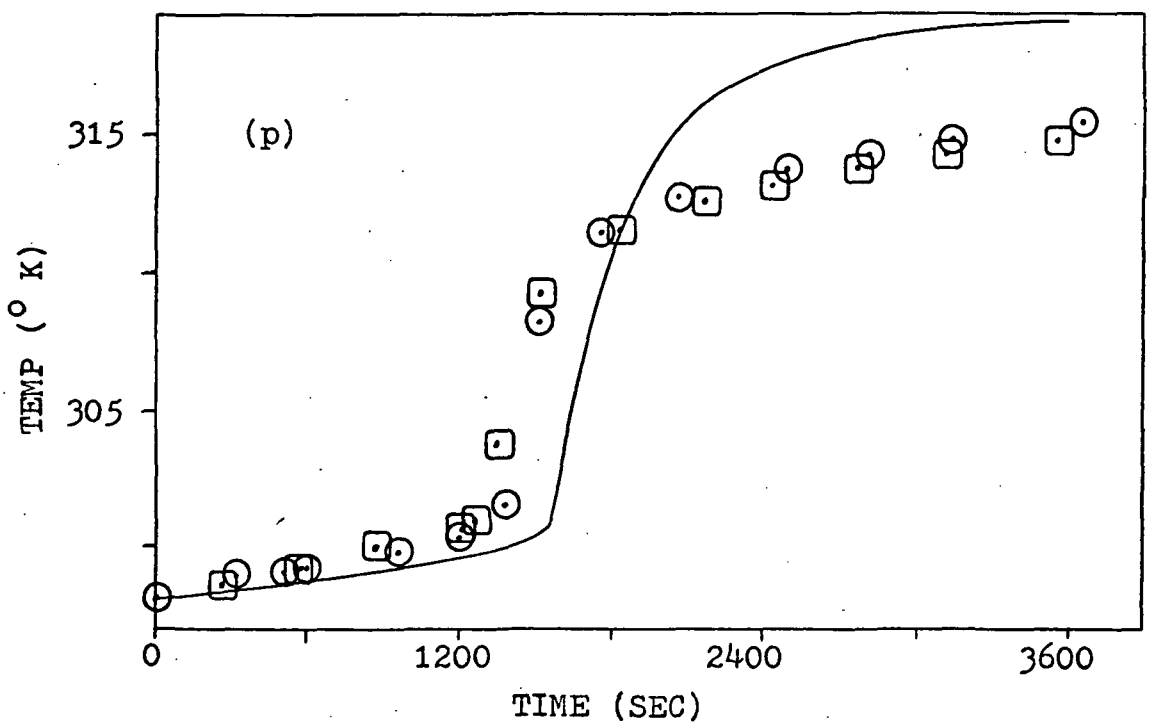

Figure 12. Comparison of Experimental Data to Theoretical Model Temperature Profiles for a Hot Wall Temperature of 330.22 ^{o}K

(a) r = 0.3175 cm, z = 1.016 cm
(b) r = 0.3175 cm, z = 2.032 cm
(c) r = 0.3175 cm, z = 3.048 cm
(d) r = 0.3175 cm, z = 4.064 cm
(e) r = 0.635 cm, z = 1.016 cm
(f) r = 0.635 cm, z = 2.032 cm
(g) r = 0.635 cm, z = 3.048 cm
(h) r = 0.635 cm, z = 4.064 cm
(i) r = 0.9525 cm, z = 1.016 cm
(j) r = 0.9525 cm, z = 2.032 cm
(k) r = 0.9525 cm, z = 3.048 cm
(l) r = 0.9525 cm, z = 4.064 cm
(m) r = 1.270 cm, z = 1.016 cm
(n) r = 1.270 cm, z = 2.032 cm
(o) r = 1.270 cm, z = 3.048 cm
(p) r = 1.270 cm, z = 4.064 cm

Legend:

⊙ = C-17-2
⊡ = C-18-2
— = Theoretical Model

Figure 12

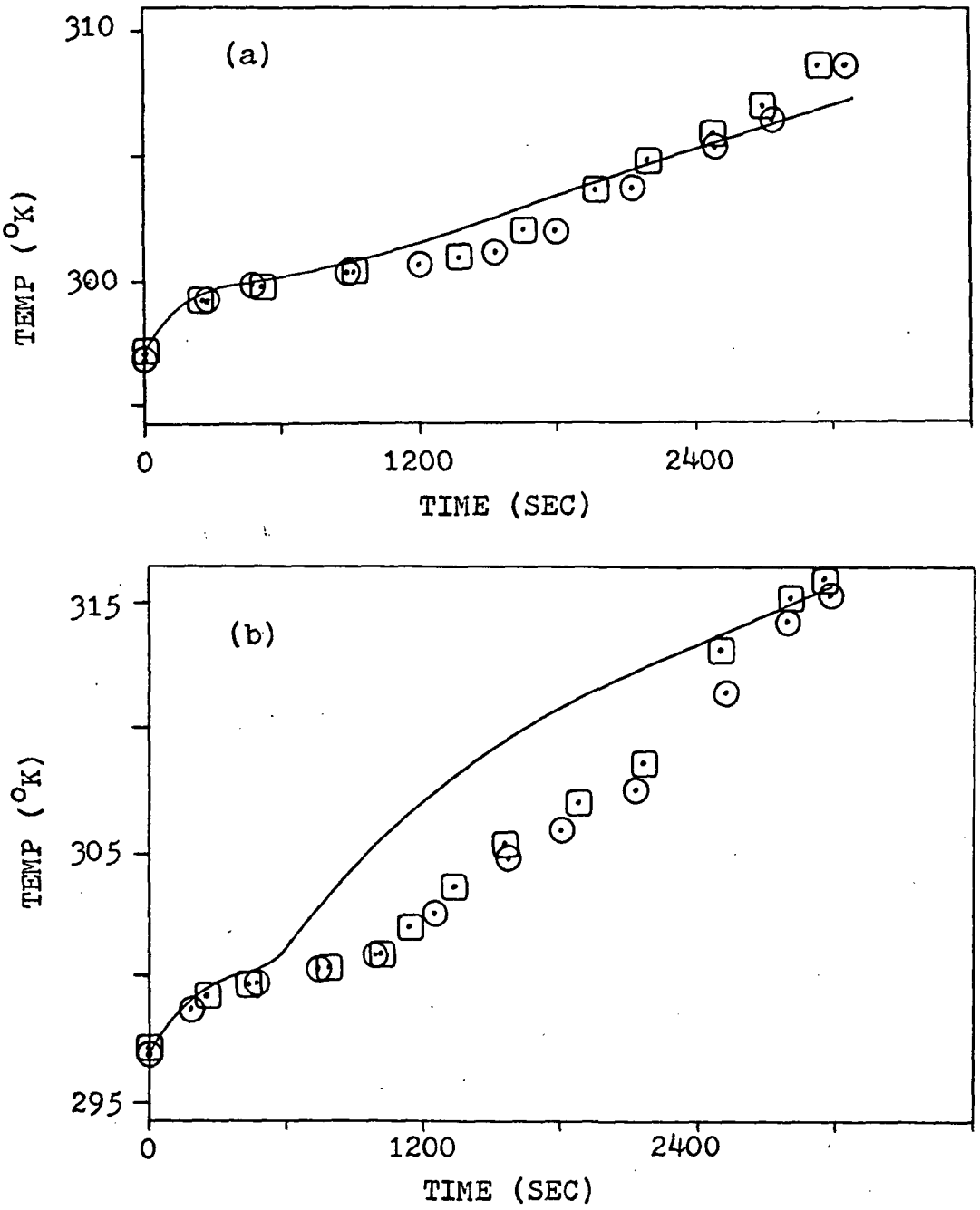
(a)
310
300
TEMP (°K)
0
1200
2400
TIME (SEC)
(b)
315
305
295
TEMP (°K)
0
1200
2400
TIME (SEC)

Figure 12 (cont)

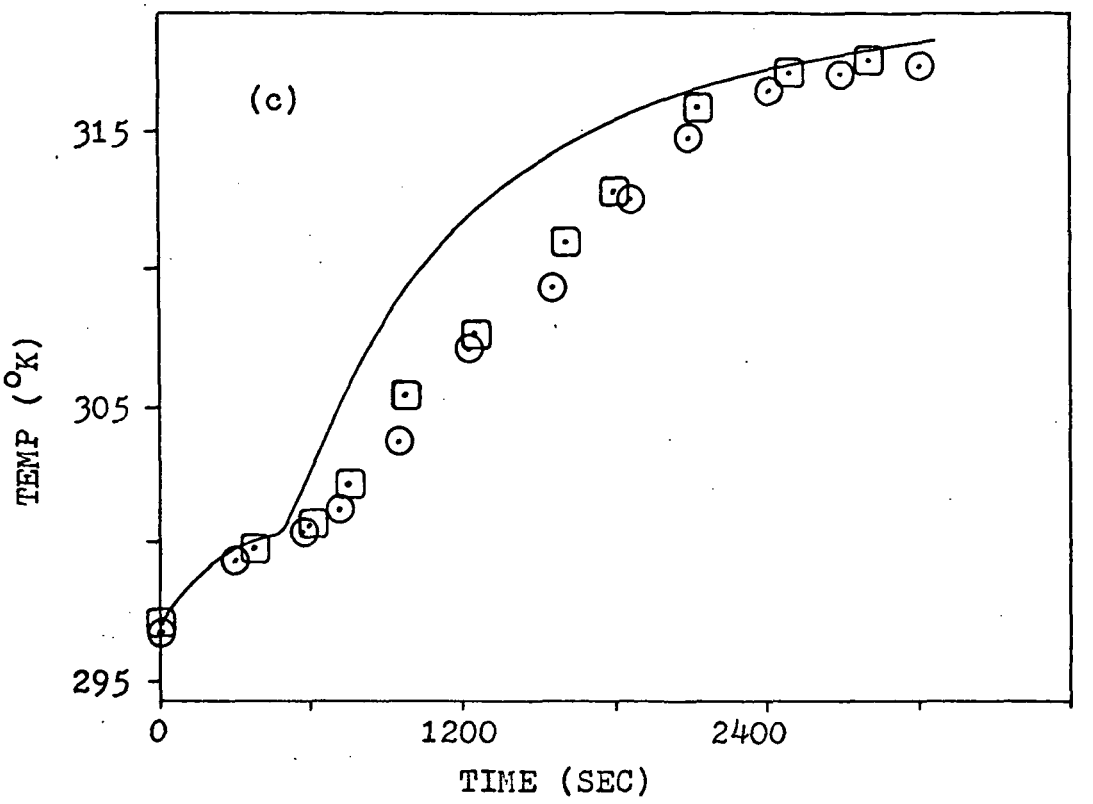

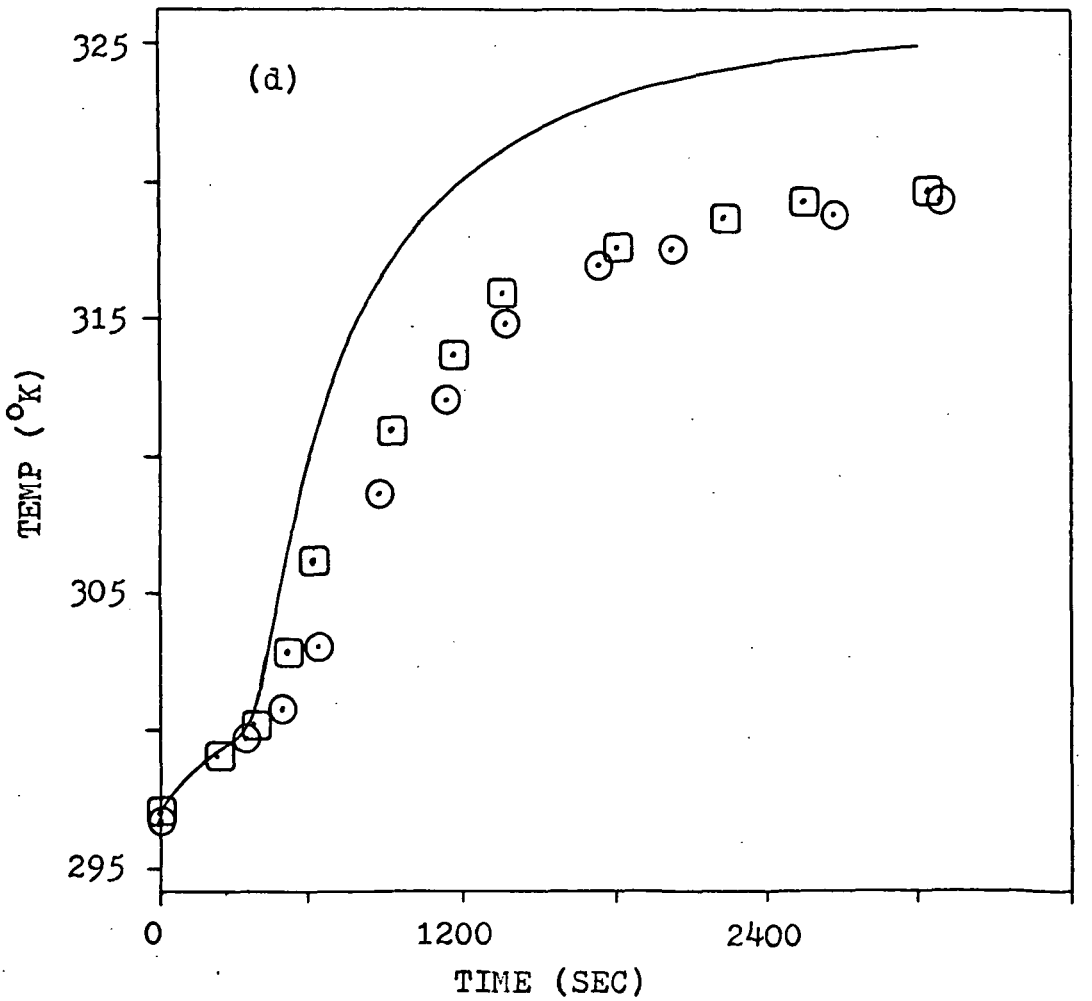

Figure 12 (cont)

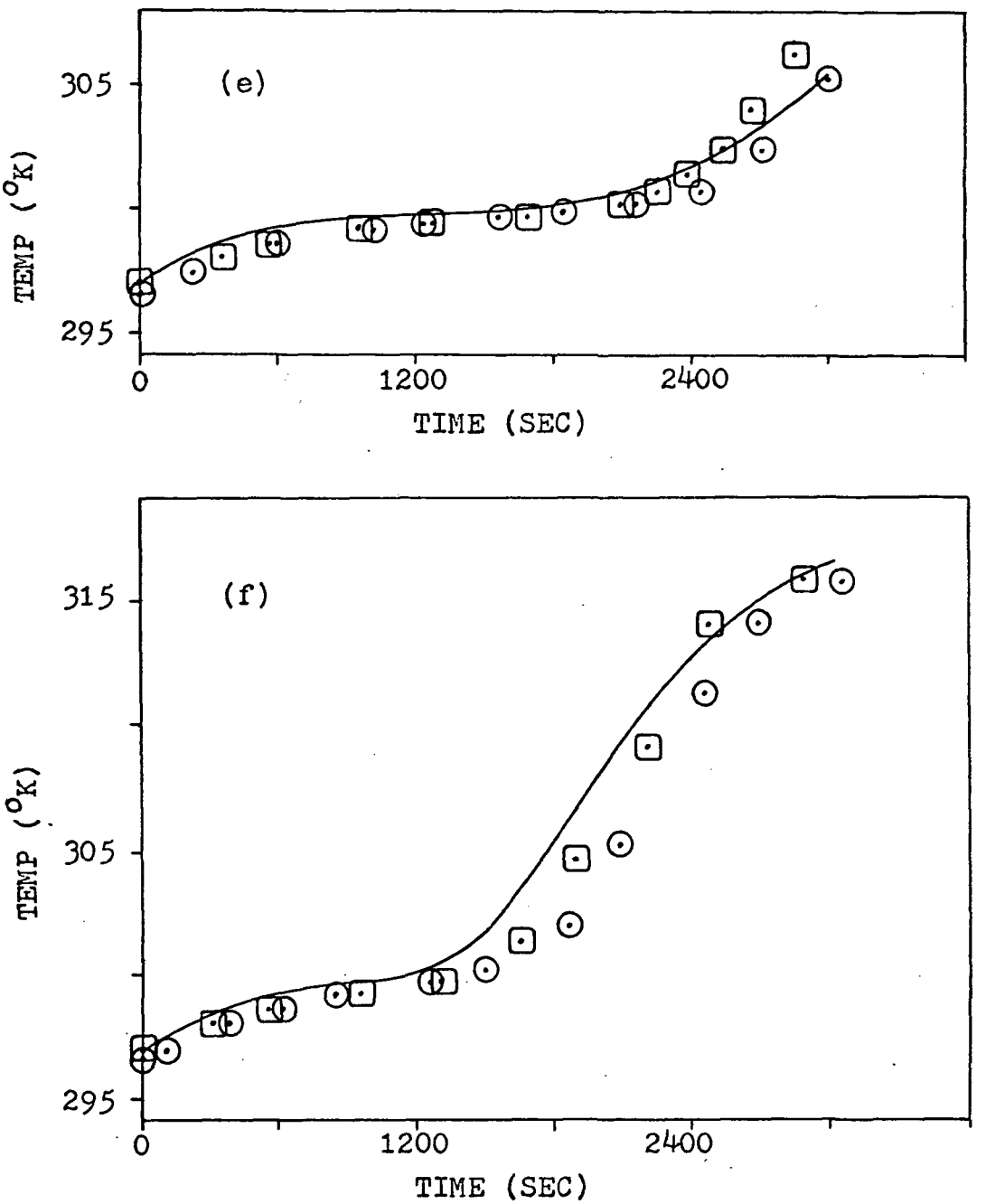

Figure 12 (cont)

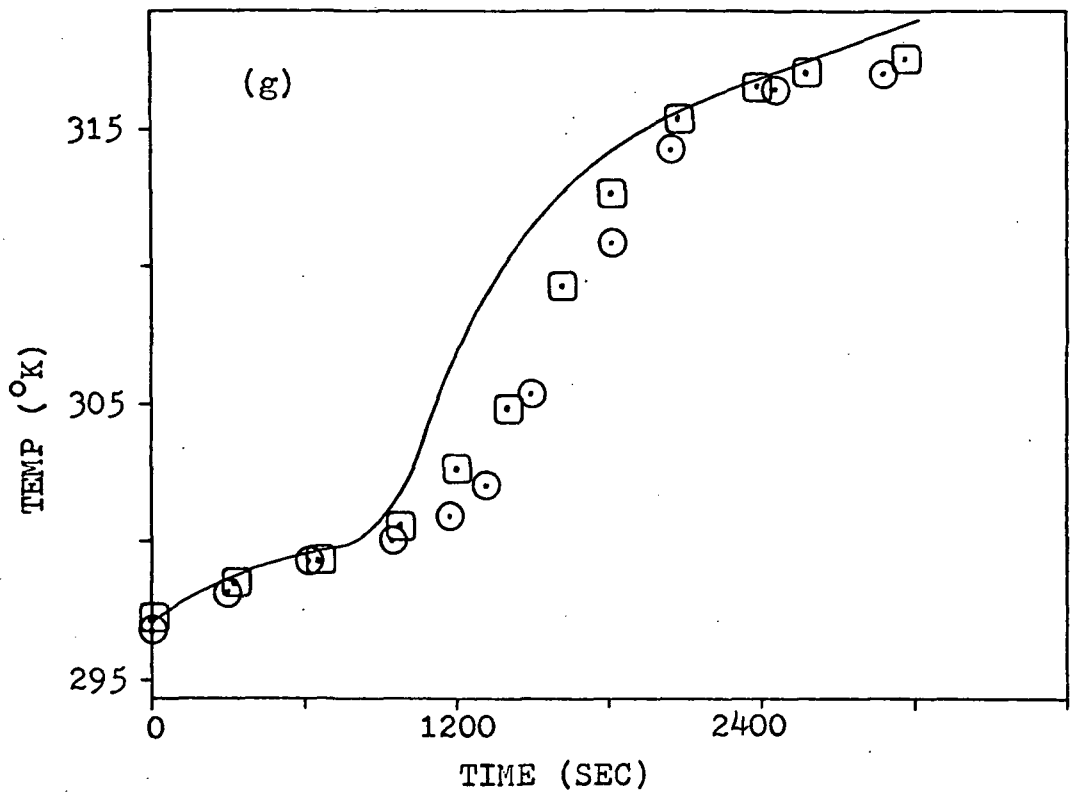

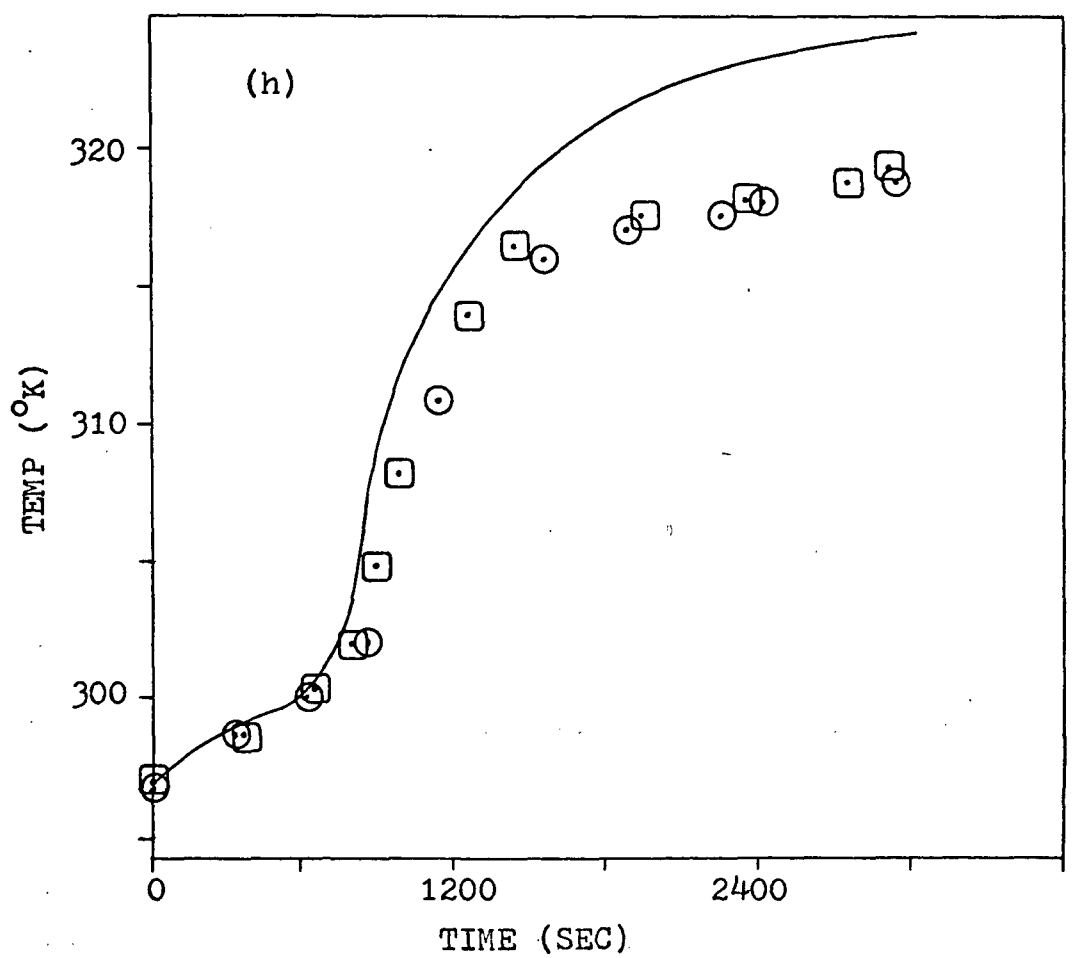

Figure 12 (cont)

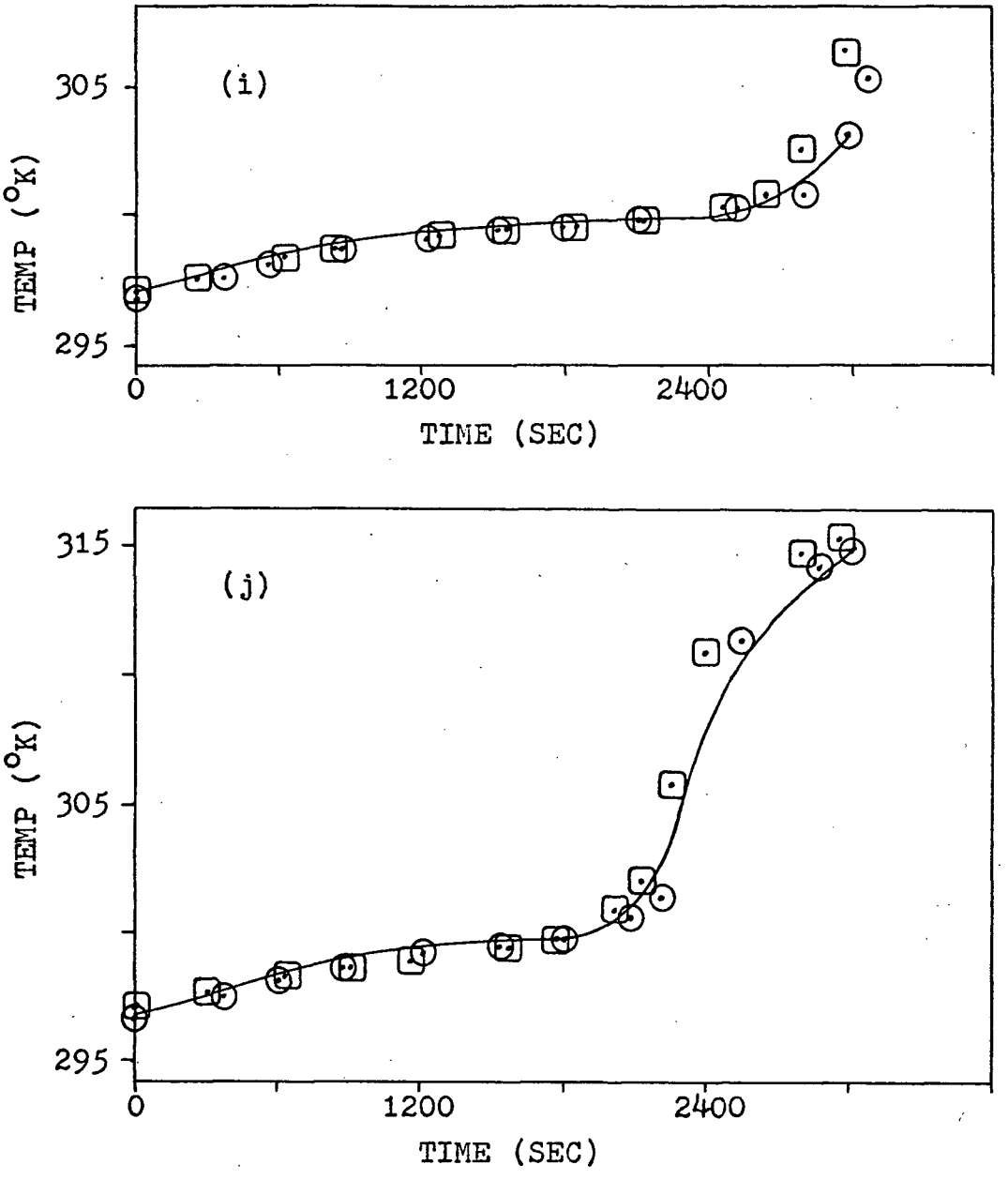

Figure 12 (cont)

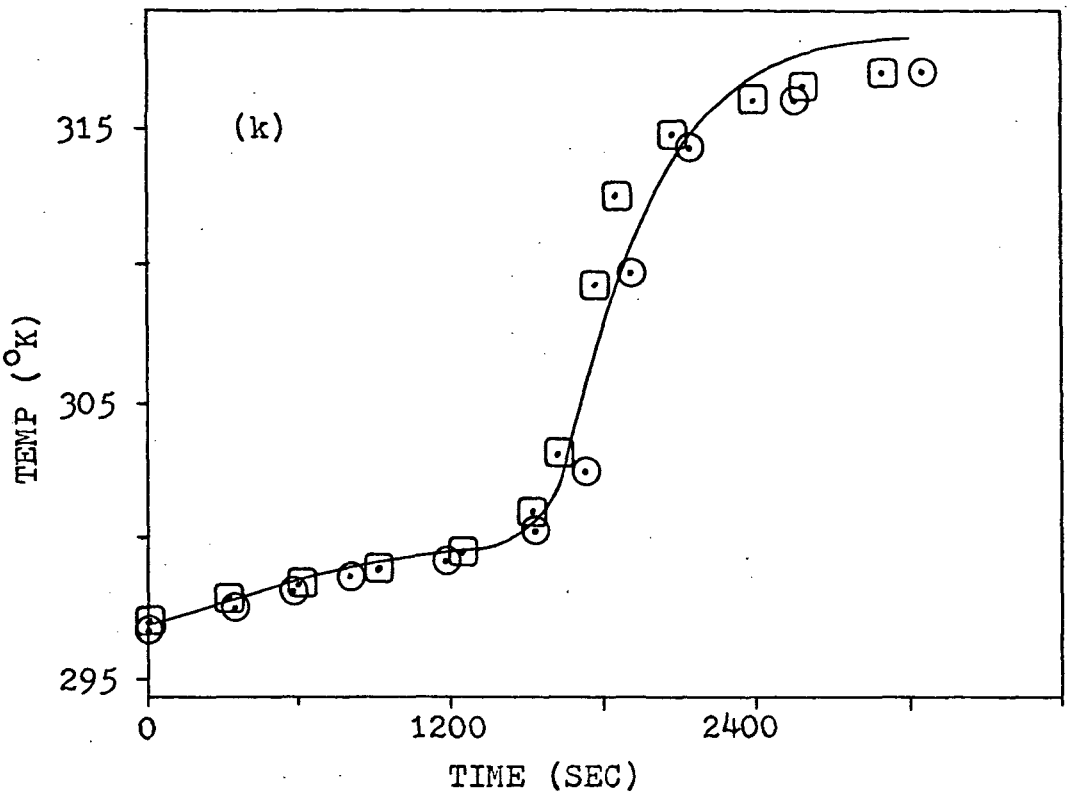

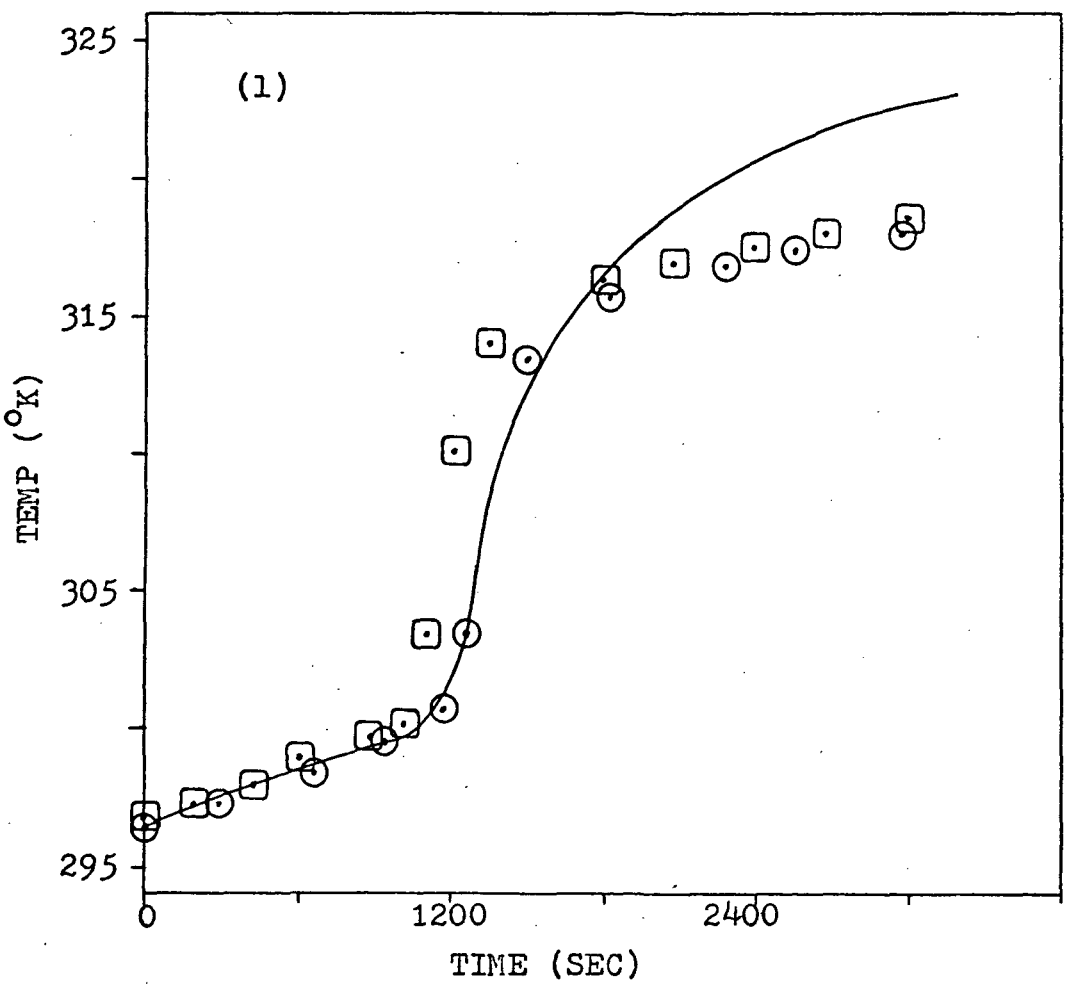

Figure 12 (cont)

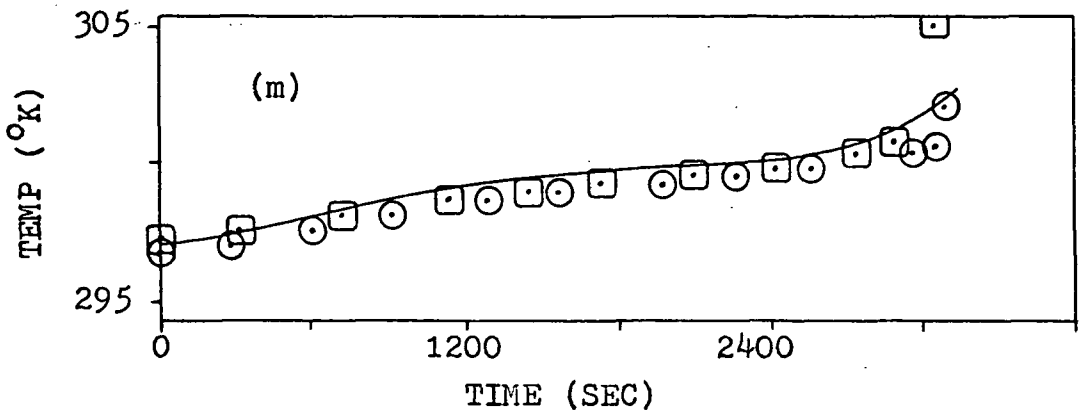

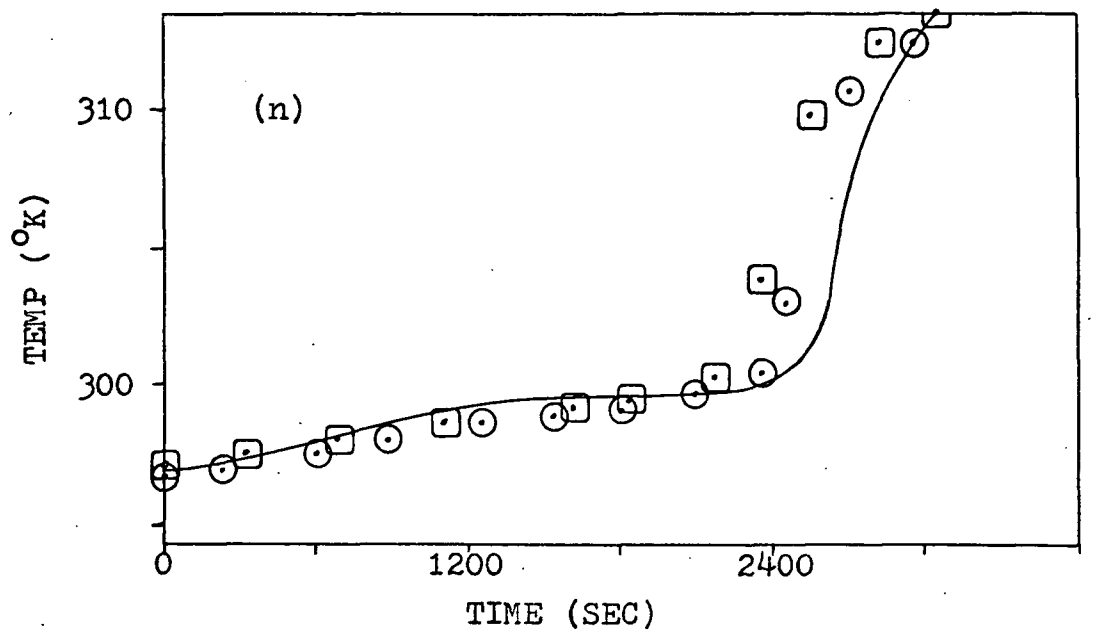

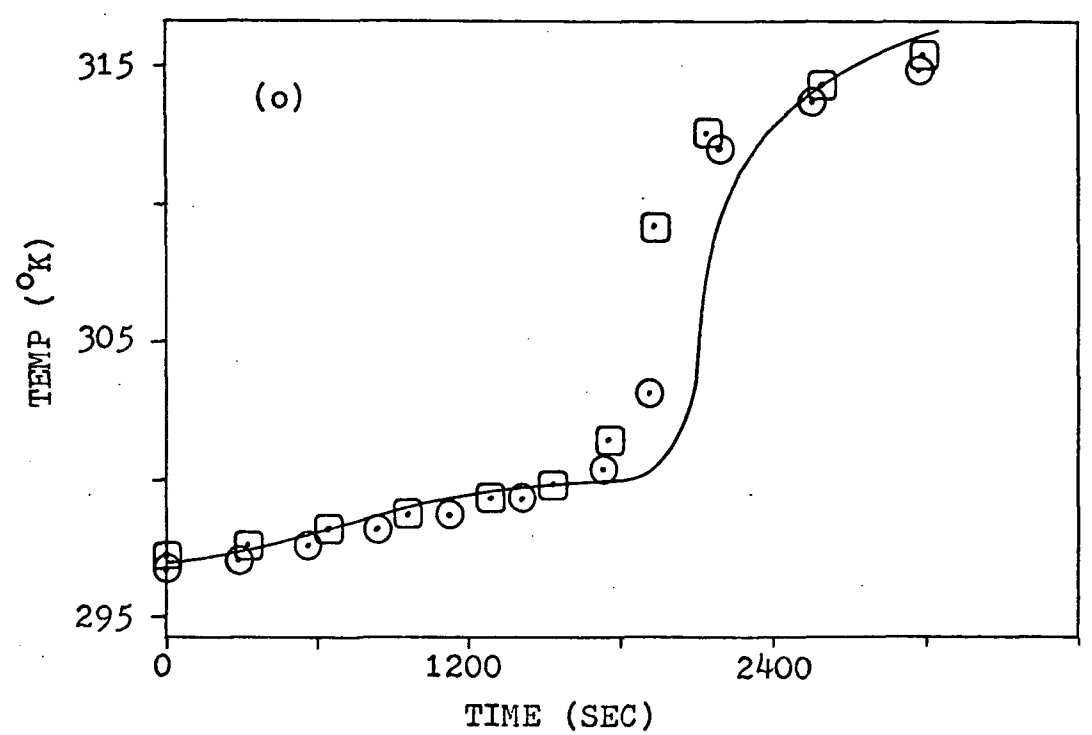

Figure 12 (cont)

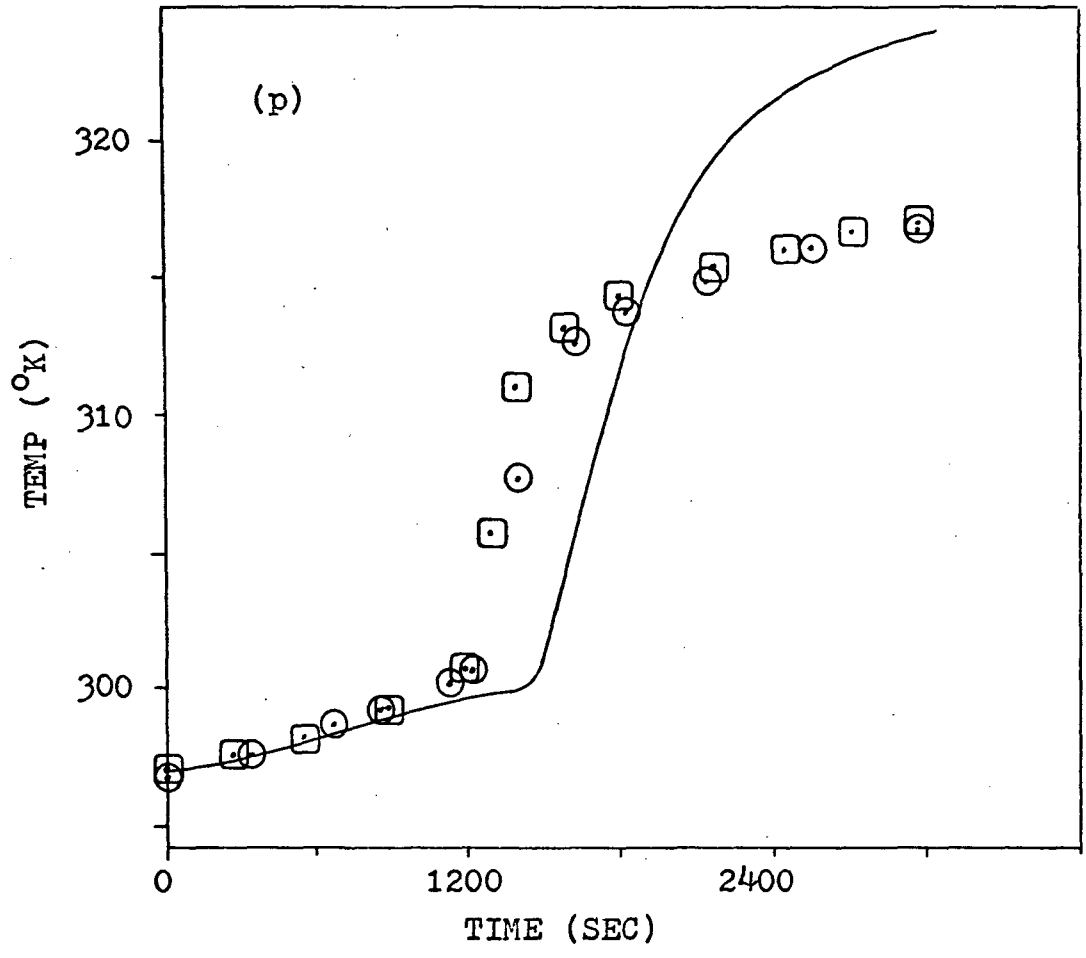

Conclusions

The following conclusions have been made from this study:

1. The determination of physical properties, especially the latent heat of fusion, is very critical for the proper modeling of the phase-change phenomena. When working with materials with a very low thermal diffusivity the latent heat of fusion becomes the governing physical property in the theoretical modeling of the system. The latent heat may be affected by purity of material, either chemical purity as manufactured or impurities introduced by chemical reactions with the test cell, and by air bubbles in the material. When using high chain normal paraffins air bubbles are the major factor to be considered in the determination of an effective latent heat of fusion.

2. Numerical dispersion is an important factor in the modeling of the solid-liquid phase-change phenomena when free convection is present. In this study we were not able to reduce the time step in the numerical solution to a small enough value to reach a convergent solution where numerical dispersion could be considered negligible.

3. Other sources of numerical error are the constant maximum velocity and the limitation placed on velocity by the stability criteria in the liquid phase energy equation.

4. An earlier study (2) has shown that it is not possible to determine a gravity level until an experimental investigation has been made to determine a critical Rayleigh number for the particular experimental system under study. However, the conclusion can be made that gravity-induced free convection is an important factor in the design of passive phase-change thermal control devices, especially when ground tests are to be made on a phase-change device. In a high gravity field gravity-induced free convection will cause the phase-change material to melt faster than predicted by a pure conduction model in certain portions of the cell. This will cause hot spots in the equipment whose temperature is being controlled, if allowance is not made for the increased melting rate in the design of the phase-change device.

5. The numerical study assumed that the velocity profiles were symmetric, in magnitude but not sign, in the development of the ideal-viscous flow model. However, the experiment was made using a cylindrical geometry test cell. Nodes further away from the tubular heating wall contain more mass than nodes close to the heating wall. Therefore, the flow model should be modified to account for the fact that velocities near the hot wall should be larger in magnitude than nodes further from the hot wall.

6. The experimental data is reproducible, which means that air bubbles in the test material did not cause hot or cold spots in the material. The only effect of air bubbles was on the latent heat of fusion. By making the heating wall vertical air bubbles rose to the top of the cell and did not affect heat transfer rates from the hot wall to the test material.

7. The study has shown that the method of solution, an ideal-viscous flow model coupled with the energy equation, will model the phase change process when liquid phase temperature gradients are small. When the liquid phase temperature gradients become larger deviations appear between final liquid phase temperatures predicted theoretically and measured experimentally. Therefore, the theoretical solution should be considered an initial solution to the problem of gravity-induced free-convection effects in the solid-liquid phase-change phenomena. Further work is needed if a complete solution to the problem is to be made.

Recommendations

The following recommendations are made as a result of this study:

1. The computer solution used in this study should be modified to account for the fact that velocity levels should become smaller in magnitude further away from the hot wall. The modified computer solution should then be compared to the experimental results of this study to see if the theoretical prediction is better than that using the present computer solution.

2. An experimental study using tracer materials in the phase change system should be made to determine the actual shape of convection induced velocity profiles in liquefaction and solidification phenomena. The measurement equipment should be photographic or microphotographic equipment.

3. Because of the problems encountered in the theoretical modeling of the convection phenomena, a material investigation study should be made to determine whether or not low density inert polymers, which exhibit solid-solid phase changes with high heats of transition, would make feasible phase-change materials. This type of material could be modeled using only a pure conduction model.

4. A study should be undertaken to determine effective thermal diffusivities that would model the phase change phenomena without solving for velocity profiles.

5. A theoretical investigation should be made to determine the proper finite difference form of the equation of state for gravity to be introduced into the equations of motion. By this means the actual equations governing the liquid phase could be solved.

Nomenclature

Definition:

Given that $s = f(z,R,t)$, then the following definitions are true:

$$s_t = \frac{\partial s}{\partial t} \quad , \quad s_z = \frac{\partial s}{\partial z} \quad , \quad s_r = \frac{\partial s}{\partial r} \quad , \quad s_{tt} = \frac{\partial^2 s}{\partial t^2} \quad , \quad s_{zz} = \frac{\partial^2 s}{\partial z^2}$$

$$s_{rr} = \frac{\partial^2 s}{\partial r^2} \quad , \quad s_{rz} = \frac{\partial^2 s}{\partial r \partial z}$$

Parallel Flow Model:

b = one-half of distance between parallel walls, cm

g = acceleration of gravity, cm^2/sec

ΔT = temperature gradient between parallel walls, $^\circ K$

y = distance from centerline, cm

$\eta = y/b$

β = coefficient of thermal expansion, $^\circ K^{-1}$

ρ = density, grams/cubic cm

μ = viscosity, gm $cm^{-1} sec^{-1}$

Ideal Flow Model:

a,b,c = real constants in ascending order of magnitude

A',B' = complex constants

t,w,z = complex planes

u = x-direction velocity, cm/sec

v = y-direction velocity, cm/sec

x = spatial dimension in complex z plane, cm

y = spatial dimension in complex z plane, cm

Finite Difference Models:

A,B,C,D,F,G = coefficients of IAD equations

C_p = heat capacity, watts sec gm^{-1} $^\circ K^{-1}$

ΔH = latent heat of fusion, watts sec gm^{-1}

q = heat flux, $watts/cm^2$

r = radial spatial dimension, cm

T = temperature, $^\circ K$

t = time, sec

u = velocity in z-direction, cm/sec

v = velocity in r-direction, cm/sec

z = longitudinal spatial dimension, cm

α = thermal diffusivity, $cm^2\ sec^{-1}$

Subscripts:

e,f,l,o,p,s = excess, fusion, liquid, cold wall, hot wall, solid, respectively

Superscripts

*,o = at end of 1st time step, at end of second time step, respectively

Tridiagonal Matrix:

a,b,c,d = coefficients of tridiagonal matrix

f,g,w = regression coefficients

Computer:

AK2 = liquid phase thermal conductivity, Btu $(ft\ sec\ °F)^{-1}$

AKP = wall thermal conductivity, Btu $(ft\ sec\ °F)^{-1}$

AKS = solid phase thermal conductivity, Btu $(ft\ sec\ °F)^{-1}$

AL = liquid phase thermal diffusivity, $ft^2\ sec^{-1}$

AS = solid phase thermal diffusivity, $ft^2\ sec^{-1}$

CPL = liquid phase heat capacity, Btu $(lb\ °F)^{-1}$

CPP = wall heat capacity, Btu $(lb\ °F)^{-1}$

CPS = solid phase heat capacity, Btu $(lb\ °F)^{-1}$

DR = spatial increment, r-direction, ft

DT = time increment, sec

DZ = spatial increment, z-direction, ft

HA = heat transfer coefficient, wall-atmosphere, Btu $(ft^2 sec\ °F)^{-1}$

HF = latent heat of fusion, Btu/lb

M1 = number of nodes in r-direction

M2 = M1 - 1

M3 = M1 - 2

MR1,MR2,MR3,MR4 = r-positions for nodes to be printed

MX1,MX2,MX3,MX4 = z-positions for nodes to be printed

N1 = number of nodes in z-direction

N2 = N1 - 1

N3 = N2 - 1

RMIN = radius of heating tube, inches

RØL = liquid phase density, $lb(ft^3)^{-1}$

RØP = wall density, $lb(ft^3)^{-1}$

RØS = solid phase density, $lb(ft^3)^{-1}$

T = temperature at old time step, °F

TA = atmospheric temperature, °F

TI = initial temperature, °F

TN = temperature at new time step, °F

U = flow model velocity for z-direction, ft sec^{-1}

UR = liquid phase velocity for r-direction, ft sec^{-1}

UZ = liquid phase velocity for z-direction, ft sec^{-1}

V = flow model velocity for r-direction, ft sec^{-1}

VMAX = allowable maximum velocity, ft sec^{-1}

Literature Cited

1. Bentilla, E. W., K. F. Stewart, and L. E. Kane, Final Report, Contract No. NAS-8-11163, Northrup Space Laboratories, Hawthorne, Calif., April 1968.

2. Bain, R. L., F. J. Stermole, and J. O. Golden, "The Effect of Gravity-Induced Free Convection Upon the Melting Phenomena of a Finite Paraffin Slab for Thermal Control," Annual Summary Report No. 1, Contract NAS-8-30511, Mod 1, Colorado School of Mines, Golden, Colorado, January 1972.

3. Carslaw, H. S. and J. C. Jaeger, Conduction of Heat in Solids, Oxford University Press, 1959.

4. Arpaci, V. S., Conduction Heat Transfer, Addison-Wesley Publishing Co., London, England, 1966.

5. Pujado, P. R., "Melting of a Finite Paraffin Slab," Thesis No. T 1215, Colorado School of Mines, Golden, Colorado, 1968.

6. Ukanwa, A. O., F. J. Stermole, and J. O. Golden, "Phase Change Solidification Phenomena for Thermal Control," Annual Summary Report No. 1, Colorado School of Mines, Golden, Colorado, January 1970.

7. Shah, A. P., "A Microscopic and Thermal Study of the Solidification of n-octadecane," Thesis No. T 1334, Colorado School of Mines, Golden, Colorado, 1970.

8. Dusinberre, G. M., Heat-Transfer Calculations by Finite Differences, International Textbook Corp., Scranton, Pennsylvania, 1961.

9. Grodzka, P. G., and C. Fan, "Thermal Control by Freezing and Melting - Space Thermal Control Study," Lockheed Missiles and Space Company, Huntsville, Alabama, Interim Report, Contract No. NAS-8-21133, March 1968.

10. Schlichting, H., Boundary Layer Theory, McGraw-Hill Book Co., New York, New York, 1960.

11. Longwell, P. A., Mechanics of Fluid Flow, McGraw-Hill Book Co., New York, New York, 1966.

12. Bird, R. B., W. E. Stewart, and E. N. Lightfoot, Transport Phenomena, John Wiley and Sons, Inc., New York, New York, 1960.

13. Vallentine, H. R., Applied Hydrodynamics, Butterworth and Co., Limited, London, England, 1959.

14. Bodoia, J. R., and J. F. Osterle, "Development of Free Convection Between Vertical Heated Plates," Jour. Heat Transfer, Trans. A.S.M.E., v. 84, no. 1, Feb. 1962, p. 40-44.

15. Dropkin, D. and S. Globe, "Natural Convection Heat Transfer in Liquids Confined by Two Horizontal Plates and Heated From Below," Jour. Heat Transfer, Trans. A.S.M.E., v. 81, no. 1, Feb. 1959, p. 24-28.

16. Dropkin, D., and E. Sumerscales, "Heat Transfer by Natural Convection in Liquids Confined by Two Parallel Plates Which are Inclined at Various Angles With Respect to the Horizontal," Jour. Heat Transfer, Trans. A.S.M.E., v. 90, no. 1, Feb. 1968, p. 77-84.

17. Gebhart, B., "Transient Natural Convection From Vertical Element," Jour. Heat Transfer, Trans. A.S.M.E., v. 83, no. 1, Feb. 1961, p. 61-70.

18. Koh, J. C., and J. F. Price, "Laminar Free Convection From a Non-Isothermal Cylinder," Jour. Heat Transfer, Trans. A.S.M.E., v. 87, no. 2, May 1965, p. 237-242.

19. Samuels, M. R., and S. W. Churchill, "Stability of a Fluid in a Rectangular Region Heated From Below," A.I.Ch.E. Jour., v. 13, no. 1, Jan. 1967, p. 77-85.

20. Chi-Tien and Yin-Chao Yen, "Approximate Solution of a Melting Problem With Natural Convection," Chem. Eng. Prog. Symposium Ser., v. 62, no. 64, 1966, p. 166-172.

21. Goodman, T. R., and J. J. Shea, "The Melting of Finite Slabs," Jour. Applied Mech., Trans. A.S.M.E., Feb. 1960, p. 16-24.

22. Wilkes, J. O., and S. W. Churchill, "The Finite-Difference Computation of Natural Convection in a Rectangular Enclosure," A.I.Ch.E. Jour., v. 12, no. 1, Jan. 1966, p. 161-166.

23. Peaceman, D. W., and H. H. Rachford, Jr., "The Numerical Solution of Parabolic and Elliptic Differential Equations," Jour. Soc. Indust. Appl. Math., v. 3, no. 1, March 1955, p. 28-41.

24. Fromm, J., "The Time Dependent Flow of an Incompressible Viscous Fluid," Methods in Computational Physics, v. 3, Academic Press, New York, New York, 1964, p. 346-382.

25. Emery, A. F., "The Effect of a Magnetic Field Upon the Free Convection of a Conducting Fluid," Jour. Heat Transfer, Trans. A.S.M.E., v. 85, no. 2, May 1963, p. 119-124.

26. Pearson, J.R.A., "On Convection Cells Induced by Surface Tension," Jour. Fluid Mechanics, v. 4, 1958, p. 489-500.

27. Nield, D. A., "Surface Tension and Buoyancy Effects in Cellular Convection," Jour. Fluid Mechanics, v. 19, 1964, p. 341-352.

28. Ukanwa, A. O., "Thermal Modeling of Phase Change Solidification in Thermal Control Devices Including Natural Convection Effects," Thesis No. T 1422, Colorado School of Mines, Golden, Colorado, 1971.

29. Lanz, R. B., "Rigorous Calculation of Miscible Displacement Using Immiscible Reservoir Simulators," S.P.E. Jour., June 1970, p. 192-195.

30. Lanz, R. B., "Quantitative Evaluation of Numerical Diffusion (Truncation Error)," S.P.E. Paper No. SPE 2811, 1970.

31. Von Rosenburg, D. N., Methods for the Numerical Solution of Partial Differential Equations, Elsevier, New York, New York, 1969.

32. White, S. P., Graduate Student, CPRE Dept., Colorado School of Mines, Golden, Colorado.

APPENDIX A - Experimental Data

Data from two solidification runs and two liquefaction runs are presented in this section. For experimental data of the other eight experimental runs contact Dr. J. O. Golden, C.P.R.E. Department, Colorado School of Mines, Golden, Colo.

RUN NUMBER C-13-2
Room Temperature - 298.67 ^{o}K
Bath Temperature - 310.75 ^{o}K

T.C.#1		T.C.#2		T.C.#3		T.C.#4		T.C.#5		T.C.#6	
TIME SEC	TEMP ^{o}K	TIME SEC	TEMP ^{o}K	TIME SEC	TEMP ^{o}K	TIME SEC	TEMP ^{o}K	TIME SEC	TEMP ^{o}K	TIME SEC	TEMP ^{o}K
0	298.11	0	298.11	0	298.11	0	298.11	0	298.11	0	298.11
750	298.67	570	298.67	570	298.67	252	299.22	300	298.39	576	298.67
1212	298.44	1170	299.22	1170	299.22	663	299.78	618	298.67	1362	299.22
1764	299.22	1767	299.5	1770	299.5	1218	300.33	1218	298.94	1821	299.5
2412	299.5	2415	299.64	2415	299.64	1815	300.6	1770	299.22	2418	299.64
3012	299.64	3012	299.78	2964	299.78	2415	300.75	1818	299.36	3162	299.78
3561	299.78	3702	299.92	3612	300.06	3015	300.75	2418	299.64	3618	299.92
4296	299.92	4209	300.06	4212	300.19	3612	300.75	3015	299.64	4215	299.92
4806	300.06	4848	300.19	4809	300.19	4212	301.03	3570	299.78	4815	300.06
5403	300.19	5406	300.19	5451	300.33	4812	301.03	4212	299.92	5412	300.19
6090	300.33	6003	300.33	6099	300.3	5454	301.17	4812	300.06	6012	300.33
6600	300.33	6648	300.33	6636	300.6	6009	301.44	5550	300.33	6564	300.6
7200	300.47	7200	300.6	7203	300.75	6882	302.0	6012	300.33	6777	300.89
						7296	302.28	6612	300.6	7212	301.44
								7254	301.17	7302	302.0

T.C.#7		T.C.8		T.C.#9		T.C.#10		T.C.#11		T.C.#12	
TIME SEC	TEMP °K	TIME SEC	TEMP °K	TIME SEC	TEMP °K	TIME SEC	TEMP °K	TIME SEC	TEMP °K	TIME SEC	TEMP °K
0	298.11	0	298.11	0	298.11	0	298.11	0	298.11	0	298.11
579	298.94	306	299.22	630	298.67	630	298.67	678	299.22	178	298.67
1128	299.22	720	299.22	1230	299.22	1230	299.22	1230	299.64	540	298.67
1818	299.5	1227	300.33	1827	299.5	1830	299.5	1740	299.78	1236	300.33
2421	299.78	1824	300.6	2427	299.64	2427	299.64	2430	300.05	2064	300.89
3021	300.06	2424	300.6	3624	299.78	2892	299.78	3030	300.33	2430	300.89
3621	300.19	3021	300.75	4221	300.19	4221	300.19	3672	300.6	3030	301.44
4266	300.33	3606	300.89	4818	300.33	4272	300.33	4131	300.88	3582	302.0
4818	300.6	4221	301.17	5418	300.75	4924	300.61	4914	301.44	4272	303.11
5508	300.89	4770	301.44	5736	301.44	5238	300.89	5100	303.11	4827	303.67
6015	301.44	5325	302.0	6063	303.67	5700	302.55	6072	305.33	5292	304.22
6612	302.56	5784	302.56	6570	304.78	6060	304.78	6390	305.89	5976	305.33
7122	303.67	6336	302.82	7122	305.33	6618	305.89	6897	306.44	6390	305.89
		6660	303.11			7320	306.44			6798	306.44
		7167	303.67							7314	306.72

T.C.#13		T.C.#14		T.C.#15		T.C.#16	
TIME SEC	TEMP °K	TIME SEC	TEMP °K	TIME SEC	TEMP °K	TIME SEC	TEMP °K
0	298.11	0	298.11	0	298.11	0	298.11
639	298.94	546	298.67	591	299.22	594	299.78
1005	299.22	1188	299.5	1242	299.78	1104	300.33
1968	299.78	1968	299.78	1974	300.33	1698	300.89
2430	300.05	2436	300.05	2436	300.89	3036	302.56
3030	300.33	2895	300.33	3084	300.89	3450	304.22
3675	300.89	3630	300.89	3312	303.11	3822	304.78
3930	301.44	3912	302.0	3636	304.22	4512	305.33
4320	303.67	4185	303.67	4230	305.89	4830	306.44
4692	304.78	4866	305.89	4830	306.72	5340	306.72
5292	305.33	5565	306.44	5616	307.0	5982	307.0
6072	305.89	6027	306.72	6120	307.28	6720	307.56
7212	306.44	6990	307.0	6720	307.56	6720	307.56
				7320	307.56	7272	307.83

RUN NUMBER C-14-2

Bath Temperature - 310.61 ^{o}K

T.C.#1		T.C.#2		T.C.#3		T.C.#4		T.C.#5		T.C.#6	
TIME SEC	TEMP ^{o}K	TIME SEC	TEMP ^{o}K	TIME SEC	TEMP ^{o}K	TIME SEC	TEMP ^{o}K	TIME SEC	TEMP ^{o}K	TIME SEC	TEMP ^{o}K
0	298.67	0	298.53	0	298.53	0	298.53	0	298.67	0	298.67
606	298.94	606	298.81	612	298.81	288	299.22	612	298.94	615	298.81
1206	299.22	1212	299.36	1212	299.36	657	299.78	1212	299.92	1215	299.22
1803	299.5	1806	299.5	1809	299.36	1257	300.33	1812	299.5	1812	299.5
2448	299.78	2406	299.78	2409	299.78	1854	300.47	2409	299.65	2409	299.78
3045	299.92	3003	299.92	3009	299.92	2409	300.61	3009	299.92	3012	299.92
3600	300.06	3603	300.06	3603	300.06	3006	300.61	3609	300.06	3612	300.06
4242	300.19	4200	300.19	4203	300.19	3609	300.75	5209	300.19	4212	300.19
5442	300.33	5445	300.33	5403	300.47	4206	300.89	4806	300.47	4809	300.47
6039	300.47	6042	300.47	6000	300.61	4803	300.89	5406	300.47	5405	300.61
6639	300.61	6642	300.61	6642	300.61	5400	301.44	6000	300.61	6003	300.75
7239	300.61	7241	300.61	7242	300.89	6000	301.72	6600	300.75	6600	301.25
						6645	302.0	7200	301.03	7200	302.0
						7242	302.28				

T.C.#7		T.C.#8		T.C.#9		T.C.#10		T.C.#11		T.C.#12	
TIME SEC	TEMP ^{o}K	TIME SEC	TEMP ^{o}K	TIME SEC	TEMP ^{o}K	TIME SEC	TEMP ^{o}K	TIME SEC	TEMP ^{o}K	TIME SEC	TEMP ^{o}K
0	298.53	0	298.67	0	298.67	0	298.67	0	298.53	0	298.53
618	298.94	294	299.22	648	299.08	621	298.81	624	299.22	168	299.22
1218	299.22	618	299.65	1176	299.22	1221	299.36	1224	299.36	627	300.06
1815	299.5	1218	300.19	1818	299.65	1821	299.65	1824	299.92	1224	300.33
2415	299.78	1815	300.47	2418	299.78	2376	299.78	2421	300.05	1824	300.61
3015	299.92	2415	300.61	3015	299.92	3066	300.05	3021	300.19	2424	300.89
3615	299.92	3015	300.61	3615	300.19	3618	300.19	3528	300.33	3021	302.0
4212	300.47	3612	300.89	4215	300.47	4218	300.33	4080	300.89	3762	302.5
4854	300.61	4305	301.44	4812	300.61	4815	300.61	4725	302.0	4494	303.67
5406	300.75	4902	302.0	5184	300.89	5457	302.0	5460	304.22	4866	304.22
6006	301.25	5454	302.5	5544	301.44	6012	305.33	6105	305.89	5646	305.33
6648	302.5	6282	303.1	5982	304.22	6432	305.89	6795	306.44	6102	305.89
7158	303.67	6930	303.67	6930	305.33	7254	306.44	7350	306.72	6672	306.44
		7248	304.22	7344	305.61					7302	306.86

T.C.#13		T.C.#14		T.C.#15		T.C.#16	
TIME SEC	TEMP ^{o}K	TIME SEC	TEMP ^{o}K	TIME SEC	TEMP ^{o}K	TIME SEC	TEMP ^{o}K
0	298.67	0	298.67	0	298.53	0	298.53
627	299.22	630	299.08	495	299.78	495	299.78
1227	299.65	1230	299.78	1233	300.05	1233	300.61
1827	299.92	1830	300.06	1830	300.33	1830	300.89
2427	300.19	2427	300.19	2382	300.89	2430	303.11
3024	300.61	3027	300.61	3030	302.5	3168	304.78
3624	301.17	3576	302.5	3582	304.78	3765	305.89
4311	304.78	4131	305.33	4410	306.44	4227	306.44
4815	305.33	4914	306.44	5424	307.0	5148	307.0
6066	305.89	5742	306.72	6018	307.28	5700	307.28
6615	306.44	6018	306.86	7032	307.55	6486	307.55
7356	306.72	6708	307.0			7272	307.83
		7302	307.14				

RUN NUMBER C-19-2

T.C.#1		T.C.#2		T.C.#3		T.C.#4		T.C.#5		T.C.#6	
TIME SEC	TEMP ^{o}K	TIME SEC	TEMP ^{o}K	TIME SEC	TEMP ^{o}K	TIME SEC	TEMP ^{o}K	TIME SEC	TEMP ^{o}K	TIME SEC	TEMP ^{o}K
0	303.11	0	303.11	0	303.39	0	303.11	0	303.25	0	303.25
204	302.55	342	302.0	300	302.0	120	302.0	258	302.55	210	302.55
387	302.0	618	301.44	480	301.44	300	299.22	534	302.0	492	302.0
753	301.44	942	301.17	666	300.89	486	296.44	762	301.44	765	301.44
936	301.17	1266	300.89	852	300.33	624	294.78	948	301.17	948	301.17
1215	301.17	1542	300.33	990	299.78	852	293.11	1272	301.04	1224	301.04
1491	301.04	1860	299.5	1266	298.67	1176	291.44	1590	301.04	1458	300.89
1860	300.89	2142	298.67	1542	297.56	1452	290.33	1824	301.04	1689	300.33
2136	300.75	2232	198.39	1866	296.44	1632	289.78	2190	300.89	1824	299.92
				2046	295.89	1866	289.22			2190	299.22
				2232	295.61	2097	288.67				

T.C.#7		T.C.#8		T.C.#9		T.C.#10		T.C.#11		T.C.#12	
TIME SEC	TEMP °K	TIME SEC	TEMP °K	TIME SEC	TEMP °K	TIME SEC	TEMP °K	TIME SEC	TEMP °K	TIME SEC	TEMP °K
0	303.25	0	303.39	0	303.39	0	303.39	0	303.39	0	303.39
273	302.55	216	300.89	306	302.55	315	302.55	270	302.55	177	301.44
396	302.0	354	299.5	588	302.0	591	302.0	450	301.44	324	299.78
582	301.44	582	295.89	912	301.44	864	301.44	588	300.89	594	295.89
720	300.89	858	293.67	1230	301.17	1236	301.17	864	299.78	870	293.67
903	300.33	954	293.11	1554	301.17	1464	400.89	1005	299.22	1191	292.89
1134	199.22	1182	292.0	1830	301.04	1785	300.33	1236	298.11	1467	290.89
1734	297.0	1458	290.89	2154	300.89	1971	299.78	1512	297.0	1698	290.33
1872	296.44	1737	290.33			2202	299.22	1836	295.89	1884	289.78
2100	295.89	1920	289.78					2202	294.78	2070	289.22
2244	295.61	2106	289.22							2250	288.89
		2241	288.89								

T.C.#13		T.C.#14		T.C.#15		T.C.#16	
TIME SEC	TEMP ^{o}K	TIME SEC	TEMP ^{o}K	TIME SEC	TEMP ^{o}K	TIME SEC	TEMP ^{o}K
0	303.39	0	303.39	0	303.39	0	303.39
408	302.55	414	302.55	348	302.55	144	302.55
639	302.0	645	302.0	504	302.0	276	300.61
870	301.44	960	301.44	750	300.89	324	299.78
1242	301.17	1245	301.17	876	300.33	462	298.11
1515	301.04	1515	300.89	1014	299.78	648	295.89
1836	301.04	1794	300.33	1152	299.22	780	294.78
2115	300.89	1932	299.78	1428	298.11	966	293.67
2250	300.75	2112	299.22	1704	297.0	1290	292.0
		2208	298.94	1842	296.44	1704	290.33
				2118	294.78	1890	289.78
				2208	294.78	2076	289.22
						2256	288.81

RUN NUMBER C-23-2

Bath Temperature - 273.67 °K

T.C.#1		T.C.#2		T.C.#3		T.C.#4		T.C.#5		T.C.#6	
TIME SEC	TEMP °K	TIME SEC	TEMP °K	TIME SEC	TEMP °K	TIME SEC	TEMP °K	TIME SEC	TEMP °K	TIME SEC	TEMP °K
0	303.11	0	303.11	0	303.11	0	303.11	0	303.11	0	303.11
270	302.0	273	302.0	132	302.55	138	300.89	372	302.0	189	302.09
552	301.44	462	301.44	408	301.44	228	299.78	648	301.44	372	302.0
732	301.17	732	301.17	600	300.89	324	298.11	924	301.17	603	301.44
966	301.33	1008	301.03	828	300.33	372	297.56	1248	301.03	927	301.17
1272	300.89	1194	300.89	1056	299.22	552	294.78	1524	300.89	1200	300.89
1518	300.89	1422	300.33	1194	298.67	738	293.11	1800	300.89	1572	300.33
1836	300.75	1590	299.78	1470	297.56	1014	291.44	2124	300.61	1800	299.78
2154	300.61	1791	299.22	1894	296.44	1290	290.33	2352	300.33	2029	299.22
2340	300.33	2022	298.67	1980	295.89	1614	289.22			2262	298.67
		2346	297.56	2208	295.33	2118	288.11				
						2352	287.56				

T.C.#7		T.C.#8		T.C.#9		T.C.#10		T.C.#11		T.C.#12	
TIME SEC	TEMP ^{o}K	TIME SEC	TEMP ^{o}K	TIME SEC	TEMP ^{o}K	TIME SEC	TEMP ^{o}K	TIME SEC	TEMP ^{o}K	TIME SEC	TEMP ^{o}K
0	303.11	0	303.11	0	303.11	0	303.11	0	303.11	0	303.11
192	302.55	147	302.0	240	302.55	243	302.55	336	302.0	150	301.44
330	302.0	240	300.05	426	302.0	474	302.0	522	300.89	294	299.5
465	301.44	330	298.67	795	301.44	654	301.44	705	300.33	384	298.11
606	300.89	468	296.44	978	301.17	933	301.17	888	299.22	660	294.78
837	300.33	699	294.22	1254	301.17	1257	300.89	1119	298.11	846	293.11
1065	299.22	930	292.55	1578	300.89	1485	300.61	1254	297.56	1215	291.44
1482	297.56	1347	290.88	1899	300.61	1668	300.33	1488	296.44	1536	290.33
1800	296.44	1668	189.78	2310	300.33	1854	299.78	1857	295.33	1950	289.22
2217	295.33	1896	189.22			2082	299.22	2040	294.78	2226	288.67
		2220	288.67			2268	298.67	2268	294.22		

T.C.#13		T.C.#14		T.C.#15		T.C.#16	
TIME SEC	TEMP ^{o}K	TIME SEC	TEMP ^{o}K	TIME SEC	TEMP ^{o}K	TIME SEC	TEMP ^{o}K
0	303.11	0	303.11	0	303.11	0	303.11
342	302.55	342	302.55	300	302.55	210	300.89
570	302.0	618	302.0	621	300.89	345	298.94
894	301.44	942	301.17	897	299.89	624	295.61
1218	301.17	1260	300.89	1200	298.89	942	293.11
1542	301.03	1542	300.61	1548	297.0	1266	291.44
1815	300.89	1818	299.78	1824	195.88	1590	290.33
2136	300.61	2136	298.67	2184	294.22	1908	289.22
2322	300.33	2277	298.11	2280	293.67	2136	288.67
						2328	288.11

APPENDIX B

Fortran IV Computer Program

This program was written to solve a two-dimensional cylindrical-coordinate liquefaction problem of n-octadecane under the influence of gravity-induced free convection. The program was run on a DEC, Model PDP-10 computer. The program was written in general terms, except for the heat capacity term in the phase change calculation. To use the program the following length to effective radius must be observed

$$N1 \geq 2M1 + 1$$

See the nomenclature for definition of terms and units to be used in the program.

Input File:

1. For execution 4 = Input file or device
2. First card - N1,N2,N3,M1,M2,M3,MR1,MR2,MR3,MR4, with a (10I) format)
3. Second card - RMIN, with a (F) format
4. Third card - MX1,MX2,MX3,MX4, with a (4I) format
5. Fourth card - DZ,DR,DT,TP,TA,TF,TI,HA,HF, with a (9F) format. TA and HA are dummy input variables, to be used if calculation of heat loss through walls is incorporated into the program
6. Fifth card - CPS,CPL,CPP,AKS,AKL,AKP,RØS,RØL,RØP with a (9E) format. CPP,AKP,RØP are dummy input variables, to be used if a heat balance of the cell walls is incorporated into the program
7. Sixth card - VMAX, with an (E) format

Flag File:

1. For execution 6 = Flag File
2. Output - 'Input File'
3. Input - FLAG, with an (F) format
   a. if FLAG < 10.0, stop execution
   b. if FLAG $\geq$ 10.0, continue execution

Output File:

1. For execution 5 = output file, 6 = output file
2. Time, t, in seconds at 120 second intervals
3. Temperatures at input nodes at 120 second intervals
4. Interface nodes at 120 second intervals

Sample Input File:

```
81,80,79,26,25,24,7,11,16,21
0.375
17,33,49,65
0.0020833,0.0020833,1.5,99.75,75.0,80.0,77.5,0.0,78.675
0.517E+00,0.522E+00,0.1E-12,0.243E-04,0.2402E-04,0.1E-12
          0.5349E+02,0.482E+02,0.1E-12
0.75E-03
```

```
C       CYLINDRICAL COORDINATE IAD PROGRAM
C   SSSSSSSSSSSSSS
      DIMENSION U(81,39),V(81,39),UZ(81,39),UR(81,39)
      DIMENSION T(81,39),TM(81,39),R(81,39)
      DIMENSION RO(81),ML(39),HR(39)
      DIMENSION A(39),C(39),D(39),W(39),Y(39)
      DIMENSION DJ(81),JZ(81),YZ(81),JR(5),JX(5)
      COMMON /S1/ A,C,D,N,Y
      COMMON /S2/ DZ,DR,DT
      COMMON /S3/ AS,AL,DJ,WZ,YZ
      COMMON /ALPHA/ U,V
      COMMON /BETA/ UZ,UR
      COMMON /GAMMA/ N1,N2,N3,M1,M2,M3
C   INPUT PARAMETERS AND CONSTANTS.....
      READ (4,8) N1,N2,N3,M1,M2,M3,MR1,MR2,MR3,MR4
8     FORMAT (12I)
      READ (4,9) RMIN
9     FORMAT (F)
      WRITE (6,8) N1,N2,N3,M1,M2,M3,MR1,MR2
      WRITE (6,9) RMIN
      READ (4,10) MX1,MX2,MX3,MX4
      WRITE (6,10) MX1,MX2,MX3,MX4
10    FORMAT (4I)
      READ (4,11) DZ,DR,DT,TP,TA,TF,TI,HA,HF
      WRITE (6,111) DZ,DR,DT,TP,TF,TI,HF
11    FORMAT (9F)
111   FORMAT (10X,' DX = ',F,' FT ',/,10X,' DR = ',F,' FT ',
     1 /,10X,' DT = ',F,' SEC ',/,10X,' TP = ',F,
     2 ' DEG F ',/,10X,' TF = ',F,' DEG F ',/,10X,' TI = ',
     3 F,' DEG F ',/,10X,' HF = ',F,' BTU/LB ',/)
C   INPUT PHYSICAL PROPERTIES.....
      READ (4,12) CPS,CPL,CPP,AKS,AKL,AKP,ROS,ROL,ROP
      WRITE (6,112) CPS,CPL,AKS,AKL,ROS,ROL
12    FORMAT (9E)
112   FORMAT (10X,' CPS = ',F,' BTU/(LB*DEG F)',/,10X,' CPL = ',
     1 F,' BTU/(LB*DEG F)',/,10X,' AKS = ',E,' BTU/(SEC*FT*DEG F)',
     2 /,10X,' AKL = ',F,' BTU/(SEC*FT*DEG F)',/,10X,' ROS = ',F,'
     3 LB/FT**3',/10X,' ROL = ',F,' LB/FT**3',/)
      READ (4,14) VMAX
14    FORMAT (E)
      CALL VIVV(VMAX)
C   INITIALIZE VARIABLES.....
      JR(1)=MR1
      JR(2)=MR2
      JR(3)=MR3
      JR(4)=MR4
      JX(1)=MX1
      JX(2)=MX2
      JX(3)=MX3
      JX(4)=MX4
      DO 15 I=1,M1
      DO 15 J=1,M1
      UZ(I,J)=0.1E-12
      UR(I,J)=0.1E-12
      R(I,J)=0.1E-12
      T(I,J)=TI
      TM(I,J)=TI
      HR(J)=HF
      NO(I)=1
15    CONTINUE
```

```
      ATI=119.95
      DO 16 I=1,M1
16    T(I,1)=TF
      TI=0.000
      IMP=1
      AS=0.893E-06
      AL=.956E-06
      A1=RMIN/DR/12.
      VT=FLOAT(M1)*AL/A1/DR
      WRITE (5,850) VT
850   FORMAT (' MAXIMUM ALLOWABLE VELOCITY ',E,' FT/SEC '/)
      G=VMAX/6.0*122
      WRITE (5,851) G
851   FORMAT (' APPROXIMATE GRAVITY LEVEL ',E,/)
20    TI=TI+DT
      DO 21 I=2,M2
21    T(I,M1)=T(I,M2)
      DO 121 J=2,M1
      T(1,J)=T(2,J)
121   T(M1,J)=T(M2,J)
      CALL SET (R,NO,ML,HR)
      CALL VEL (NO)
      IF (IMP.EQ.2) GO TO 30
      DO 22 IL=2,M2
      CALL TSR (IL,NO,AS,TN,T,RMIN)
      CALL TLR (IL,NO,AL,TM,T,RMIN)
22    CONTINUE
      IMP=2
      GO TO 40
30    DO 32 JL=2,M2
      CALL TSZ (JL,ML,TN,T,RMIN)
      CALL TLZ (JL,ML,TM,T,RMIN)
32    CONTINUE
      IMP=1
C   PHASE CHANGE CALCULATIONS.....................................
40    DO 70 J=2,M2
      DO 70 I=2,M2
      IF (TN(I,J).LT.TF) GO TO 70
      IF ((R(I,J)*0.517).GT.HR(J)) GO TO 70
      AHF=HR(J)
      SUM=TN(I,J)-T(I,J)
      SUM=SUM+R(I,J)
      SA=SUM*3.5170
      IF (SA-AHF) 61,61,62
61    R(I,J)=SUM
      TN(I,J)=TF+SA/AHF*3.
      GO TO 70
62    R(I,J)=HR(J)/0.517+1.
      TN(I,J)=3.+TF+(SA-AHF)/3.5170
70    CONTINUE
      DO 92 I=2,M2
      DO 92 J=2,M2
92    T(I,J)=TN(I,J)
C   PRINT RESULTS.................................................
      IF (TI.LT.ATI) GO TO 20
      ATI=ATI+120.0
      RTI=TI/60.0
      WRITE (5,194) RTI
194   FORMAT (' TIME = ',F,' MIN ',/)
      DO 95 I=1,4
```

```
      DO 95 JJ=1,4
      J=JR(I)
      K=JX(JJ)
      WRITE (6,94) J,K,T(K,J-1),T(K,J),T(K,J+1)
94    FORMAT (2I5,3F12.3)
95    CONTINUE
      WRITE (6,600) (NO(I),I=2,N2)
600   FORMAT (15I3)
      WRITE (6,96)
96    FORMAT (' INPUT FLAG '/)
      READ (6,97) FLAG
97    FORMAT (F)
      IF (FLAG.GE.10.0) GO TO 22
102   STOP
      END
      SUBROUTINE VEL(NO)
      DIMENSION U(81,30),V(81,30),UZ(81,30),UR(81,30),NO(81)
      COMMON /ALPHA/ U,V
      COMMON /BETA/ UZ,UR
      COMMON /GAMMA/ N1,N2,N3,M1,M2,M3
      DO 13 N=2,N2
      L=NO(N)-1
      DO 13 I=2,L
      IF (L.LT.3) GO TO 12
      II=I-1
      JJ=NO(N)-1
      IF (JJ.LT.1) JJ=NO(N)
      S1=FLOAT(II)/FLOAT(JJ)
      IF (S1.GE.0.999) GO TO 12
      DO 8 J=2,M2
      JK=J-1
      S2=FLOAT(JK)/FLOAT(M2)
      IF (S2.LT.S1) GO TO 8
      UZ(N,I)=U(N,J)
      UR(N,I)=V(N,J)
      GO TO 13
8     CONTINUE
      GO TO 13
12    UZ(N,I)=0.1E-12
      UR(N,I)=0.1E-12
13    CONTINUE
      RETURN
      END
      SUBROUTINE VIVV(VMAX)
      DIMENSION U(81,30),V(81,30),VV(30),SF(30),US(30),VB(30),VO(30)
      COMMON /ALPHA/ U,V
      COMMON /GAMMA/ N1,N2,N3,M1,M2,M3
      R1=FLOAT (M2)
      YV=-1.0
      B=1.0
      A=-1.2/SQRT(3.0)
      DO 10 I=2,M2
      YV=YV+2.0/R1
      C=YV/B
      RA=(C**3.0-C)/(A**3.0-A)
10    VV(I)=VMAX*RA
      PI=3.1415962
      Y=0.0
      DO 15 I=2,M2
      Y=Y+1.0/R1
```

```
      X=1.3
      SF(I)=COSH(PI*X)*SIN(PI*Y)
      UB(I)=-SINH(PI*X)*COS(PI*Y)*PI
15    VB(I)=COSH(PI*X)*SIN(PI*Y)*PI
      X=0.3
      Y=0.50
      DO 18 J=2,M2
      X=X+1.0/91
18    VO(M1+1-J)=PI*COSH(PI*X)*SIN(PI*Y)
      Y=0.50-1.0/R1
      J1=(M1+1)/2
      DO 36 M=J1,M2,1
      Y=Y+1.0/R1
      X=0.0
      DO 36 N=2,N2
      X=X+1.0/R1
      SFT=SINH(PI*X)*SIN(PI*Y)
      U1=-PI*SINH(PI*X)*COS(PI*Y)
      L1=M2/2
      DO 31 I=1,L1
      KK=M1-I
      IF (SFT.GE.SF(KK)) GO TO 30
      GO TO 31
30    CONTINUE
      KK=J1
31    UMAX=UB(KK)
      UBO=VV(KK)
      U(N,M)=U1*UBO/UMAX
      V1=PI*COSH(PI*X)*SIN(PI*Y)
      V(N,M)=(1.0-ABS(V1/VB(KK)))*UBO
      IF (ABS(V1/VB(KK)).GE.1.00) V(N,M)=0.001*UBO
36    CONTINUE
      DO 42 M=2,L1
      DO 42 N=2,N2
      U(N,M)=-U(N,M1-M)
      V(N,M)=V(N,M1-M)
40    CONTINUE
      NR1=M1-M2
      NR2=NR1-1
      NR3=N2-1
      DO 50 M=2,M2
      DO 50 N=M1,NR1
      V(N,M)=0.1E-12
      U(N,M)=VV(M)
      IF (M.EQ.J1) U(N,M)=0.1E-12
50    CONTINUE
      DO 60 M=2,M2
      DO 60 N=NR1,N3
      NN=N-NR2
      U(M1-NN,M)=U(N-NR3,M)
      V(M1-NN,M)=-V(N-NR3,M)
60    CONTINUE
      RETURN
      END
      SUBROUTINE SET (R,NO,ML,HR)
      DIMENSION R(81,31),NO(81),ML(30),HR(30)
      COMMON /GAMMA/ N1,N2,N3,M1,M2,M3
      DO 10 I=2,N2
      DO 8 J=2,M2
      IF (R(I,J)*0.517.GE.HR(J)) GO TO 8
```

```
      NO(I)=J
      GO TO 14
    8 CONTINUE
      NO(I)=M2
   10 CONTINUE
      DO 22 J=2,M2
      ML(J)=2
      DO 18 I=2,M2
      IF (R(I,J)*2.517.LT.RR(J)) GO TO 18
      ML(J)=I
      GO TO 22
   18 CONTINUE
      ML(J)=M1
   20 CONTINUE
      RETURN
      END
      SUBROUTINE TSR (I,NO,AS,TN,T,RMIN)
      DIMENSION TN(81,32), T(81,32),NO(81),A(32),C(32)
      DIMENSION D(32),W(32),Y(33)
      COMMON /S1/ A,C,D,W,Y
      COMMON /S2/ DZ,DR,DT
      COMMON /GAMMA/ N1,N2,N3,M1,M2,M3
      IF (NO(I).GT.M2) GO TO 10
      IF (NO(I).EQ.M2) GO TO 20
      IF (NO(I).EQ.M3) GO TO 25
      K=NO(I)
      RAD=FLOAT(K-1)*DR+RMIN/12.
      A(K)=-AS*DT/DR/DR+0.5*AS*DT/RAD/DR
      B=1.+2.*AS*DT/DZ/DZ
      C(K)=-AS*DT/DR/DR-0.5*AS*DT/RAD/DR
      D(K)=T(I,K)+AS*DT/DZ/DZ*(T(I-1,K)+T(I+1,K)-2.*T(I,K))
      D(K)=D(K)-A(K)*T(I,K-1)
      KK=K+1
      DO 10 J=KK,N3
      RAD=FLOAT(J-1)*DR+RMIN/12.
      A(J)=-AS*DT/DR/DR+0.5*AS*DT/RAD/DR
      C(J)=-AS*DT/DR/DR-0.5*AS*DT/RAD/DR
   10 D(J)=T(I,J)+AS*DT/DZ/DZ*(T(I+1,J)+T(I-1,J)-2.*T(I,J))
      J=M2
      RAD=FLOAT(J-1)*DR+RMIN/12.
      A(J)=-AS*DT/DR/DR+0.5*AS*DT/RAD/DR
      C(J)=A(J)-AS*DT/RAD/DR
      D(J)=T(I,J)+AS*DT/DZ/DZ*(T(I+1,J)+T(I-1,J)-2.*T(I,J))
      D(J)=D(J)-C(J)*T(I,J+1)
      W(K)=B
      Y(K)=D(K)/W(K)
      DO 12 J=KK,M2
      BB=C(J-1)/A(J-1)
      W(J)=B-A(J)*BB
   12 Y(J)=(D(J)-A(J)*Y(J-1))/W(J)
      TN(I,M2)=Y(M2)
      DO 15 J=M3,K,-1
      L=J
      BB=C(L)/W(L)
   15 TN(I,L)=Y(L)-BB*TN(I,L+1)
      GO TO 100
   20 RAD=FLOAT(M3)*DR+RMIN/12.
      AA=-AS*DT/DR/DR+0.5*DT*AS/RAD/DR
      BB=1.0+2.0*AS*DT/DR/DR
      CC=AA-AS*DT/RAD/DR
```

```
      DD=T(I,M2)+AS*DT/DZ/DZ*(T(I+1,M2)+T(I-1,M2)-2.*T(I,M2))
      TN(I,M2)=(DD-AA*T(I,M3)-CC*T(I,M1))/BB
      GO TO 100
25    RAD=FLOAT(M3)*DR+RMIN/12.0
      RA=-AS*DT/DR/DR+0.5*AS*DT/RAD/DR
      CC=RA-AS*DT/DR/RAD
      RAD=RAD-DR
      RC=-AS*DT/DR/DR-0.5*AS*DT/RAD/DR
      AA=RC+AS*DT/RAD/DR
      BB=1.0+2.0*AS*DT/DR/DR
      D1=T(I,M3)+AS*DT/DZ/DZ*(T(I+1,M3)+T(I-1,M3)-2.*T(I,M3))
      D1=D1-AA*T(I,M3-1)
      D2=T(I,M2)+AS*DT/DZ/DZ*(T(I+1,M2)+T(I-1,M2)-2.*T(I,M2))
      D2=D2-CC*T(I,M1)
      F=D1/BB-D2/RA
      G=RC/BB-RB/RA
      TN(I,M2)=F/G
      TN(I,M3)=D1/BB-RC*TN(I,M2)/BB
100   RETURN
      END
      SUBROUTINE TLR (I,NO,AL,TN,T,RMIN)
      DIMENSION TN(81,30),T(81,30),NO(81),A(30),C(30),UZ(81,30)
      DIMENSION UR(81,30)
      DIMENSION D(30), (30),Y(30)
      COMMON /S1/A,C,D, ,Y
      COMMON /S2/ DZ,DR,DT
      COMMON /BETA/ UZ,UR
      COMMON /GAMMA/ M1,M2,M3, 1,M2,M3
      LN=NO(I)-1
      IF (LN.LE.1) GO TO 100
      IF (LN.EQ.2) GO TO 22
      IF (LN.EQ.3) GO TO 25
      RAD=RMIN/12.0+DR
      A(2)=-UR(I,2)*DT/2.0/DR-AL*DT/DR/DR+0.5*AL*DT/RAD/DR
      B=1.0+2.0*AL*DT/DR/DR
      C(2)=0.5*UR(I,2)*DT/DR-AL*DT/DR/DR-0.5*AL*DT/RAD/DR
      D(2)=0.5*DT*UZ(I,2)*(T(I-1,2)-T(I+1,2))/DZ+T(I,2)
      D(2)=D(2)+AL*DT*(T(I+1,2)+T(I-1,2)-2.0*T(I,2))/DZ/DZ-A(2)*T(I,1)
      LO=LN-1
      DO 10 J=3,LO
      RAD=FLOAT(J-1)*DR+RMIN/12.0
      A(J)=-0.5*UR(I,J)*DT/DR-AL*DT/DR/DR+0.5*AL*DT/RAD/DR
      C(J)=0.5*UR(I,J)*DT/DR-AL*DT/DR/DR-0.5*AL*DT/RAD/DR
      D(J)=0.5*DT*UZ(I,J)*(T(I-1,J)-T(I+1,J))/DZ+T(I,J)
10    D(J)=D(J)+AL*DT*(T(I+1,J)+T(I-1,J)-2.0*T(I,J))/DZ/DZ
      RAD=FLOAT(LN)*DR+RMIN/12.0
      A(LN)=-0.5*UR(I,LN)*DT/DR-AL*DT/DR/DR+0.5*AL*DT/RAD/DR
      C(LN)=0.5*UR(I,LN)*DT/DR-AL*DT/DR/DR-0.5*AL*DT/RAD/DR
      D(LN)=0.5*DT*UZ(I,LN)*(T(I-1,LN)-T(I+1,LN))/DZ+T(I,LN)
      D(LN)=D(LN)+AL*DT*(T(I+1,LN)+T(I-1,LN)-2.*T(I,LN))/DZ/DZ
      D(LN)=D(LN)-C(LN)*T(I,LN+1)
      B(2)=B
      Y(2)=D(2)/B(2)
      DO 12 J=3,LN
      BB=C(J-1)/B(J-1)
      B(J)=B-A(J)*BB
12    Y(J)=(D(J)-A(J)*Y(J-1))/B(J)
      TN(I,LN)=Y(LN)
      DO 15 J=LO,2,-1
      L=J
```

```
      BB=C(L)/W(L)
15    TN(I,L)=Y(L)-BB*TN(I,L+1)
      GO TO 100
20    RAD=RMIN/12.0+DR
      RA=-AL*DT/DR/DR+ .5*AL*DT/RAD/DR
      RB=1.0+2.0*AL*DT/DR/DR
      RC=RA+AL*DT/RAD/DR
      RD=T(I,2)+AL*DT/DZ/DZ*(T(I+1,2)+T(I-1,2)-2.*T(I,2))
      TN(I,2)=(RD-RA*T(I,1)-RC*T(I,3))/RB
      GO TO 100
25    RAD=RMIN/12.0+2.5*DR
      RA=-0.5*UR(I,LN)*DT/DR-AL*DT/DR/DR+0.5*AL*DT/RAD/DR
      RC=RA+UR(I,LN)*DT/DR-AL*DT/RAD/DR
      RB=1.0+2.0*AL*DT/DR/DR
      RAD=RAD-DR
      CR=0.5*UR(I,LN-1)*DT/DR-AL*DT/DR/DR-0.5*AL*DT/RAD/DR
      AR=-0.5*UR(I,LN-1)*DT/DR-AL*DT/DR/DR+0.5*DT*AL/RAD/DR
      D1=0.5*UZ(I,LN-1)*DT/DZ*(T(I-1,LN-1)-T(I+1,LN-1))+T(I,LN-1)
      D1=D1+AL*DT*(T(I+1,LN-1)+T(I-1,LN-1)-2.*T(I,LN-1))/DZ/DZ
      D1=D1-AR*T(I,LN-2)
      D2=0.5*DT*UZ(I,LN)*(T(I-1,LN)-T(I+1,LN))/DZ+T(I,LN)
      D2=D2+AL*DT*(T(I+1,LN)+T(I-1,LN)-2.*T(I,LN))/DZ/DZ
      D2=D2-RC*T(I,LN+1)
      F=D1/RB-D2/RA
      G=CR/RB-RB/RA
      TN(I,LN)=F/G
      TN(I,LN-1)=D1/RB-CR*TN(I,LN)/RB
100   RETURN
      END
      SUBROUTINE TSZ (J,ML,TN,T,RMIN)
      DIMENSION T(81,31)
      DIMENSION ML(30),TN(81,31),DJ(81),WZ(81),YZ(81)
      COMMON /S2/ DZ,DR,DT
      COMMON /S3/ AS,AL,DJ,WZ,YZ
      COMMON /GAMMA/ N1,N2,N3,M1,M2,M3
      RAD=FLOAT(J-1)*DR+RMIN/12.0
      IF (ML(J)-1,LT,2) GO TO 100
      L=ML(J)-1
      LL=L-1
      AA=-AS*DT/DZ/DZ
      BB=1.0+2.0*AS*DT/DZ/DZ
      CC=AA
      D1=AS*DT/DR/DR
      D2=0.5*AS*DT/RAD/DR
      IF (L.EQ.2) GO TO 20
      IF (L.EQ.3) GO TO 25
      I=2
      DJ(I)=D1*(T(I,J+1)+T(I,J-1)-2.*T(I,J))+D2*(T(I,J+1)-T(I,J-1))
      DJ(I)=DJ(I)+T(I,J)-AA*T(I-1,J)
      DO 5 I=3,LL
      DJ(I)=D1*(T(I,J+1)+T(I,J-1)-2.*T(I,J))+T(I,J)
5     DJ(I)=DJ(I)+D2*(T(I,J+1)-T(I,J-1))
      I=L
      DJ(I)=D1*(T(I,J+1)+T(I,J-1)-2.*T(I,J))+T(I,J)-CC*T(I+1,J)
      DJ(I)=DJ(I)+D2*(T(I,J+1)-T(I,J-1))
      WZ(2)=BB
      YZ(2)=DJ(2)/WZ(2)
      DO 10 K=3,L
      X=CC/WZ(K-1)
      WZ(K)=BB-AA*X
```

```
10      YZ(K)=(DJ(K)-AA*YZ(K-1))/WZ(K)
        TN(L,J)=YZ(L)
        DO 12 K=LL,2,-1
        KJ=K
        X=CC/WZ(KJ)
12      TN(KJ,J)=YZ(KJ)-X*TN(KJ+1,J)
        GO TO 100
20      TN(2,J)=(D1*(T(2,J+1)+T(2,J-1)-2.*T(2,J))-AA*T(1,J)+T(2,J)
     1  +D2*(T(2,J+1)-T(2,J-1))-CC*T(3,J))/BB
        GO TO 100
25      E1=D1*(T(2,J+1)+T(2,J-1)-2.0*T(2,J))+T(2,J)-AA*T(1,J)
        E1=E1+D2*(T(2,J+1)-T(2,J-1))
        E2=D1*(T(3,J+1)+T(3,J-1)-2.*T(3,J))+T(3,J)-CC*T(4,J)
        E2=E2+D2*(T(3,J+1)-T(3,J-1))
        F=E1/BB-E2/AA
        G=CC/BB-BB/AA
        TN(3,J)=F/G
        TN(2,J)=E1/BB-CC*TN(3,J)/BB
100     RETURN
        END
        SUBROUTINE TLZ (J,ML,TN,T,RMIN)
        DIMENSION ML(30),TN(61,30),T(61,30),DJ(61),WZ(61)
        DIMENSION YZ(61),UZ(61,30),UR(61,30),AA(61),CC(61)
        COMMON /S2/ DZ,DR,DT
        COMMON /S3/ AS,AL,DJ,WZ,YZ
        COMMON /BETA/ UZ,UR
        COMMON /GAMMA/ N1,N2,N3,M1,M2,M3
        L=ML(J)
        RAD=FLOAT(J-1)*DR+RMIN/12.0
        IF (L.GE.N1) GO TO 10
        BB=1.0+2.*AL*DT/DZ/DZ
        IF (L.EQ.N2) GO TO 20
        IF (L.EQ.N3) GO TO 25
        AA(L)=-0.5*UZ(L,J)*DT/DZ-AL*DT/DZ/DZ
        CC(L)=0.5*UZ(L,J)*DT/DZ-AL*DT/DZ/DZ
        DJ(L)=0.5*UR(L,J)*DT/DR*(T(L,J-1)-T(L,J+1))+AL*DT*(T(L,J+1)+T(L
     1  ,J-1)-2.*T(L,J))/DR/DR
        DJ(L)=DJ(L)+AL*DT*(T(L,J+1)-T(L,J-1))/2./RAD/DR-AA(L)*T(L-1,J
     1  )+T(L,J)
        LL=L+1
        DO 5 I=LL,N3
        AA(I)=-UZ(I,J)*DT/2./DZ-AL*DT/DZ/DZ
        CC(I)=UZ(I,J)*DT/2./DZ-AL*DT/DZ/DZ
        DJ(I)=0.5*UR(I,J)*(T(I,J-1)-T(I,J+1))/DR+AL*DT*(T(I,J+1)+
     1  T(I,J-1)-2.*T(I,J))/DR/DR-AL*DT*(T(I,J-1)-T(I,J+1))/2./RA
     2  D/DR+T(I,J)
5       CONTINUE
        I=N2
        AA(I)=-UZ(I,J)*DT/2./DZ-AL*DT/DZ/DZ
        CC(I)=UZ(I,J)*DT/2./DZ-AL*DT/DZ/DZ
        DJ(I)=0.5*UR(I,J)*DT/DR*(T(I,J-1)-T(I,J+1))+AL*DT*(T(I,J+1)+
     1  T(I,J-1)-2.0*T(I,J))/DR/DR+AL*DT*(T(I,J+1)-T(I,J-1))/2./RA
     2  D/DR-CC(I)*T(I+1,J)+T(I,J)
        WZ(L)=BB
        YZ(L)=DJ(L)/WZ(L)
        DO 10 K=LL,N2
        X=CC(K)/WZ(K-1)
        WZ(K)=BB-AA(K)*X
10      YZ(K)=(DJ(K)-AA(K)*YZ(K-1))/WZ(K)
        TN(N2,J)=YZ(N2)
```

```
      DO 12 KJ=N3,L,-1
      X=CC(KJ)/AZ(KJ)
12    TN(KJ,J)=YZ(KJ)-X*TN(KJ+1,J)
      GO TO 100
20    A=-UZ(L,J)*DT/2./DZ-AL*DT/DZ/DZ
      C=UZ(L,J)*DT/2./DZ-AL*DT/DZ/DZ
      B=0.5*UR(L,J)*DT/DR*(T(L,J-1)-T(L,J+1))+AL*DT*(T(L,J+1)+T(
     1L,J-1)-2.0*T(L,J))/DR/DR+AL*DT*(T(L,J+1)-T(L,J-1))/2./RAD/
     2DR-A*T(L-1,J)-C*T(L+1,J)+T(L,J)
      TN(L,J)=D/BB
      GO TO 100
25    A=-UZ(L+1,J)*DT/2./DZ-AL*DT/DZ/DZ
      C=UZ(L,J)*DT/2./DZ-AL*DT/DZ/DZ
      D1=0.5*UR(L,J)*DT/DR*(T(L,J-1)-T(L,J+1))+AL*DT*(T(L,J+1)
     1+T(L,J-1)-2.0*T(L,J))/DR/DR+T(L,J)+AL*DT*(T(L,J+1)
     2-T(L,J-1))/2./RAD/DR+(UZ(L,J)*DT/2./DZ+AL*DT/DZ/DZ)*T(L-1,J)
      D2=0.5*UR(L+1,J)*DT/DR*(T(L+1,J-1)-T(L+1,J+1))+AL*DT*(T(L+1,J+1
     1)+T(L+1,J-1)-2.0*T(L+1,J))/DR/DR+T(L+1,J)+AL*DT*(T(L+1,J+1)-T(L
     2+1,J-1))/2./RAD/DR-(UZ(L+1,J)*DT/2./DZ-AL*DT/DZ/DZ)*T(L+2,J)
      F=D1/BB-D2/A
      G=C/BB-BB/A
      TN(L+1,J)=F/G
      TN(L,J)=D1/BB-C*TN(L+1,J)/BB
100   RETURN
      END
```